**DOT/FAA/TC-12/44**

Federal Aviation Administration
William J. Hughes Technical Center
Aviation Research Division
Atlantic City International Airport
New Jersey 08405

# Neck Injury Criteria for Side-Facing Aircraft Seats—Phase II

May 2013

Final Report

This document is available to the U.S. public through the National Technical Information Services (NTIS), Springfield, Virginia 22161.

This document is also available from the Federal Aviation Administration William J. Hughes Technical Center at actlibrary.tc.faa.gov.

U.S. Department of Transportation
**Federal Aviation Administration**

## NOTICE

This document is disseminated under the sponsorship of the U.S. Department of Transportation in the interest of information exchange. The U.S. Government assumes no liability for the contents or use thereof. The U.S. Government does not endorse products or manufacturers. Trade or manufacturers' names appear herein solely because they are considered essential to the objective of this report. The findings and conclusions in this report are those of the author(s) and do not necessarily represent the views of the funding agency. This document does not constitute FAA policy. Consult the FAA sponsoring organization listed on the Technical Documentation page as to its use.

This report is available at the Federal Aviation Administration William J. Hughes Technical Center's Full-Text Technical Reports page: actlibrary.tc.faa.gov in Adobe Acrobat portable document format (PDF).

**Technical Report Documentation Page**

| | | |
|---|---|---|
| 1. Report No.<br>DOT/FAA/TC-12/44 | 2. Government Accession No. | 3. Recipient's Catalog No. |
| 4. Title and Subtitle<br>NECK INJURY CRITERIA FOR SIDE-FACING AIRCRAFT SEATS—PHASE II | | 5. Report Date<br>May 2013 |
| | | 6. Performing Organization Code<br>Medical College of Wisconsin |
| 7. Author(s)<br>Narayan Yoganandan, Frank A. Pintar, John R. Humm, James Rinaldi, Christopher E. Wolfla, and Dennis J. Maiman | | 8. Performing Organization Report No.<br>MCW-FAA-20110715 |
| 9. Performing Organization Name and Address<br>Department of Neurosurgery<br>9200 West Wisconsin Avenue<br>Medical College of Wisconsin<br>Milwaukee, WI 53226 | | 10. Work Unit No. (TRAIS) |
| | | 11. Contract or Grant No.<br>DTFACT-09-R-00029 |
| 12. Sponsoring Agency Name And Address<br>U.S. Department of Transportation<br>Federal Aviation Administration<br>Northwest Mountain Region—Transport Airplace Directorate<br>FAA Northwest Mountain Regional Office<br>1601 Lind Ave., SW<br>Renton, WA 98057 | | 13. Type of Report and Period Covered<br>Final Report |
| | | 14. Sponsoring Agency Code<br>ANM-115 |

15. Supplementary Notes

The Federal Aviation Administration William J. Hughes Technical Center Aviation Research Division COR was Allan Abramowitz.

16. Abstract

The Federal Aviation Administration (FAA) is conducting research to support the development of aircraft side-facing neck injury criteria and tolerances for Title 14 Code of Federal Regulations (CFR). Recent research conducted for the FAA involved the use of dynamic sled tests with postmortem human subjects (PMHS) and the EuroSID-2 (ES-2) anthropomorphic test dummy, which was designed for automotive side-impact applications. The purpose of the current study was to obtain PMHS injury and neck load data associated with lateral, high-moment/low-tension loading at the neck, conduct comparable tests on an ES-2, correlate results, and develop Injury Assessment Reference Values (IARV) for the ES-2 based on current and previous FAA-sponsored research.

To obtain the necessary data, a component test methodology was developed to induce a high lateral bending moment with low axial tensile force at the occipital condyles (OC) of the human head-neck complex. The test methodology was developed, and tests were conducted on whole-body PMHS and intact and isolated head-neck complexes. Head angular and linear accelerations and angular velocities were computed using a custom pyramid nine-accelerometer package on the head; PMHS-specific physical properties, including center of gravity and moments of inertia in the three dimensions; and equations of equilibrium. These data were used to compute neck loads (i.e., forces and moments at the OC). Although these magnitudes correspond to PMHS, matched pair tests were conducted on an ES-2. The ES-2 was subjected to lateral bending moment loads using the same loading fixtures and experimental setups as the PMHS. IARVs specific to the ES-2 were obtained using current and previous PMHS and ES-2 results. The data supports the development of performance standards for the certification of aircraft side-facing seats and associated protection systems and development of ES-2 IARV test certification criteria to demonstrate compliance to the CFR.

| | |
|---|---|
| 17. Key Words<br>Anthropomorphic test device, Biomechanics, Certification, ES-2, Injury Assessment Reference Values, Lateral bending moment, Occipital condyle loads, Postmortem human subjects, Side-facing seat, Tolerance | 18. Distribution Statement<br>This document is available to the U.S. public through the National Technical Information Service (NTIS), Springfield, Virginia 22161. This document is also available from the Federal Aviation Administration William J. Hughes Technical Center at actlibrary.tc.faa.gov. |

| | | | |
|---|---|---|---|
| 19. Security Classif. (of this report)<br>Unclassified | 20. Security Classif. (of this page)<br>Unclassified | 21. No. of Pages<br>79 | 22. Price |

**Form DOT F 1700.7** (8-72) Reproduction of completed page authorized

ACKNOWLEDGEMENTS

Allan Abramowitz of the Federal Aviation Administration (FAA) William J. Hughes Technical Center was the Contracting Office Representative for this research. The authors thank Mr. Abramowitz for his guidance and management of the project. The authors also acknowledge Steve J. Soltis, retired FAA Chief Scientific and Technical Advisor for Crash Dynamics, for providing important consultations and insight during the initial phase of the study. The authors are also grateful to Matt M.G.M. Philippens, TNO Defence, Security, and Safety, The Netherlands, who assisted during various stages of the study, for his efforts and experience. The authors thank Jac S.H.M. Wismans, Safeteq, Inc., The Netherlands, for his consultation. Rick W. DeWeese and David Moorcroft, Civil Aerospace Medical Institute, Oklahoma City, OK, are acknowledged for sharing aviation-related experiences and assisting the authors to achieve the goals of this project. Joseph Pellettiere, FAA Chief Scientific and Technical Advisor for Crash Dynamics, Aviation Safety, is also acknowledged for assisting the authors in the review of the first draft of the report and participating in several discussions with Allan Abramowitz and Rick DeWeese to finalize this report.

The authors thank the clinical faculty of the Department of Neurosurgery of the Medical College of Wisconsin. Also acknowledged are Michael Schlick's technical consultations, and the support of the Neuroscience Research Staff, including Christy Stadig and Kristin Kiehl, while conducting the experiments. This study was also supported by the Department of Veterans Affairs Medical Research.

TABLE OF CONTENTS


| | | Page |
|---|---|---|
| EXECUTIVE SUMMARY | | xi |
| 1. | INTRODUCTION | 1 |
| | 1.1 Objective | 1 |
| 2. | BACKGROUND | 1 |
| 3. | METHODS—THE PMHS TESTS | 3 |
| | 3.1 The PMHS Preparation and Mounting | 3 |
| | 3.2 Loading | 4 |
| | 3.3 The PMHS Instrumentation | 5 |
| | 3.4 Physical Properties | 5 |
| | 3.5 Coordinate System | 6 |
| | 3.6 Biomechanical Data | 6 |
| 4. | THE PMHS TEST RESULTS | 7 |
| | 4.1 The PMHS Data | 7 |
| | 4.2 The PMHS 1 Test, Series 1 | 7 |
| | 4.3 The PMHS 1 Test, Series 2 | 12 |
| | 4.4 The PMHS 2 Test Series | 14 |
| 5. | DISCUSSION—THE PMHS TESTS | 17 |
| | 5.1 Overall Goals | 17 |
| | 5.2 Rationale for the Present Model | 17 |
| | 5.3 Importance of Specimen-Specific Properties | 17 |
| | 5.4 Importance of Head Kinematics | 17 |
| | 5.5 Role of Coupled Motions in the Human Neck | 18 |
| | 5.6 Limitations | 18 |
| | 5.7 The Applications of PMHS Findings | 19 |
| 6. | THE PMHS-BASED IRVs | 20 |
| 7. | SUMMARY AND CONCLUSIONS—THE PMHS TESTS | 21 |
| 8. | METHODS—THE ES-2 TESTS | 21 |
| | 8.1 The ES-2 Preparation and Mounting | 21 |
| | 8.2 Loading | 22 |

8.3 Instrumentation 22
8.4 Coordinate system 22
8.5 Mechanical data 22

9. RESULTS—THE ES-2 TESTS 22

9.1 Applied Moment and Force Histories 22
9.2 Summary of Data 24

10. DISCUSSION—THE ES-2 TESTS 26

10.1 Overall Goals 26
10.2 The ES-2 Responses 26

11. THE ES-2-BASED IARVs 27

12. CONCLUSIONS 28

13. BIBLIOGRAPHY 29

LIST OF FIGURES


| Figure | | Page |
|---|---|---|
| 1 | Fixture Used to Apply Lateral Bending Moments | 4 |
| 2 | Pyramid-Shaped, Nine-Accelerometer Package | 5 |
| 3 | Right-Handed Cartesian Coordinate System | 6 |
| 4 | The PMHS 1, Series 1 Representative Integrated Moment Data | 9 |
| 5 | The PMHS 1, Series 1 Head Angular Velocity Corresponding to Representative Integrated Moment Data | 9 |
| 6 | Representative Applied Moments | 10 |
| 7 | Representative Applied Forces | 10 |
| 8 | Representative Moments at the OC | 11 |
| 9 | Representative Forces at the OC | 12 |
| 10 | The PMHS 1, Series 1 | 14 |
| 11 | The PMHS 1, Series 2 | 14 |
| 12 | The PMHS 2 | 16 |
| 13 | Photograph Showing the Test Setup for ES-2 Experiments | 21 |
| 14 | The ES-2 Representative Measured Applied Moments | 23 |
| 15 | The ES-2 Representative Measured Applied Forces | 23 |
| 16 | The ES-2 Representative Upper-Neck Load Cell Moments | 25 |
| 17 | The ES-2 Representative Upper-Neck Load Cell Forces | 25 |
| 18 | Variations of Integrated and OC Moments in PMHS and ES-2 | 27 |

LIST OF TABLES


| Table | | Page |
|---|---|---|
| 1 | Physical Properties of the Head | 7 |
| 2 | The PMHS 1, Series 1 Head Angular Velocity, Integrated Moment, and Head Angle Data | 8 |
| 3 | The PMHS 1, Series 1 Summary of Applied Loads | 8 |
| 4 | The PMHS 1, Series 1 Summary of Loads at the OC | 11 |
| 5 | The PMHS 1, Series 2 Head Angular Velocity, Integrated Moment, and Head Angle Data | 13 |
| 6 | The PMHS 1, Series 2 Summary of Applied Loads | 13 |
| 7 | The PMHS 1, Series 2 Summary of Loads at the OC | 13 |
| 8 | The PMHS 2, Head Angular Velocity, Integrated Moment, and Head Angle Data | 15 |
| 9 | The PMHS 2, Summary of Applied Forces and Moments | 15 |
| 10 | The PMHS 2, Summary of Forces and Moments at the OC | 16 |
| 11 | The ES-2 Head Angular Velocity and Integrated Moment Data | 24 |
| 12 | The ES-2 Peak Applied Forces and Moments | 24 |
| 13 | The ES-2 Upper-Neck Load Cell Forces and Moments | 26 |

LIST OF SYMBOLS, ABBREVIATIONS, AND ACRONYMS

| | |
|---|---|
| $F$ | Force |
| $F_x$ | Anteroposterior shear force |
| $F_y$ | Lateral shear force |
| $F_z$ | Axial force |
| $I_{xx}$ | Moment of inertia along x-axis |
| $I_{yy}$ | Moment of inertia along y-axis |
| $I_{zz}$ | Moment of inertia along z-axis |
| $M_x$ | Lateral or coronal bending moment |
| $M_y$ | Sagittal or flexion-extension bending moment |
| $M_z$ | Axial (twisting) moment |
| $N_{ij}$ | Neck injury criteria |
| kN | kilonewton |
| ms | Millisecond |
| m/s | Meter per second |
| N | Newton |
| Nm | Newton meter |
| rad | Radian |
| rad/s | Radians per second |
| AIS | Abbreviated Injury Scale |
| AP | Anteroposterior |
| ATD | Anthropomorphic test dummy |
| CFR | Code of Federal Regulations |
| c.g. | Center of gravity |
| CT | Computed tomography |
| ES-2 | EuroSID-2 (anthropomorphic test dummy) |
| FAA | Federal Aviation Administration |
| FMVSS | Federal Motor Vehicle Safety Standards |
| IARV | Injury Assessment Reference Value |
| IRV | Injury Reference Value |
| LVDT | Linear variable differential transformer |
| MCW | Medical College of Wisconsin |
| OC | Occipital condyles |
| PMHS | Postmortem human subject |

# EXECUTIVE SUMMARY

The Federal Aviation Administration (FAA) is conducting research to support the development of aircraft side-facing neck injury criteria and tolerances for Title 14 Code of Federal Regulations (CFR). Recent research conducted for the FAA involved the use of dynamic sled tests using postmortem human subjects (PMHS) and the EuroSID-2 (ES-2) anthropomorphic test dummy, which was designed for automotive side-impact applications. The purpose of the current study was to obtain PMHS injury and neck load data associated with lateral high-moment/low-tension loads at the neck, conduct comparable tests on an ES-2, correlate the results, and develop Injury Assessment Reference Values (IARV) for the ES-2 based on current and previous FAA-sponsored research.

To obtain the necessary data, a component test methodology was developed to induce a high lateral or lateral bending moment with low axial tensile force at the occipital condyles (OC) of the human head-neck complex. A series of tests were conducted on whole-body PMHS and intact and isolated head-neck complexes. Head angular and linear accelerations and angular velocities were computed using a custom pyramid nine-accelerometer package on the head; PMHS-specific physical properties, including center of gravity and moments of inertia in the three dimensions; and equations of equilibrium. These data were used to compute neck loads (i.e., forces and moments at the OC). Data from 24 tests indicated that lateral moments up to 74 Newton meter (Nm) at the OC associated with very low levels of axial tensile forces—less than 300 Newton (N)—produced no injuries. This was assessed using palpation, x-rays, computed tomography, and a detailed autopsy.

Using a matched pair test procedure, the ES-2 was subjected to lateral bending moment loads using the same loading fixtures and experimental setups as the PMHS. An IARV specific to the ES-2 was developed using the current PMHS and ES-2 research data. A peak lateral bending moment of 115 Nm IARV is recommended for the ES-2.

The data support the development of performance standards for the certification of aircraft side-facing seats and associated protection systems and the development of ES-2 IARV test certification criteria to demonstrate compliance to the CFR.

## 1. INTRODUCTION.

The Federal Aviation Administration (FAA) is conducting research to support the development of aircraft side-facing seat neck injury criteria and tolerances for Title 14 Code of Federal Regulations (CFR). Recent research conducted for the FAA (Philippens et al., 2011) involved the use of dynamic sled tests using postmortem human subjects (PMHS) and the EuroSID-2 (ES-2) anthropomorphic test dummy (ATD), which was designed for automotive side-impact applications. The purpose of the current study was to obtain additional data to support the development of the requirement. Specifically, the Medical College of Wisconsin (MCW) obtained PMHS injury and neck load data associated with coronal or lateral high-moment/low-tension loads at the neck; conducted comparable tests on an ES-2; correlated the results; and developed an Injury Assessment Reference Value (IARV) for the ES-2 based on the current and previous FAA research. These results support the FAA in the development of the requirement and ES-2 test certification criteria to demonstrate compliance.

### 1.1 OBJECTIVE.

The overall objectives of this study were (1) to investigate the biomechanics of the human head-neck complexes with a focus on neck injuries in side-facing aircraft seats, and (2) to develop neck injury assessment values that can be used to establish FAA requirements.

In the first phase of the study (PMHS tests), a component-level test was developed to obtain PMHS injury data and establish Injury Reference Values (IRV).

In the second phase of the study (ES-2 tests), a matched pair test procedure was conducted using the ES-2 (matched to the PMHS).

In the third phase of the study, IARV specific to the ES-2 was obtained. The IARV criteria from the past FAA study and the current research supports performance standards for the certification of side-facing aircraft seats and associated protection systems.

## 2. BACKGROUND.

To determine human injury tolerances due to impacts, PMHS are used as experimental models in aviation, motor vehicle, athletics, and other environments (Soltis et al., 2003; Yoganandan et al., 1998; Yoganandan et al., 2007a). From side-impact perspectives, the test subject is exposed to impacts using free-fall (Fayon et al., 1977; Tarriere et al., 1979; Walfisch et al., 1980); sled (Eppinger et al., 1984; Pintar et al., 1997; Yoganandan et al., 2009b; and Yoganandan et al., 2008a); and pendulum (Nusholtz et al., 1982; Viano et al., 1989; Yoganandan et al., 1997; and Yoganandan et al., 1996) devices. Intact PMHS have also been used in full-scale vehicle tests in this mode (Douglas et al., 2007; Klaus and Kalleris, 1982, 1983; Klaus et al., 1984). Following the application of the external load, parameters (such as accelerations and deformations) are obtained using techniques including x-rays and autopsy, and the resulting injuries are documented. The connection between the PMHS and in vivo humans, particularly with respect to features such as the musculoskeletal structure, allows the specification of human tolerance to trauma. This methodology has been used to establish injury criteria and applications to crash test

dummies (Eppinger et al., 1984 and Kuppa et al., 2000). The primary focus of these studies was thoracic trauma.

With regard to external loads, considerable efforts have focused on motor vehicle crashes (Yoganandan et al., 2009b and Yoganandan et al., 2008a). Data generated from models replicating specific trauma scenarios have led to the development of safety-engineered systems, such as torso airbags and head curtains, and the promulgation of requirements, including those in the U.S. Federal Motor Vehicle Safety Standards (FMVSS). FMVSS 214 (NHTSA, 1990, 1999) is an example, and in other countries there are similar requirements. The primary focus of these previous studies was to define, quantify, and mitigate injuries to the thorax, abdomen, and pelvic regions of the human body. Research efforts have been conducted for aircraft environments, with a focus on the head and neck regions of the human body (Philippens et al., 2009 and Soltis, 2001). Although Soltis' proposed neck injury criteria are based on the literature, the analysis emphasized the need to obtain data from PMHS experiments. Currently, specific IRVs for the head-neck region in lateral impacts do not exist, and this includes motor vehicle and aircraft environments. Therefore, it was necessary for the FAA to develop the necessary neck injury data.

The FAA sponsored an earlier study (Philippens et al., 2011) to investigate neck injuries in side-facing aircraft seats, develop injury criteria, and advance IARVs for the ES-2. Ten PMHS tests provided data on neck injuries and injury criteria in side-impact loading. Computer simulations and ES-2 sled tests were conducted to guide the definition of test conditions and establish corresponding values for injury criteria and ES-2 tolerance values. A rigid seat without cushion was initially used to minimize the influence of the seat on the results. A rigid seat with cushions was used for the three-point seat belt tests. Due to the stiffness of in-service, side-facing seats, the performance of the rigid seat with cushions was considered comparable. Since the kinematics of the occupant dominates the results (injury mechanisms), the effect of the seat (cushion) was not considered significant.

Ten tests with PMHS and ES-2 were used for this previous study. Two test configurations were used: a rigid seat with the thorax and pelvis restrained to the seat and an aircraft seat (including bottom, back panel, and armrest cushions) using a current in-service, three-point aircraft seatbelt. Two pulse types were used for the rigid-seat configuration tests: a 12.5-g sled deceleration with the velocity change prescribed in 14 CFR 25.562 and a 15.5-g sled deceleration with a 44% increase in velocity (twice the kinetic energy). Similarly, two pulse types were used for the aircraft seat configuration tests: a 12.5-g sled deceleration with the velocity prescribed in 14 CFR 25.562, and a 8.5-g sled deceleration with a 30% decrease in velocity.

Using the Abbreviated Injury Scale, (AIS) (Association for the Advancement of Automotive Medicine, 1990), minor neck injuries (AIS 1) occurred with the 12.5-g rigid-seat tests, and higher-severity injuries (AIS 3+) occurred with the same impact severity using the aircraft seat and a three-point seat belt restraint system. As serious injuries were attributed to the kinematics of the three-point seat belt-restrained occupant, it was expected that serious neck injury could occur using a standard three-point restraint system. The lowest-severity aircraft seat tests resulted in AIS 3 injuries in one PMHS and no injury in the other. The severe 15.5-g, rigid-seat tests resulted in AIS 2 injuries in one PMHS and AIS 3+ in the other PMHS.

Tensile force was found to be the discriminating parameter for predicting AIS 3+ neck injuries. The ES-2 upper-neck forces of 2300 and 1800 Newtons corresponding to 50% and 25% risks were suggested IARVs when combined with a minimum shear force, bending, or torque. The report stated: "explicit tolerance values for pure bending or shear loads would be helpful to complete the dataset" (Philippens et al., 2011).

The objective of the present study was to (1) develop a methodology to induce loading such that a high level of lateral bending moment accompanied by a low level of axial tensile force is applied to the head-neck complex, (2) determine the axial tensile and lateral bending moment from the developed experimental and computational methodologies, and (3) determine the potential head-neck injury criteria applicable to lateral impact loads with a primary focus on aviation environments. Specifically, the overall goal in the first phase of the study was to provide a PMHS-based IRV, and the second phase was to provide an ES-2-based IARV criteria.

## 3. METHODS—THE PMHS TESTS.

Prior to conducting the tests, unembalmed PMHS were screened for human immunodeficiency virus (HIV) and hepatitis A, B, and C. Pretest x-rays were obtained and anteroposterior (AP) and lateral radiographs were examined to ensure the integrity of the head-neck complex.

### 3.1 THE PMHS PREPARATION AND MOUNTING.

An analysis of existing methodologies for testing intact and isolated PMHS head-neck complexes indicated pure moment testing of functional units and segmented cervical columns, direct impact loading of head-neck complexes, and inverted drops of osteoligamentous cervical columns with the head and torso mass (Pintar et al., 2005; Pintar et al., 1998; Yoganandan et al., 1998; Yoganandan et al., 1986; and Yoganandan et al., 2008b). Drop tests result in vertical loads and always involve an axial-force component. Likewise, pure moment tests conducted using quasi-static rates are not applicable to traumatic situations, such as those considered in this study. These techniques were therefore deemed unsuitable to meet the present objectives as the intent was to achieve a unique loading condition (i.e., high lateral bending moment accompanied by low tensile force). The following novel methodology was used in this study.

The PMHS intact and isolated head-neck complexes were subjected to external loads using an electrohydraulic loading device (MTS Systems, Minneapolis, MN). Preparation included clothing the PMHS in tight-fitting leotards and positioning it on a custom-designed seat fixture, rigidly fixed to the platform of the testing device. The PMHS was seated upright with the head Frankfort plane horizontal, and a diagonal seat belt was used to restrain the torso supported by the back plate. To apply lateral flexion moment at varying rates of loading, the occiput (back part of the head) was connected to the loading device via a custom apparatus (figure 1). The cable shown in the figure was coupled to the load device piston to apply a torque to the PMHS occiput via a shaft. The shaft was aligned with the occipital condylar axis of the PMHS. The shaft was connected to a load cell that was attached to an interface plate that was screwed to the occiput to ensure rigid fixation. For isolated head-neck complex tests, the caudal end of each PMHS was fixed in polymethyl-methacrylate with the C3-C4 disc maintained horizontal. This fixative and procedure is commonly used in spine biomechanics studies (Yoganandan et al.,

1998). After rigid fixation of the caudal end of the PMHS to the test fixture, the occiput was coupled to the loading device to apply the lateral bending moment.

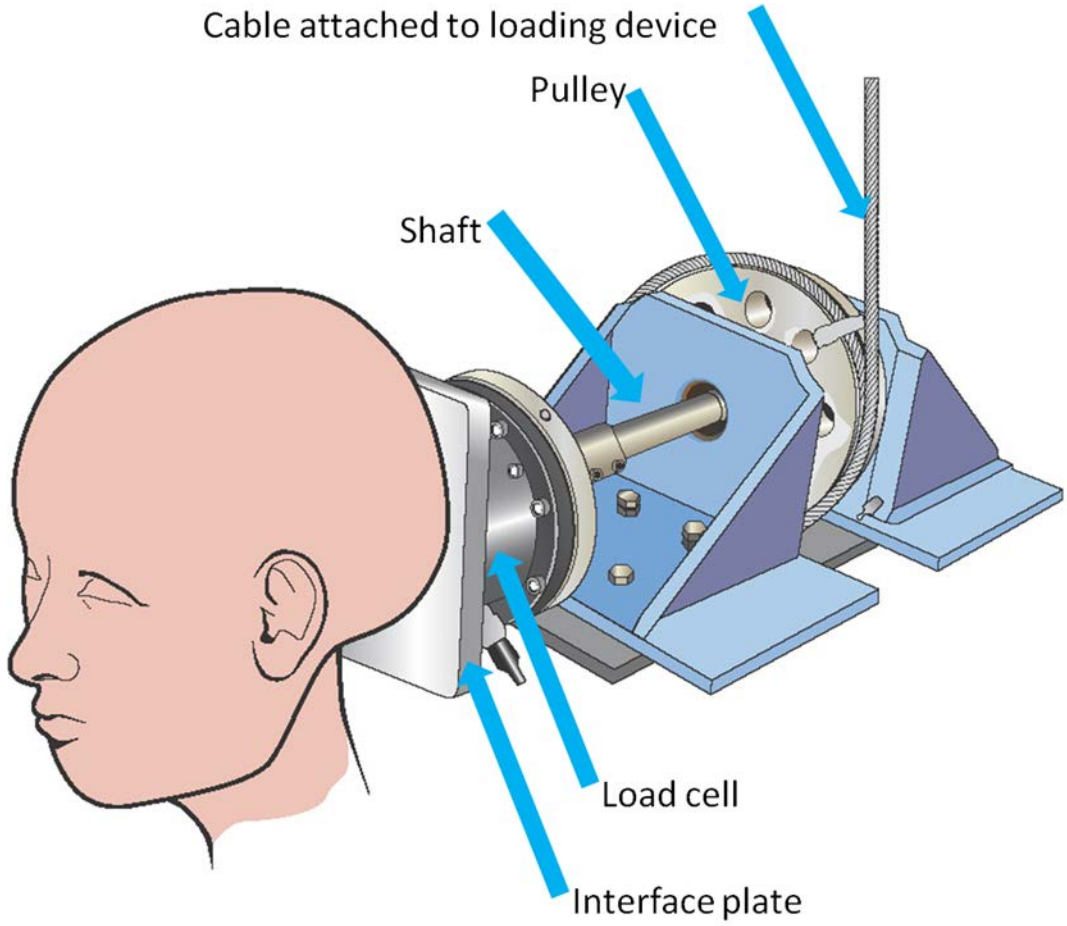


Figure 1. Fixture Used to Apply Lateral Bending Moments

3.2 LOADING.

The PMHS was loaded incrementally using a displacement control protocol with piston velocities from 2.0 to 7.0 m/s. To control the external load, feedback from a linear variable differential transformer (LVDT) displacement transducer connected in-series to the piston of the load device was used. Piston displacements were preset to limit excursions during loading. The PMHS was palpated after each loading test, and the PMHS was subjected to a higher velocity loading test if no injury was detected. Experienced personnel, including the clinical members of the research study, performed the palpations. The experimental protocol ceased testing when injury was confirmed or when reaching the limits of the testing apparatus. Subsequent to the final test, the PMHS was palpated, radiographs were taken, and computed tomography (CT) images were obtained at 1.0-mm intervals using a high-resolution CT scanner (Siemens, Germany).

3.3 THE PMHS INSTRUMENTATION.

Accelerometer instrumentation consisted of a pyramid-shaped, nine-accelerometer package secured to the lateral region of the head (Yoganandan et al., 2006). The package, shown in figure 2, had three linear accelerometers along the three orthogonal axes at the vertex, and two linear accelerometers at each of the three legs of the pyramid (Endevco® Model 7264, San Juan Capistrano, CA). These were used to obtain translational accelerations from which angular accelerations and velocities and linear accelerations at the center of gravity (c.g.) of the head were computed. In addition, a six-axis load cell (Denton, Inc., Rochester Hills, MI) attached to the occiput recorded the lateral bending moment induced to the PMHS. These data were used to determine the axial force and lateral bending moment at the head-neck junction (force and moment at the occipital condyles (OC)).

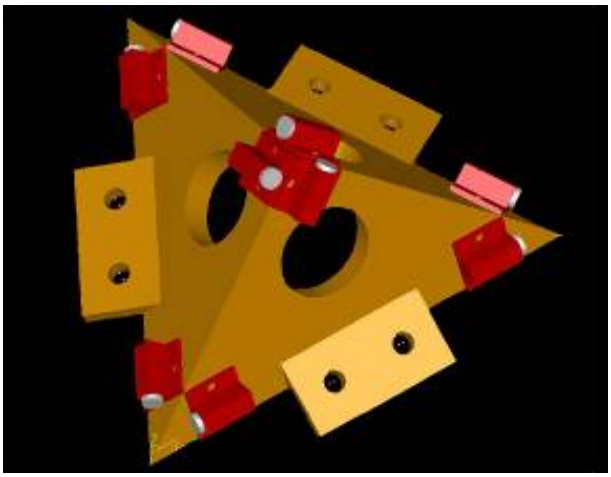

Figure 2. Pyramid-Shaped, Nine-Accelerometer Package

3.4 PHYSICAL PROPERTIES.

Following the testing sequence and imaging, the inertial properties of the head were determined. An incision was made on the posterior aspect of the skull along the superior nuchal line. This was continued anteriorly through the OC joint to the mandible, following the ramus bilaterally to the angle, and laterally through the soft tissues along a line connecting both mandibular angles. The head c.g. was determined by attaching a mass equivalent to one-half the mass of the load cell and suspending the PMHS in two orientations. Reasons for defining the mass of the head in this manner are provided in section 5. The three-dimensional locations of the head c.g. and OC were obtained using a FaroArm coordinate measuring device (Faro® Technologies, Inc., Lake Mary, FL). The c.g. to the OC vector was quantified. To determine the moments of inertia, the PMHS was oriented on the triangular plate of a torsion pendulum in six different positions along the three anatomic axes and midline between the anatomical planes. From these measurements the full moment of inertia tensor was calculated. The external marks of the c.g. and Frankfort plane were made on the head. Laser line levels were used to align the head in the appropriate orientation on the triangular plate, and the head was supported using a ring and low-mass pellets. Moments of inertia were determined using the mean period of 25 oscillations, three wire lengths, radii, head mass, and tare moment of inertia of the pendulum.

3.5 COORDINATE SYSTEM.

The right-handed Cartesian coordinate system of reference was used in this study. The origin of the head was at the c.g. with the x-axis parallel along the midline and parallel to the Frankfort plane, which included the left and right porions and left and right infraorbital notches. The y-axis was parallel to the Frankfort plane from left to right porion. The z-axis was perpendicular to the Frankfort plane along the superior to inferior direction (figure 3).

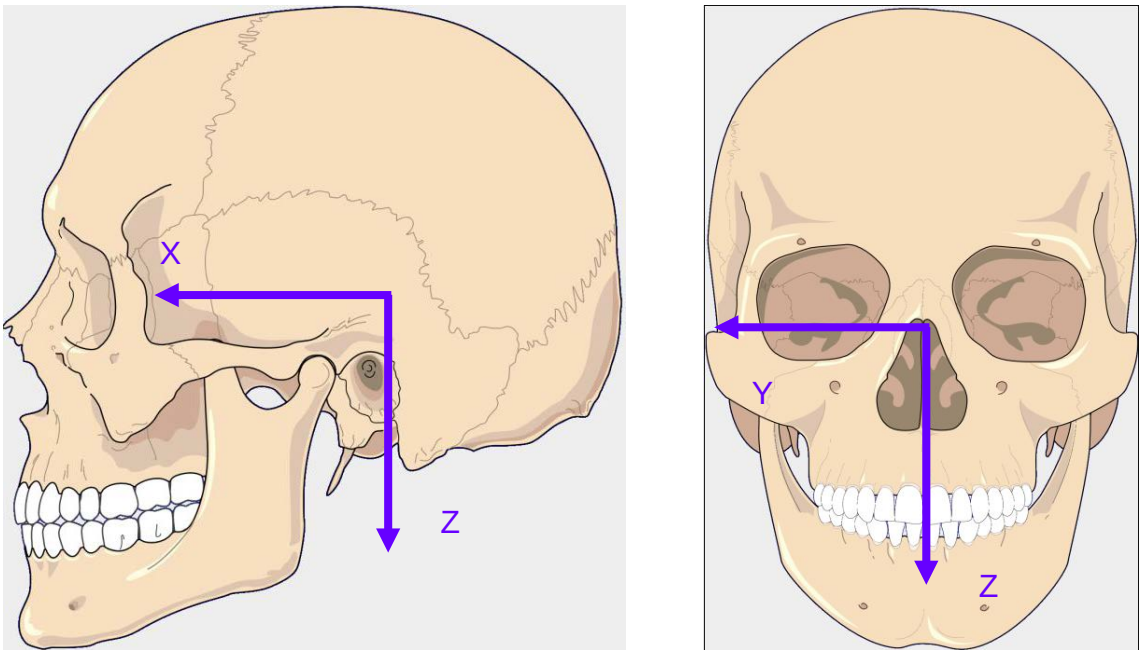


Figure 3. Right-Handed Cartesian Coordinate System (origin is at c.g.)

The polarity of the forces and moments are those defined in SAE 1994. At the upper neck, positive axial z force indicates neck tension; positive AP shear represents pushing the head in the -x direction while pushing the neck in the +x direction; positive lateral shear corresponds to pushing the head in the -y direction while pushing the neck in the +y direction. According to the convention, forward flexion, right-to-left lateral bending, and right-to-left axial twisting moments are positive.

3.6 BIOMECHANICAL DATA.

PMHS accelerometer signals, applied moment, and LVDT displacement data were gathered using a digital data acquisition system. Head c.g., angular and linear accelerations, angular velocity, axial and shear forces, lateral bending moments at the OC, and the applied integrated lateral moment were obtained using the dynamic equations of equilibrium and the applied lateral bending moment. The data were recorded at 20,000 samples per second and filtered using an SAE International Channel Frequency Class 60 digital filter (SAE International, 2007). The PMHS and test-specific results are presented in section 4.

## 4. THE PMHS TEST RESULTS.

### 4.1 THE PMHS DATA.

The age, stature, and total body mass of the two male subjects were 52 and 53 years, 1.83 and 1.86 m, and 72 and 82 kg, respectively. The first PMHS (PMHS 1) underwent nine tests (Series 1) with the PMHS intact, followed by three tests (Series 2) using the isolated head-neck complex. The second PMHS (PMHS 2) underwent 12 tests using only the isolated head-neck complex. This resulted in a total of 24 experiments. The physical properties of the head, such as mass and moments of inertia, are given in table 1.

Table 1. Physical Properties of the Head

| Parameter | Details | Units | PMHS | |
|---|---|---|---|---|
| | | | 1 | 2 |
| Head mass | - | kg | 5.54 | 5.60 |
| OC to CG vector | x-axis | mm | 0.0160 | 0.0181 |
| | z-axis | mm | 0.0476 | 0.0509 |
| Moment of inertia | $I_{xx}$ | kg-m s$^2$ | 0.0237 | 0.0216 |
| | $I_{xy}$ | kg-m s$^2$ | -0.0029 | -0.003 |
| | $I_{xz}$ | kg-m s$^2$ | -0.0038 | 0.0005 |
| | $I_{yy}$ | kg-m s$^2$ | 0.0426 | 0.0438 |
| | $I_{yz}$ | kg-m s$^2$ | 0.0055 | 0.0056 |
| | $I_{zz}$ | kg-m s$^2$ | 0.0376 | 0.0386 |

### 4.2 THE PMHS 1 TEST, SERIES 1.

Series 1 consisted of nine tests conducted on the intact PMHS 1. Table 2 includes a summary of the head angular velocity, integrated bending moment, head angulation data, and piston velocity for each test. The integrated bending moment was calculated using the applied lateral bending moment with respect to time. The period of integration occurred during the time the bending moment value exceeded a threshold of 1% of the peak bending moment during the interval of interest. Representative plots of integrated bending moment and the resulting head angular velocity are shown in figures 4 and 5. Data from a six-axis load cell were used to obtain applied lateral bending moments, axial twist, and flexion and extension moments; axial forces; and lateral and AP shear forces. Table 3 shows the values at the peak lateral bending moment, which ranged from 35.86 to 138.62 Nm.

Table 2. The PMHS 1, Series 1 Head Angular Velocity, Integrated Moment, and Head Angle Data

| Identification Number | Head Angular Velocity (x) (rad/s) | Integrated Moment (Nm-s) | Head Angle (degrees) | Piston Velocity (m/s) |
|---|---|---|---|---|
| FNMC124 | 12.96 | 0.46 | 37.09 | 2.20 |
| FNMC125 | 12.96 | 0.37 | 35.96 | 3.20 |
| FNMC126 | 15.10 | 0.44 | 35.52 | 4.30 |
| FNMC127 | 15.31 | 0.41 | 32.67 | 5.20 |
| FNMC128 | 16.20 | 0.42 | 35.22 | 5.20 |
| FNMC129 | 21.90 | 0.65 | 40.50 | 6.10 |
| FNMC130 | 31.90 | 1.11 | 48.05 | 6.40 |
| FNMC131 | 28.25 | 0.92 | 48.43 | 6.90 |
| FNMC132 | 34.84 | 1.41 | 52.80 | 6.60 |

Table 3. The PMHS 1, Series 1 Summary of Applied Loads

| Identification Number | Force (N) | | | Moment (Nm) | | |
|---|---|---|---|---|---|---|
| | $F_x$ | $F_y$ | $F_z$ | $M_x$ | $M_y$ | $M_z$ |
| FNMC124 | 13.08 | 60.81 | -17.61 | 35.86 | 1.09 | 7.50 |
| FNMC125 | 24.95 | 39.75 | -51.00 | 41.48 | -3.26 | 7.29 |
| FNMC126 | 66.09 | 50.56 | -13.35 | 49.43 | -1.47 | 7.66 |
| FNMC127 | -108.80 | 78.78 | 8.35 | 53.16 | 10.27 | 9.74 |
| FNMC128 | -173.82 | 76.60 | 63.43 | 57.13 | 6.19 | 9.76 |
| FNMC129 | -152.48 | 149.53 | 60.84 | 66.51 | 3.49 | 5.51 |
| FNMC130 | 125.31 | 162.56 | 0.56 | 81.04 | -17.28 | 13.58 |
| FNMC131 | -169.76 | 88.55 | 51.02 | 72.31 | 9.13 | 18.16 |
| FNMC132 | -79.20 | 195.22 | 10.57 | 138.62 | 0.47 | 7.91 |

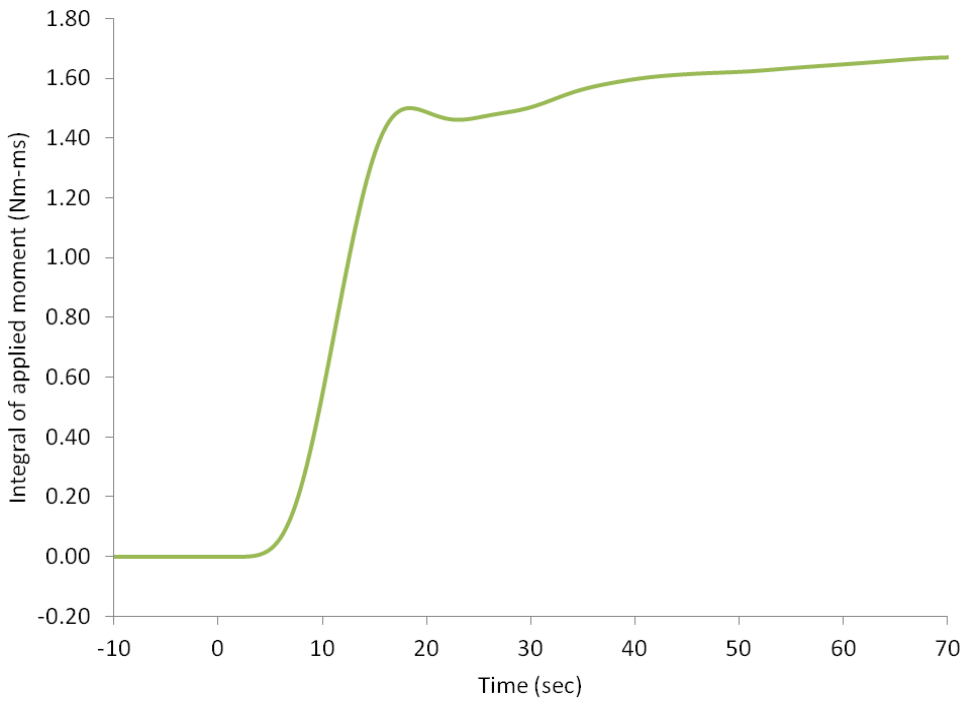


Figure 4. The PMHS 1, Series 1 Representative Integrated Moment Data

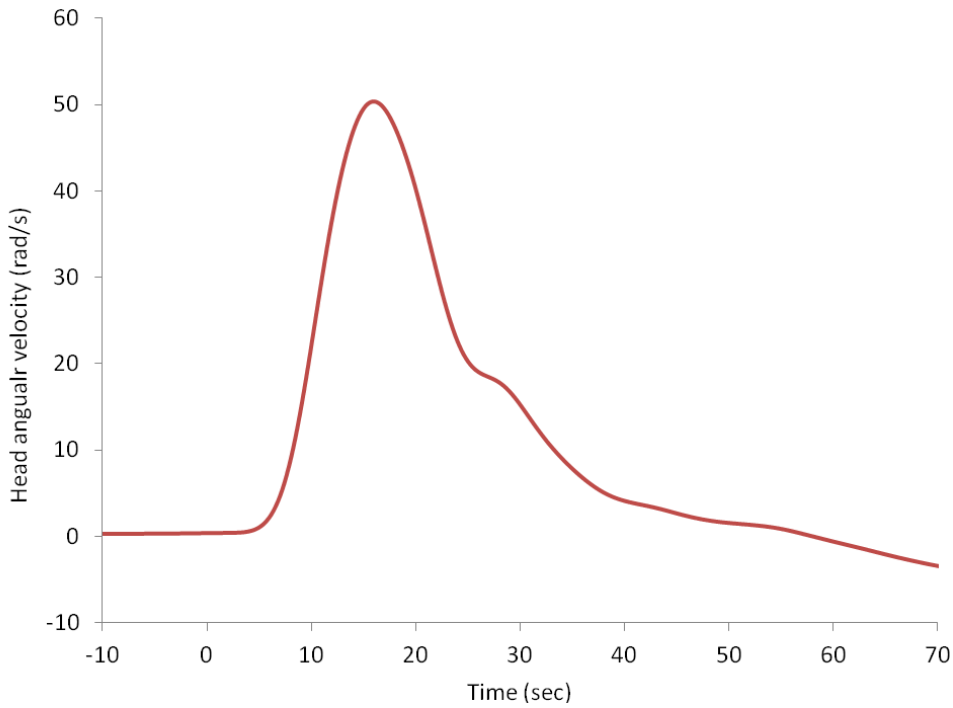


Figure 5. The PMHS 1, Series 1 Head Angular Velocity Corresponding to Representative Integrated Moment Data

Figure 6 shows representative applied moments, and figure 7 shows the corresponding force time histories recorded from the load cell attached to the occiput. The lateral flexion ($M_x$), flexion and extension ($M_y$), and axial twist ($M_z$) moments are shown in figure 6. Forces along the x (AP shear, $F_x$), y (lateral shear, $F_y$), and z (axial, $F_z$) directions are shown in figure 7. The dotted lines indicate the time of peak lateral-flexion moment.

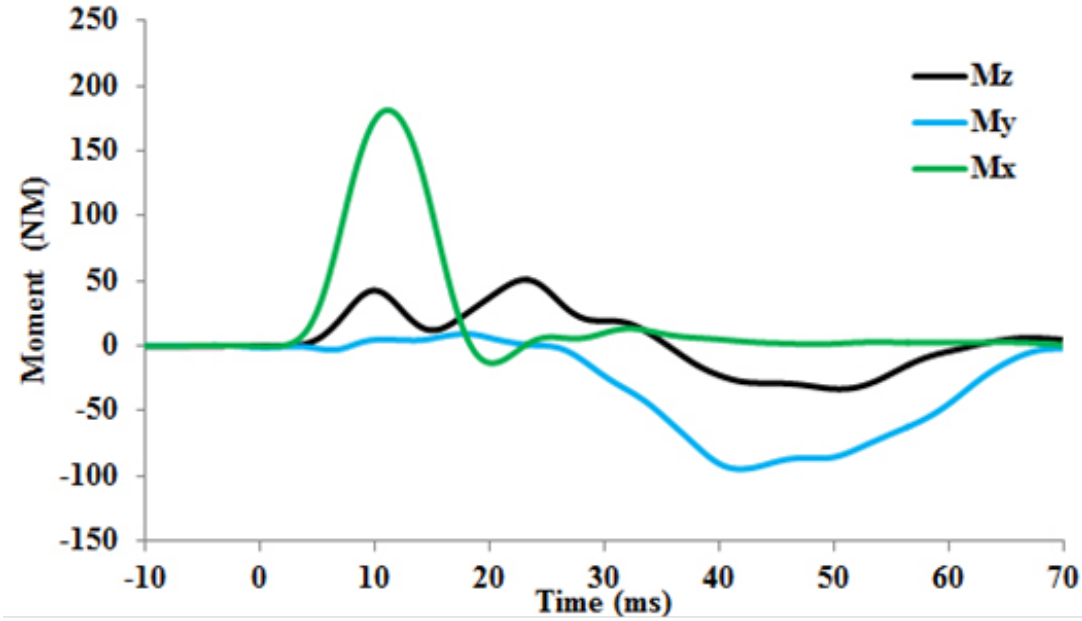


Figure 6. Representative Applied Moments

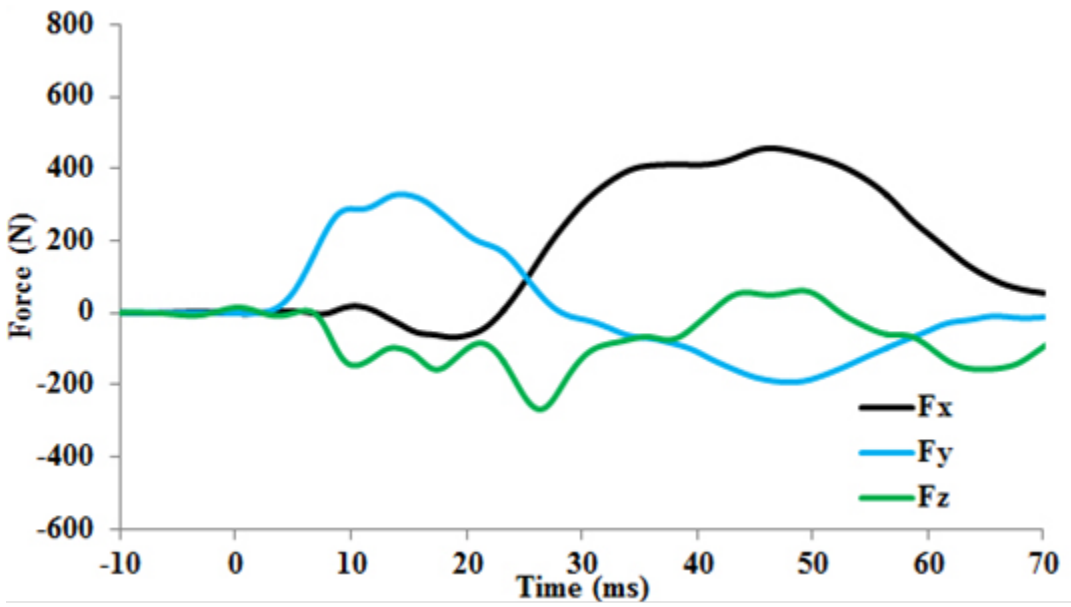


Figure 7. Representative Applied Forces

Figure 8 shows representative time histories of moments, and figure 9 shows forces at the OC for the same data set shown in figures 4 through 7. To determine peak forces and moments at the

OC, initial loads stemming from inertial effects were not considered, and a dotted line is drawn in figures 8 and 9 to indicate the time at which these loads were obtained. Reasons for omitting the inertial spikes are described in section 5.4. The derived values at the OC at the time of the peak lateral bending moment are shown in table 4. They include peak lateral bending moments, axial twist, and flexion and extension moments; axial forces; and lateral and AP shear forces. Peak lateral bending moments ranged from 12.46 to 36.38 Nm.

Table 4. The PMHS 1, Series 1 Summary of Loads at the OC

| Identification Number | Force (N) | | | Moment (Nm) | | |
|---|---|---|---|---|---|---|
| | $F_x$ | $F_y$ | $F_z$ | $M_x$ | $M_y$ | $M_z$ |
| FNMC124 | -18.64 | 69.60 | -132.16 | -14.95 | 0.93 | 8.55 |
| FNMC125 | -14.52 | 60.15 | -111.35 | -12.76 | 0.72 | 8.08 |
| FNMC126 | -21.06 | 60.33 | -127.60 | -15.42 | 0.58 | 8.78 |
| FNMC127 | -4.69 | 58.55 | -109.93 | -12.46 | 0.88 | 6.88 |
| FNMC128 | -5.35 | 63.91 | -107.48 | -12.56 | 0.94 | 6.72 |
| FNMC129 | -35.45 | 68.48 | -127.46 | -18.02 | 0.60 | 11.52 |
| FNMC130 | -88.00 | 70.58 | -64.81 | -26.36 | -18.27 | -9.07 |
| FNMC131 | -23.35 | 76.73 | -146.44 | -20.87 | -0.68 | 11.29 |
| FNMC132 | -16.37 | 182.43 | -139.97 | -36.38 | -14.06 | 3.69 |
| FNMC124 | -18.64 | 69.60 | -132.16 | -14.95 | 0.93 | 8.55 |

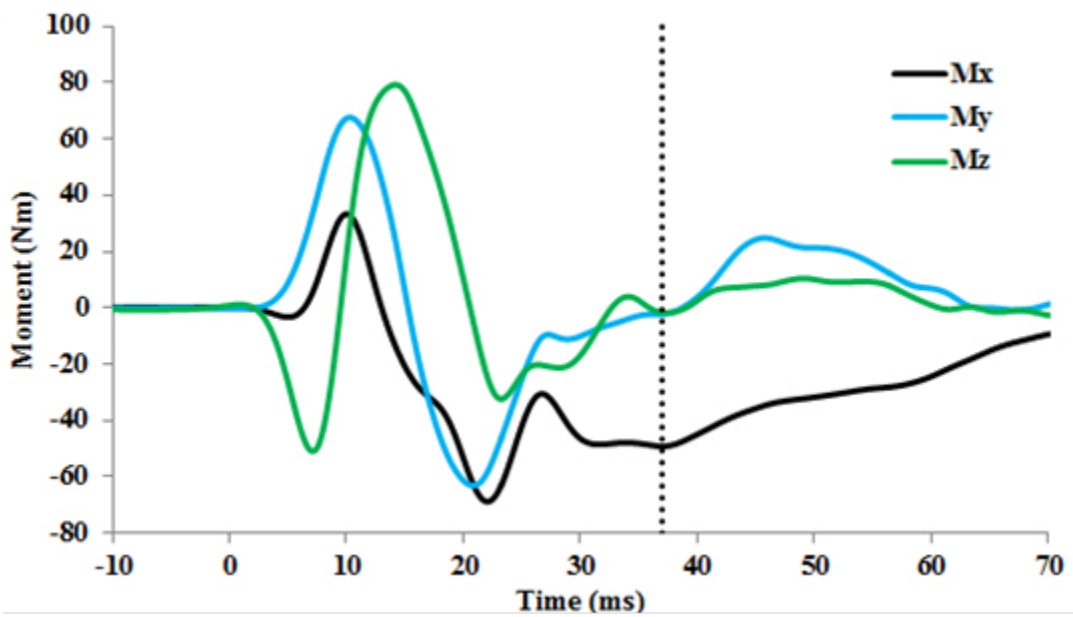


Figure 8. Representative Moments at the OC (The dotted line corresponds to peak data without inertial effects.)

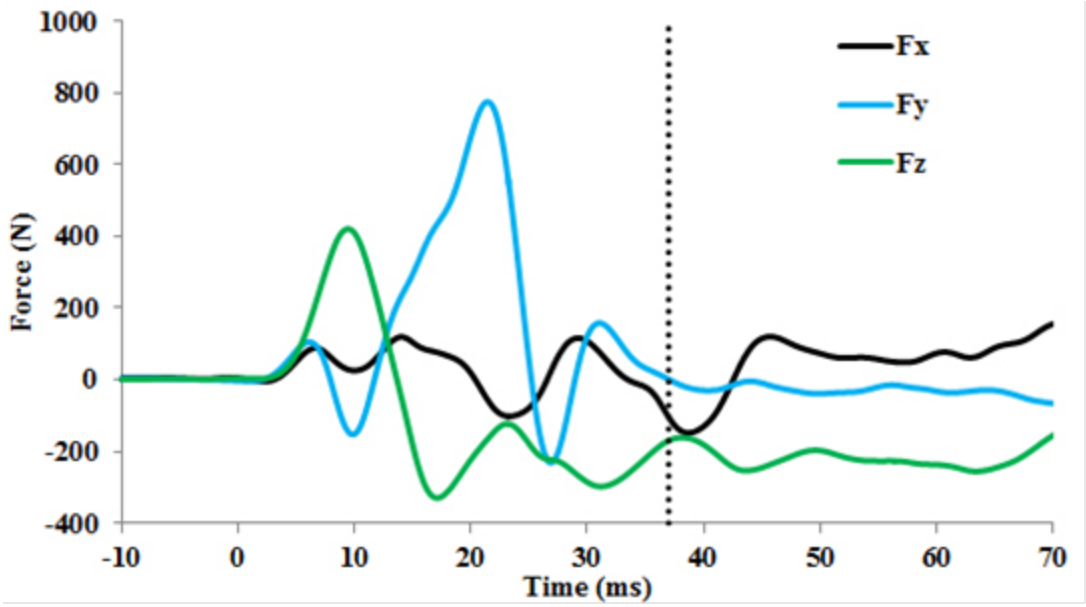


Figure 9. Representative Forces at the OC (The dotted line corresponds to peak data without inertial effects.)

The PMHS 1, Series 1 tests did not result in moments at OCs greater than 36.4 Nm. Because oscillations were found to occur at higher velocities, testing was discontinued, the PMHS was palpated, and x-rays were obtained. The PMHS was prepared for isolated head-neck complex tests and pretest CT scans were performed. No injuries were detected in these images; in addition, no clinical signs of abnormality were identified during PMHS 1, Series 1 tests.

4.3 THE PMHS 1 TEST, SERIES 2.

Series 2 consisted of three tests performed on the isolated head-neck complex of PMHS 1. Figures 4 through 9 (section 4.2) are also representative of results obtained in PMHS 1 Test, Series 2. Table 5 includes a summary of the head angular velocity, integrated bending moment, head angulation, and piston velocity on a test-by-test basis. Peak applied lateral bending moments ranged from 32.86 to 181.47 Nm. Axial twist and flexion and extension moments; axial forces; and lateral and AP shear forces at the time of the application of the peak lateral bending moment are shown in table 6.

Table 5. The PMHS 1, Series 2 Head Angular Velocity, Integrated Moment, and Head Angle Data

| Identification Number | Head Angular Velocity (x) (rad/s) | Integrated Moment (Nm-s) | Head Angle (degrees) | Piston Velocity (m/s) |
|---|---|---|---|---|
| FNMC133 | 12.0 | 0.40 | 36.48 | 2.20 |
| FNMC134 | 14.8 | 0.54 | 30.60 | 2.30 |
| FNMC135 | 50.3 | 1.50 | 51.30 | 6.00 |

Table 6. The PMHS 1, Series 2 Summary of Applied Loads

| Identification Number | Force (N) | | | Moment (Nm) | | |
|---|---|---|---|---|---|---|
| | $F_x$ | $F_y$ | $F_z$ | $M_x$ | $M_y$ | $M_z$ |
| FNMC133 | -72.66 | 67.91 | -3.89 | 32.86 | 4.55 | 11.12 |
| FNMC134 | -71.62 | 82.02 | 5.93 | 45.28 | 4.00 | 15.82 |
| FNMC135 | -105.03 | 204.91 | -9.08 | 181.47 | 3.42 | 39.06 |

Derived peak lateral bending moments, axial and flexion and extension moments; axial forces; and lateral and AP shear forces at the time of the peak lateral bending moment are given in table 7. Peak lateral bending moments ranged from 13.33 to 48.54 Nm.

Table 7. The PMHS 1, Series 2 Summary of Loads at the OC

| Identification Number | Force (N) | | | Moment (Nm) | | |
|---|---|---|---|---|---|---|
| | $F_x$ | $F_y$ | $F_z$ | $M_x$ | $M_y$ | $M_z$ |
| FNMC133 | 34.89 | 10.79 | -131.81 | -13.33 | 3.60 | 3.10 |
| FNMC134 | 48.48 | 18.04 | -200.09 | -20.27 | 5.29 | 4.60 |
| FNMC135 | 54.91 | 150.14 | -296.27 | -48.54 | -7.26 | -6.69 |

After the third test, clinical examinations raised uncertainty for potential injury, and, therefore, further tests were discontinued. However, posttest radiographs and CT images did not reveal fractures or dislocations to cervical spine vertebrae or to the OC junction. An AIS 0 was assigned for each of the three tests. In addition, no clinical signs of instability were found after the second test series. Figures 10 and 11 show the pretest and posttest images of the head-neck complex of PMHS 1 after test Series 1 and 2, respectively.

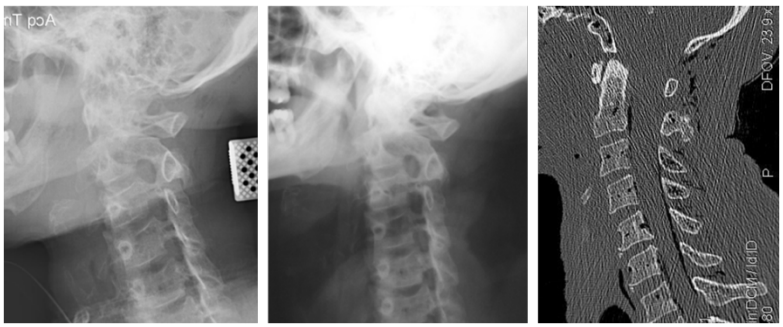

(a) (b) (c)

Figure 10. The PMHS 1, Series 1 (a) Preseries X-Rays, (b) Postseries X-Rays, and (c) Postseries CT Scan

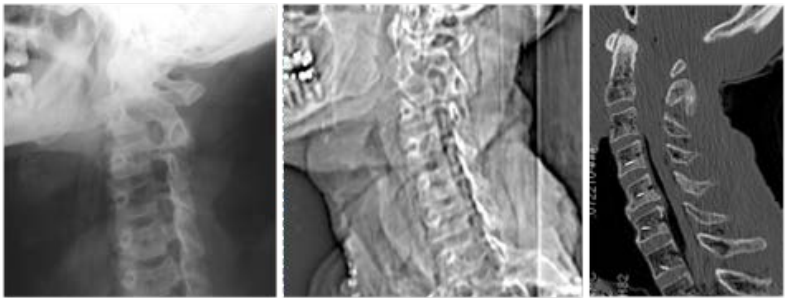

(a) (b) (c)

Figure 11. The PMHS 1, Series 2 (a) Preseries X-Rays, (b) Postseries, and (c) Postseries CT Scan

4.4 THE PMHS 2 TEST SERIES.

The PMHS 2 test series consisted of 12 tests using the isolated head-neck complex from PMHS 2. Table 8 includes a summary of the head angular velocity, integrated bending moment, head angulation, and piston velocity data. Peak applied lateral bending moments, axial twist and flexion and extension moments; axial forces; and lateral and AP shear forces at the time of the peak lateral bending moment are given in table 9. Peak applied lateral bending moments ranged from 14.02 to 182.98 Nm.

Table 8. The PMHS 2, Head Angular Velocity, Integrated Moment, and Head Angle Data

| Identification Number | Head Angular Velocity (x) (rad/s) | Integrated Moment (Nm-s) | Head Angle (degrees) | Piston Velocity (m/s) |
|---|---|---|---|---|
| FNMC137 | 5.30 | 0.23 | 22.17 | 2.20 |
| FNMC138 | 7.20 | 0.30 | 29.00 | 2.10 |
| FNMC139 | 7.40 | 0.25 | 26.84 | 2.90 |
| FNMC140 | 13.40 | 0.37 | 33.16 | 4.20 |
| FNMC141 | 36.75 | 1.26 | 48.84 | 4.60 |
| FNMC142 | 33.00 | 0.93 | 45.32 | 4.90 |
| FNMC143 | 39.77 | 1.18 | 43.02 | 5.80 |
| FNMC144 | 42.80 | 1.22 | 49.80 | 5.70 |
| FNMC145 | 39.59 | 1.17 | 45.08 | 6.00 |
| FNMC146 | 51.51 | 1.51 | 50.50 | 6.10 |
| FNMC147 | 43.50 | 1.42 | 46.19 | 6.50 |
| FNMC148 | 38.13 | 1.72 | 47.91 | 6.60 |

Table 9. The PMHS 2, Summary of Applied Forces and Moments

| Identification Number | Force (N) | | | Moment (Nm) | | |
|---|---|---|---|---|---|---|
| | $F_x$ | $F_y$ | $F_z$ | $M_x$ | $M_y$ | $M_z$ |
| FNMC137 | -2.39 | 33.21 | -3.94 | 14.02 | 1.90 | 2.99 |
| FNMC138 | -17.06 | 47.31 | 9.19 | 15.01 | 2.55 | 7.16 |
| FNMC139 | -20.81 | 40.45 | -24.76 | 17.76 | 4.36 | 3.40 |
| FNMC140 | -14.33 | 113.37 | -16.51 | 47.78 | -1.72 | 10.21 |
| FNMC141 | -196.53 | 215.45 | -40.15 | 143.37 | 1.85 | 39.34 |
| FNMC142 | 62.41 | 223.19 | -7.13 | 116.53 | -14.48 | 27.14 |
| FNMC143 | 22.86 | 236.22 | 29.27 | 159.36 | -17.54 | 46.09 |
| FNMC144 | 218.05 | 289.36 | -80.13 | 162.57 | -17.73 | 69.77 |
| FNMC145 | -32.76 | 271.52 | 189.36 | 156.12 | 13.14 | 50.27 |
| FNMC146 | 61.77 | 406.00 | -52.35 | 184.22 | 9.86 | 60.48 |
| FNMC147 | 71.99 | 668.04 | -211.85 | 165.37 | 13.45 | 79.75 |
| FNMC148 | -198.24 | 670.51 | -91.57 | 182.98 | 24.89 | 61.39 |

At the OC, derived peak lateral bending moments, flexion and extension moments; axial forces; and lateral and AP shear forces at the time of peak lateral bending moment are shown in table 10. Peak lateral bending moments ranged from 4.34 to 73.60 Nm.

Table 10. The PMHS 2, Summary of Forces and Moments at the OC

| Identification Number | Force (N) | | | Moment (Nm) | | |
|---|---|---|---|---|---|---|
| | $F_x$ | $F_y$ | $F_z$ | $M_x$ | $M_y$ | $M_z$ |
| FNMC137 | 7.13 | 48.69 | 3.45 | -4.34 | -1.78 | -0.36 |
| FNMC138 | -10.46 | 52.76 | -51.18 | -5.38 | 1.07 | 4.64 |
| FNMC139 | -17.32 | 47.32 | -29.14 | -3.70 | 0.77 | 3.63 |
| FNMC140 | -37.87 | 85.55 | -111.47 | -9.84 | 1.70 | 9.38 |
| FNMC141 | -66.70 | 44.43 | -55.59 | -31.18 | -9.87 | -9.80 |
| FNMC142 | -29.45 | 159.11 | -87.98 | -21.27 | -3.44 | 8.31 |
| FNMC143 | -196.68 | 0.32 | -93.62 | -18.78 | -10.53 | 8.45 |
| FNMC144 | 57.63 | -73.37 | -134.78 | -28.76 | 3.92 | 15.02 |
| FNMC145 | -202.53 | 325.85 | -49.35 | -38.08 | -29.66 | -20.38 |
| FNMC146 | 145.15 | -174.08 | -297.83 | -47.37 | 4.00 | 30.78 |
| FNMC147 | 53.43 | -213.18 | -401.46 | -48.12 | -11.04 | 12.27 |
| FNMC148 | -210.87 | -359.31 | -166.18 | -73.60 | -42.48 | -2.27 |

Posttest radiography raised uncertainty for instability at the atlas axis level (figure 12). No fractures of any vertebra were identified in these x-rays, CT scans, or during the autopsy. Palpations of the PMHS between successive loadings did not reveal any spinal instability. Posttest CT scans were also negative for any abnormality. Thus, the PMHS was deemed to have no injury.

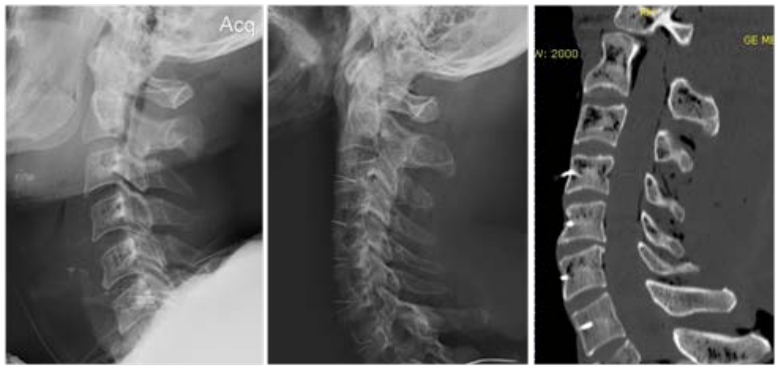


(a) (b) (c)

Figure 12. The PMHS 2 (a) Preseries X-Rays, (b) Postseries X-Rays, and (c) Postseries CT Scan

## 5. DISCUSSION—THE PMHS TESTS.

### 5.1 OVERALL GOALS.

The goals of the first phase of the project were to develop a methodology to rotate the PMHS in the sagittal plane using a fixture attached to the electrohydraulic testing device and develop an IRV. The load cell connected to the back of the specimen head was used to obtain the force and moments at the OC using the dynamic equations of equilibrium. This novel methodology was specifically designed for this project. A brief analysis of the literature expanding on the need to accurately determine the occipital loads is discussed in this section.

### 5.2 RATIONALE FOR THE PRESENT MODEL.

Side-impact sled tests were conducted using an intact PMHS to determine injuries and biomechanical metrics such as forces and moments at the OC. A recent study analyzed tests conducted in Germany in the 1980s to estimate neck loads (Kallieris et al., 1981; McIntosh et al., 2007). Out of the 63 sled tests, only 15 were deemed suitable for analysis. Although peak forces and moments at the OC were calculated based on experimental records and various assumptions, the author of the report underscored its preliminary nature and urged caution in the interpretation of their findings. Thus, these data cannot be relied on to provide IRVs in the lateral mode. In addition, the study implied the need to follow specific protocols for recording accurate data and deriving loads at the OC.

Therefore, this study included all critical components in the experimental design to obtain neck loads using PMHS tests—i.e., the use of sophisticated instrumentation devices, data acquisition and analyses techniques, optical tracking of kinematics at high speeds, computational validations of inverse dynamics, specimen-specific properties such as c.g. locations, OCs, and moments of inertia (Pintar et al., 2005; Pintar et al., 2010; Yoganandan et al., 2009a; Yoganandan et al., 2009c; Yoganandan et al., 2008a; and Yoganandan et al., 2006). Cited studies provide details on experimental (piston-based, electro- and hydraulic-system and sled-induced loadings) and computational methodologies to obtain accurate neck loads using a PMHS.

### 5.3 IMPORTANCE OF SPECIMEN-SPECIFIC PROPERTIES.

Specimen-specific properties had been used in previous FAA-sponsored studies (Yoganandan et al., 2009b; and Yoganandan et al., 2008a). This included the determination of the three-dimensional c.g. and moments of inertia along the three anatomical axes. However, to derive accurate OC loads, cross terms in the moment of inertia matrix (i.e., products of inertia) were used in the computations. To the authors' knowledge, this methodology had not been used in any previous PMHS studies. Inertial effects were assumed to be fully in force as soon as the specimen was subjected to the initiation of the applied coronal bending moment. Consequently, the moment of inertia and mass terms were independent of the time duration of the applied loads.

### 5.4 IMPORTANCE OF HEAD KINEMATICS.

From a practical perspective, a longer time is required to accelerate the head because the head has a larger mass than the neck, and the system has to drive the head, which is at rest before the

application of the external coronal bending moment. By assuming the full mass and moment of inertia properties to be active with the instantaneous application of the coronal moment, a spike or artifact results in the OC load distribution. This manifests as an initial, inertia-driven peak in the response (figures 6 and 9). This type of artifact was also found in other studies (Pintar, et al., 2005). It is attributed to the nonrigid nature of the PMHS response during the early stages of high-speed loading. The cited study confirmed this unique behavior by conducting tests using ATDs, including the Hybrid III, and the Test Device for Human Occupant Restraint. As this study was designed to determine the neck response, it was deemed necessary to determine injury-related biomechanical metrics only when the head mass was fully in force. The initial period representing the spurious response was determined as the time prior to the application of the peak lateral bending moment to the specimen that represented the accelerating phase of the initially rested head-neck complex when the full moment of inertia is not in force. In other words, the head-neck complex initiated its acceleration from a static state as soon as the external load cell began to induce and record the applied moment from the electrohydraulic piston. Furthermore, after reaching the peak bending moment, the specimen continued to laterally bend. This phase in the response is associated with a decrease in the external moment recorded by the load cell (figure 6). The head-neck system stabilizes to a near-zero value following the return of the lateral bending moment and, at this time, the specimen bends laterally with full inertial effects, and the determined physical properties are applicable in this domain. This process leads to the identification of peak loads beyond the artifact. Thus, it was appropriate to extract the peak left lateral bending moment and associated forces and the other two moments at that time. As shown in tables 4, 6, and 8, peak axial and flexion and extension moments were smaller than the lateral bending moment. The off-axes loads were expected due to the complexity of the human head-neck complex. Although not shown as combined plots for all tests, the above methodology was followed in this study. Appendix A shows generalized time histories of loads at the OC (i.e., axial and shear forces and lateral bending moments) on a test-by-test basis. Test numbers shown in each plot correspond to the identification numbers in respective tables in this report.

## 5.5 ROLE OF COUPLED MOTIONS IN THE HUMAN NECK.

Because the experimental model did not use conventional pure moment-type loading, forces were introduced in addition to the lateral bending moment, as described in Section 5.4. Unlike flexion and extension, the application of lateral bending or axial twisting moments result in coupled moments (Clark, 1998). The magnitude of coupling depends on the type and severity of the applied moment (Yoganandan et al., 1998). Although quasi-static studies have quantified coupling factors, similar data were not available in the literature about dynamic loads (Yoganandan et al., 2007b; Yoganandan et al., 2008b). From this perspective, this study provides dynamic coupling data for an intact PMHS head-neck complex.

## 5.6 LIMITATIONS.

Despite the limited sample size, the experimental protocol included multiple tests on the same specimen, a methodology adopted in other PMHS tests (Pintar et al., 2005 and Stemper et al., 2003). This method was used to optimize tests from the same specimen. It is also known that repeated loading alters the biomechanical response and has the potential to decrease human tolerance. Such tests may increase laxity of the joints in the osteoligamentous column and affect

local kinematics. From this perspective, the loads applied during this test might be considered to be conservative estimates. Another potential issue is the effect of a secondary load path from the in vivo musculature. Active musculature cannot be accommodated in all PMHS studies. Researchers have used PMHS data as a first step in computational models to delineate the role of muscles in modulating the spinal response on a parametric basis. It should be noted that, to the authors' knowledge, the precise roles of muscle activation are not known in the lateral mode. However, the data obtained during this study may be considered as lower bounds and serve as a valuable set to delineate effects of musculature. This approach was used in the design of test dummy necks and frontal impact motor vehicle safety standards in the United States (Kleinberger et al., 1998 and Shams and Rangarajan, 2005).

## 5.7 THE APPLICATIONS OF PMHS FINDINGS.

While the use of two PMHS is too small to conduct statistical analysis, results from these 24 tests provide fundamental data on lateral loading injury metrics. This data set is critical and needed for side-facing seat certification processes in aviation environments, when one acknowledges the paucity of biomechanical information in this mode, including static and dynamic loading paradigms (Yoganandan et al., 1998). In fact, almost all static loading experiments under lateral bending have been conducted using isolated functional units or segmented columns without including the intact upper-cervical, spine-head complex in any PMHS experimental model (Clark 1998; Nightingale et al., 2002; Yoganandan et al., 2007b, and Yoganandan et al., 2008b). Lateral moments were limited to low levels, often less than 5 Nm. It should also be recognized that sled tests with lateral impacts have largely focused on chest, abdomen, and pelvic injuries; a review is available of PMHS studies indicating the paucity of sled test data regarding head-neck loads and injuries using various PMHS models (Yoganandan et al., 2007a). Very few studies have been done to determine the biomechanics of the human head-neck complexes in the lateral mode (Yoganandan et al., 2009b). In the cited study, like this study, two specimens were tested under different initial conditions. Sled tests with four initial conditions (a fully restrained torso and a torso with three-point seat belt restraints under three velocity changes) identified the need to develop an experimental protocol for inducing high-magnitude, lateral bending moments accompanied by low-level, axial tensile forces to the PMHS head-neck complex to define human tolerance and injury criteria in the lateral impact mode. These sled tests are referred to as the previous tests in the following discussion.

Repeated tests conducted on the same specimen might lead to progressive loosening of the cervical joints and affect (lower) failure thresholds. As no injuries were found, metrics in this study might represent conservative estimates of unique importance to IRV. Fixing the inferior end of the specimen constrained the effects of T1 vertebral motions. Additional tests with intact and isolated head-neck complexes will delineate the influence of the T1 vertebrae on upperneck loads. However, literature data indicate that this may have a secondary influence on neck loads (Stemper et al., 2005). Although active musculature was not included, effects of passive muscles were included in the intact head-neck complex model. Variables, such as age and gender, known to affect cervical spine responses were not included (Pintar et al., 1998 and Stemper et al., 2003). Enhancing the sample size should relax such limitations and provide a more accurate assessment of neck responses.

The results from this study clearly indicate that PMHS head-neck complexes can resist a lateral bending moment of 75 Nm (73.6-Nm data rounded to nearest 5 Nm) accompanied by a low-magnitude axial tensile force (less than 300 N) at the OCs without neck injury (determined during the testing process using palpation, x-rays, CT scans, and autopsy). This high level of lateral moment without an accompanying high axial tensile force was not attained in any of the eight specimens used in the sled tests in previous research, as discussed above. Therefore, the principal objective of this research was achieved: developing a methodology to induce loading such that a high level of coronal moment accompanied by low level of axial tensile force is applied to two PMHS specimens, and determining the axial tensile and lateral bending moment from the developed experimental and computational methodologies.

The practical application of these data was to anticipate the use of active safety systems. Previous sled tests at MCW involved only head inertial forces to strain the neck (Philippens et al., 2011). This always resulted in some high level of axial loading in the neck (above 1.1 kN). Some tests with active safety systems using a shoulder belt-mounted pyrotechnic airbag produced relatively high coronal neck moments with relatively low axial load (DeWeese et al., 2007). Because the neck has the potential to be injured in pure tension and pure bending, and combinations in between, our approach was to cover the spectrum of these loading modes. This study, in other words, was meant to derive the pure lateral bending end of the extreme.

Coronal bending moments ranging from 23 to 41 Nm were suggested to represent AIS 1 and 41 to 60 Nm to represent AIS 2-level neck traumas in the lateral mode (Soltis, 2001). The results from this study exceeded these suggested magnitudes. It should be acknowledged that the suggested IRVs were based on very limited literature data and without any specific experiments targeted to the side-impact mode which, as indicated earlier, were not developed with specific protocols necessary to determine OC loads. The discrepancy is thus attributed to these factors. From this perspective, this study provided reliable data for OC loads in the side-impact modality, which is a critical need for the FAA side-facing seat safety and certification process.

OC moment data derived in this study were accompanied by off-axis loads, a consequence of the nature of the human cervical spinal column and experimental model used to apply lateral bending moments. Therefore, the resulting moments were not fully unimodel. Acknowledging these factors, a peak moment of 75 Nm can be considered an initial conservative estimate below which injury does not occur to the PMHS head-neck complex in the tested side-impact mode.

## 6. THE PMHS-BASED IRVs.

The biomechanical response criteria of the human neck are often expressed as peak force or moment (i.e., loads at the OC). An interaction-based criterion, such as $N_{ij}$, incorporates both force and bending moment parameters. This type of criteria is used for sagittal plane loading with axial force and flexion and extension bending moments as the variables defining the interaction. Regarding the side-impact mode, axial tensile force and coronal or lateral bending moment are appropriate candidates for the interaction-based metric. None of the 24 tests in this study exceeded these levels of peak tensile forces, as indicated earlier, and the maximum coronal bending moment was 73.6 Nm. Data from this study suggest that this magnitude of moment can be used (rounded off to 75 Nm) as a conservative estimate as the IRV associated with high lateral bending moment and low axial tensile force, which meets the objective of this study.

## 7. SUMMARY AND CONCLUSIONS—THE PMHS TESTS.

The objective of this phase of the investigation was to develop a test methodology to induce high lateral bending moment with low axial tensile force at the OC of the human head-neck complex and to determine the lateral bending moment injury threshold under lateral loading. The PMHS whole-body and isolated head-neck complexes with intact musculature were used. Lateral bending moments were applied using an electrohydraulic test device. Specimen-specific physical properties, including c.g. and moments of inertia, as well as equations of equilibrium were used to determine loads at the OC. Early peaks in the signals were associated with the inertial response, and subsequent peaks in the loads represented forces and moments transmitted to the upper neck. Off-axes moments were smaller than lateral bending moments. No specimens sustained injuries based on palpation, x-rays, CT, and autopsy. The peak lateral bending moment of 75 Nm associated with low axial tensile force represents the estimated IRV from this PMHS study. These data provide a baseline to conduct matched-pair tests to obtain ATD-related IARV for aviation applications.

## 8. METHODS—THE ES-2 TESTS.

Matched-pair tests were conducted using the ES-2 to obtain correlative injury metrics for side-impact loading. In principle, the testing methodology was essentially similar to the PMHS with the elimination of the biological part in the experimental processes.

### 8.1 THE ES-2 PREPARATION AND MOUNTING.

The head-neck complex of the ES-2 was exposed to lateral external loading using the same custom fixture and loading device used for the PMHS tests (figure 1). The preparation consisted of fixing the inferior end of the neck of the ES-2 to a rigid metal plate that was secured to the custom fixture (figure 13).

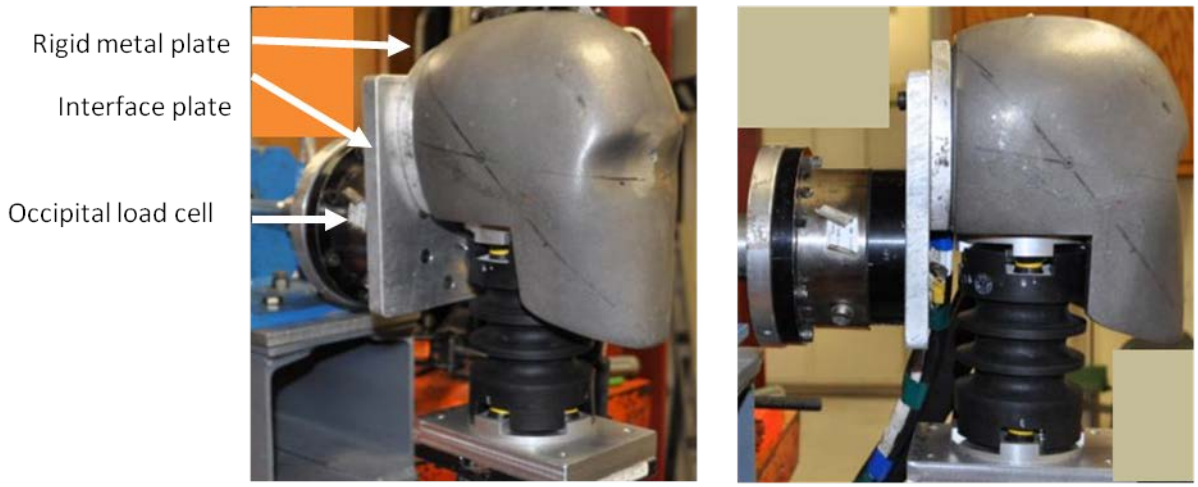


(a) (b)

Figure 13. Photograph Showing the Test Setup for ES-2 Experiments (a) Front Offset View and (b) Side View

## 8.2 LOADING.

Using the same loading system as in the PMHS tests, the prepared ES-2 was loaded incrementally using the displacement control protocol with piston velocities from 1 to 6 m/s. The experimental protocol was such that repeat tests were conducted and intended to apply similar levels of lateral bending moments to the ES-2. Sufficient time was allowed between two consecutive tests to minimize viscoelastic effects.

## 8.3 INSTRUMENTATION.

The six-axis load cell attached to the occiput recorded the applied lateral bending moments. In addition, the upper-neck load cell in the ES-2 was used to gather forces and moments at the head-neck junction (i.e., OC). In some tests, the ES-2 was instrumented with an internal nine-accelerometer package in its head. Three linear accelerometers were secured at the c.g. of the head, and two linear accelerometers were secured to the frontal and right and left lateral regions of head.

## 8.4 COORDINATE SYSTEM.

The right-handed Cartesian coordinate system of reference was used. The origin of the head was at its c.g. with the x-axis parallel to the head Frankfort plane. The y-axis was parallel to the Frankfort plane from left to right ears. The z-axis was perpendicular to the Frankfort plane along the superior to inferior direction (figure 3). The polarity of the reactive forces and moments are defined in SAE J211. At the upper neck, positive z force indicates neck tension (i.e., axial force); positive AP shear represents pushing the head in the -x direction while pushing neck in the +x direction; positive lateral shear corresponds to pushing the head in the -y direction while pushing the neck in the +y direction. According to the convention, forward flexion, right-to-left lateral bending, and right-to-left axial twisting moments are positive.

## 8.5 MECHANICAL DATA.

The applied moment, acceleration, and LVDT displacement data were gathered using a digital data acquisition system. The axial and shear forces and lateral bending moments were obtained from recorded data from the upper neck load cell of the ES-2. As in the case of PMHS tests, a CFC 60 SAE digital filter was used to facilitate comparison of the data.

# 9. RESULTS—THE ES-2 TESTS.

## 9.1 APPLIED MOMENT AND FORCE HISTORIES.

Figure 14 shows representative moments, and figure 15 shows forces recorded from the six-axis load cell attached to the back of the ES-2 head. The lateral bending ($M_x$), flexion and extension ($M_y$), and axial twist ($M_z$) moments are shown in figure 14. The forces along the x (AP shear, $F_x$), y (lateral shear, $F_y$), and z (axial, $F_z$) directions are shown in figure 15.

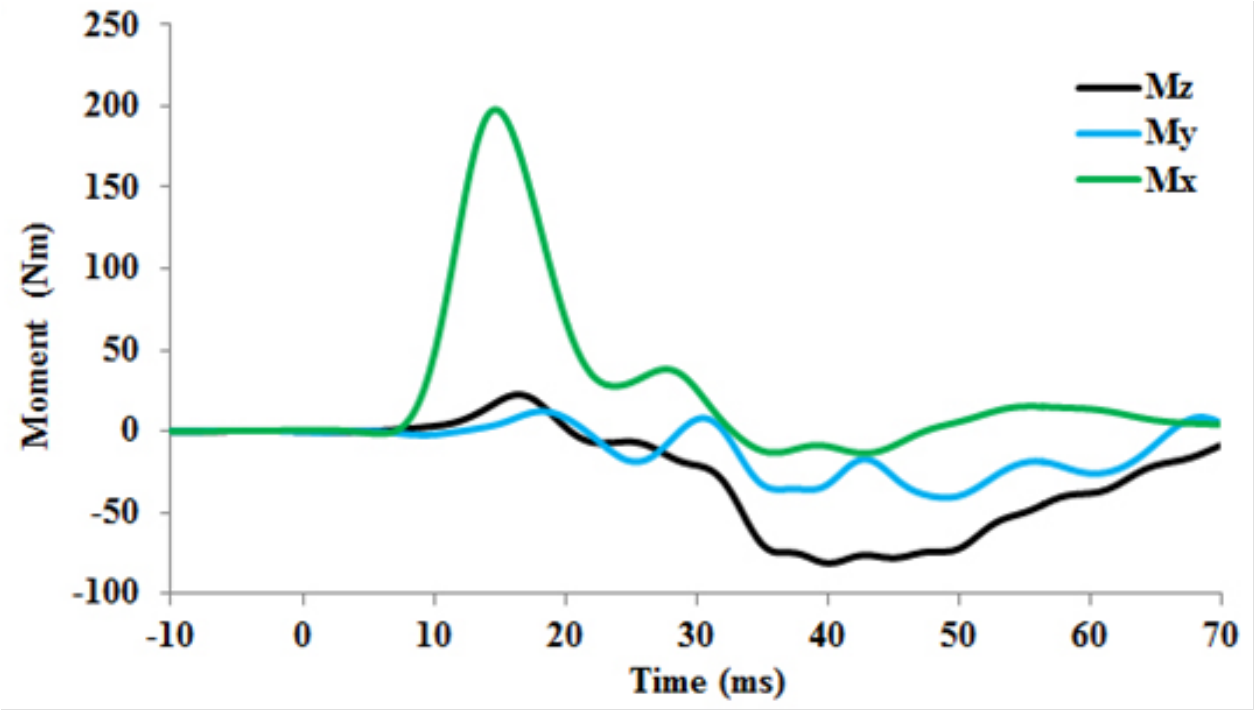


Figure 14. The ES-2 Representative Measured Applied Moments

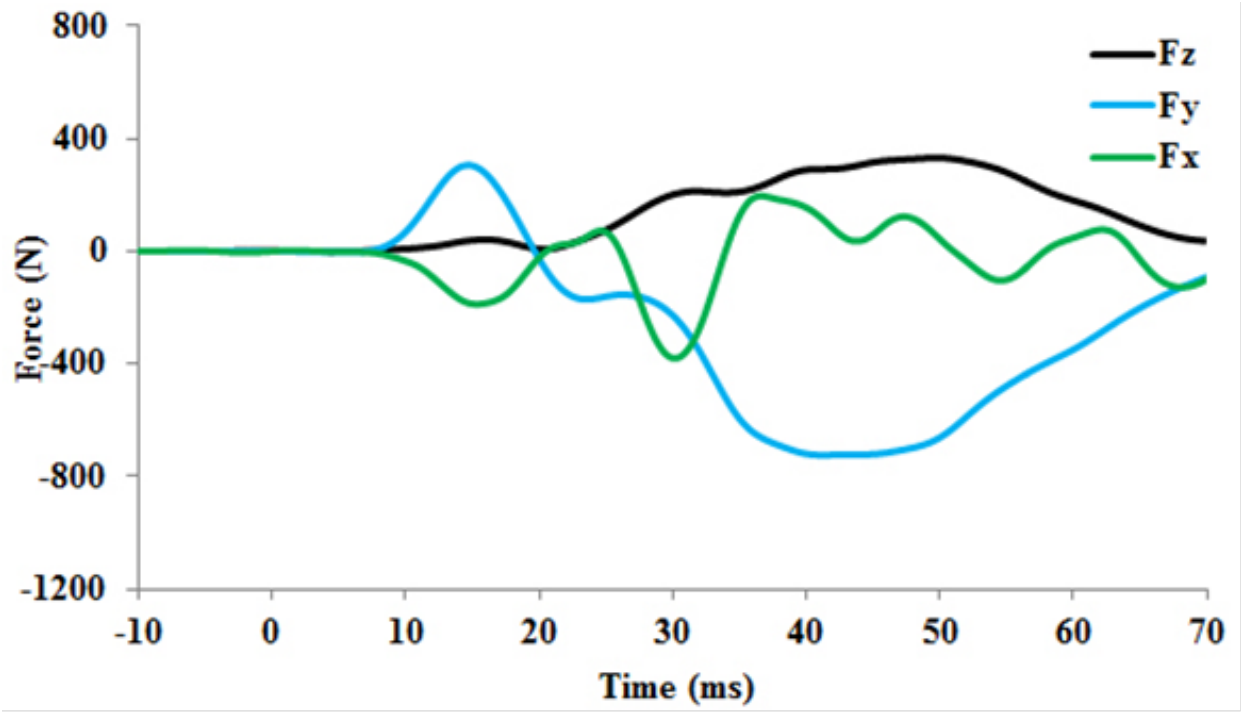


Figure 15. The ES-2 Representative Measured Applied Forces

## 9.2 SUMMARY OF DATA.

Table 11 includes a summary of the head angular velocity, integrated bending moment, and piston velocity data on a test-by-test basis. Peak lateral bending, axial twist, and flexion and extension moments; axial forces; and lateral and AP shear forces at the time of the peak lateral bending moment are included in table 12. Peak applied lateral bending moments ranged from 38.93 to 197.98 Nm.

Table 11. The ES-2 Head Angular Velocity and Integrated Moment Data

| Identification Number | Head Angular Velocity -x (rad/s) | Integrated Moment (Nm-s) | Piston Velocity (m/s) |
|---|---|---|---|
| FNMD209 | 11.50 | 1.77 | 0.98 |
| FNMD210 | 12.35 | 1.62 | 0.98 |
| FNMD211 | 16.50 | 1.40 | 2.10 |
| FNMD212 | 17.94 | 1.31 | 2.00 |
| FNMD213 | 29.07 | 1.17 | 2.90 |
| FNMD214 | 30.99 | 1.19 | 2.90 |
| FNMD215 | 48.04 | 1.58 | 4.30 |
| FNMD216 | 47.22 | 1.48 | 4.20 |
| FNMD217 | 62.30 | 1.84 | 5.40 |
| FNMD218 | 55.82 | 1.60 | 5.30 |

Table 12. The ES-2 Peak Applied Forces and Moments

| Identification Number | Force (N) | | | Moment (Nm) | | |
|---|---|---|---|---|---|---|
| | $F_x$ | $F_y$ | $F_z$ | $M_x$ | $M_y$ | $M_z$ |
| FNMD209 | 17.74 | -185.89 | 84.65 | 38.93 | -4.91 | -20.14 |
| FNMD210 | 11.59 | -152.38 | 75.04 | 39.59 | -2.84 | -17.08 |
| FNMD211 | 9.97 | -77.87 | 57.07 | 51.80 | -0.64 | -8.34 |
| FNMD212 | 5.96 | -80.51 | 57.82 | 47.06 | -0.65 | -9.17 |
| FNMD213 | -72.03 | 123.95 | 7.19 | 77.29 | 3.13 | 7.68 |
| FNMD214 | -70.58 | 129.42 | 8.30 | 80.53 | 2.87 | 8.70 |
| FNMD215 | -117.04 | 223.90 | 21.63 | 145.76 | 5.45 | 15.30 |
| FNMD216 | -102.49 | 223.54 | 25.51 | 140.11 | 4.49 | 14.41 |
| FNMD217 | -184.08 | 306.05 | 37.77 | 197.98 | 3.82 | 17.29 |
| FNMD218 | -161.03 | 278.95 | 37.86 | 180.49 | 2.46 | 14.32 |

Figure 16 shows representative moments, and figure 17 shows forces in the ES-2 as measured by the upper-neck load cell. The lateral flexion ($M_x$), flexion and extension ($M_y$), and axial twist ($M_z$) moments are shown in figure 16. The forces along the x (AP shear, $F_x$), y (lateral shear, $F_y$), and z (axial, $F_z$) directions are shown in figure 17. The dotted line indicates the time the peak lateral flexion moment was attained, and forces and other moments corresponding to this time were extracted from the various curves.

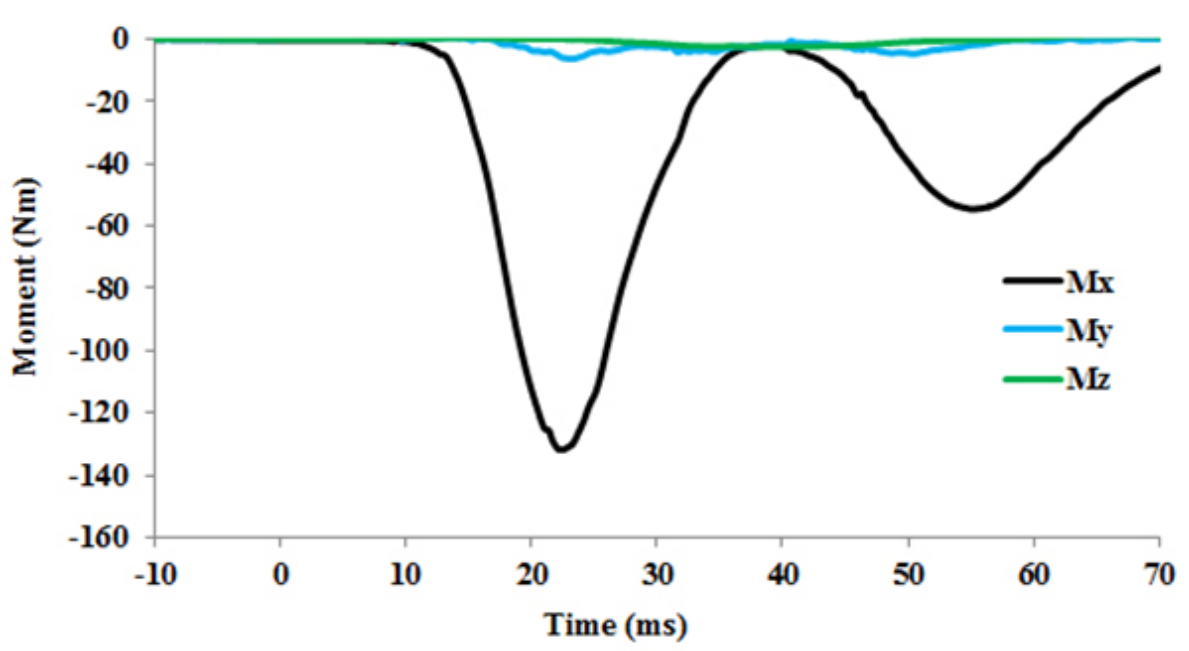


Figure 16. The ES-2 Representative Upper-Neck Load Cell Moments

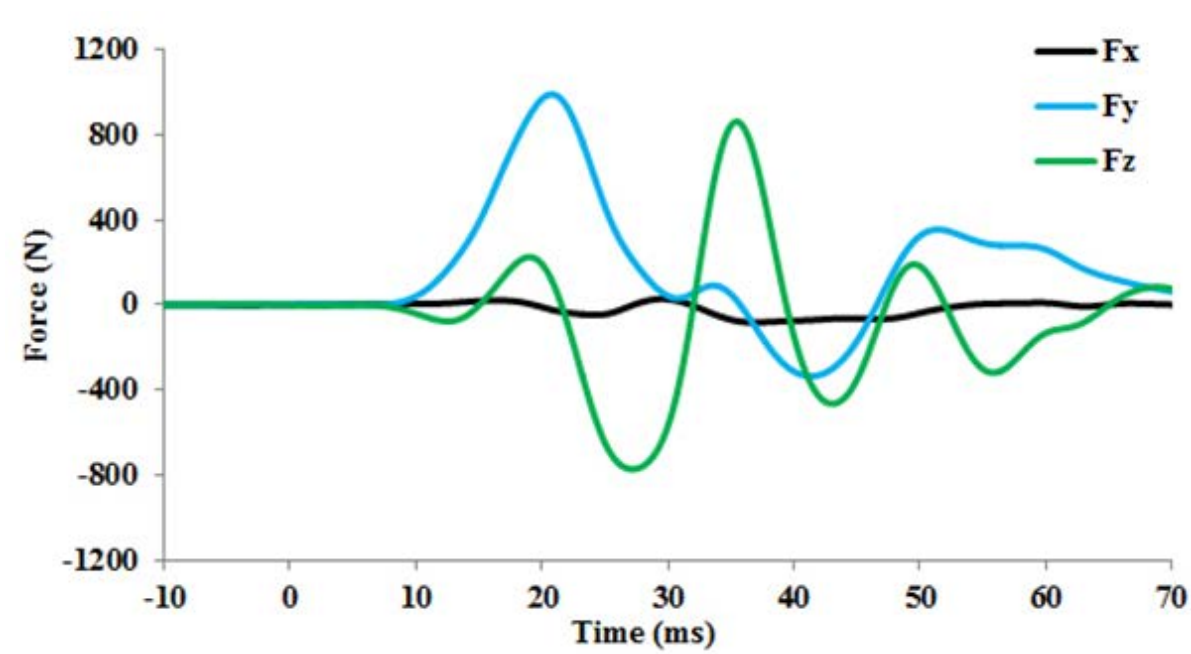


Figure 17. The ES-2 Representative Upper-Neck Load Cell Forces

Peak lateral bending, axial, and flexion and extension moments; axial forces; and lateral and AP shear forces at the time of the peak lateral bending moment are shown in table 13. Peak lateral bending moments, as measured by the upper-neck load cell, ranged from 45.14 to 131.82 Nm.

Table 13. The ES-2 Upper-Neck Load Cell Forces and Moments

| Identification Number | Force (N) | | | Moment (Nm) | | |
|---|---|---|---|---|---|---|
| | $F_x$ | $F_y$ | $F_z$ | $M_x$ | $M_y$ | $M_z$ |
| FNMD209 | -43.37 | 271.18 | -133.83 | -47.19 | -5.81 | -1.92 |
| FNMD210 | -45.84 | 256.80 | -121.31 | -45.14 | -5.80 | -1.86 |
| FNMD211 | -33.53 | 344.67 | -103.93 | -51.67 | -5.84 | -0.50 |
| FNMD212 | -31.93 | 324.70 | -96.54 | -46.90 | -5.49 | -0.26 |
| FNMD213 | -41.28 | 438.22 | -144.60 | -64.26 | -6.50 | 0.35 |
| FNMD214 | -42.24 | 457.21 | -141.94 | -67.36 | -6.70 | 0.34 |
| FNMD215 | -58.19 | 720.50 | -238.19 | -108.63 | -9.27 | 0.53 |
| FNMD216 | -85.45 | 676.55 | -203.38 | -100.50 | -12.53 | 1.00 |
| FNMD217 | -39.22 | 897.82 | -142.29 | -131.82 | -5.62 | 0.03 |
| FNMD218 | -23.27 | 720.70 | -169.33 | -110.10 | -6.30 | -0.01 |

## 10. DISCUSSION—THE ES-2 TESTS.

### 10.1 OVERALL GOALS.

The goals of the second phase of the research were to conduct experiments using the ES-2 with a matched-pair test procedure. The matched-pair design was used so the PMHS and the ES-2 would be exposed to identical loading scenarios with the same testing device. The same fixture and test setup was used in all the experiments. This process enabled the extraction of upper-neck forces and moments from the ES-2, as measured by the same load cell, at similar levels of lateral bending moments applied to the PMHS. Using the developed IRV as a basis from the PMHS tests, an IARV for the ES-2 was derived using this protocol.

### 10.2 THE ES-2 RESPONSES.

ES-2 responses indicated that the peak moments at the upper neck were predominantly in the frontal plane—i.e., peak off-axis moments in the lateral (flexion and extension moment) and transverse (axial twisting moment) planes were almost insignificant. In contrast, peak forces demonstrated a relatively more combined behavior with considerably greater lateral than AP shear forces. In fact, lateral shear forces were greater in magnitude than the axial tensile force in the ES-2, and this was true in all tests. This was attributed to the ES-2 construction and design features and the coupling at the head-neck junction. In addition, all tests showed a similar and consistent behavior in terms of trends in the upper-neck forces and moments (i.e., AP shear and axial forces were negative, and lateral shear forces were positive) according to the convention

used in this research. Likewise, lateral and flexion and extension moments were negative with very minimal axial twisting moments. These responses indicated that the ES-2 did not show coupled behavior like the PMHS, and this was expected since ES-2 is not an anatomical replica of a human. For example, its uniform design representing the human cervical spinal column does not have a posterior column with facet joints and other structures, the anterior column does not incorporate nonuniform and saddle-shaped vertebral body anatomy, and the uncovertebral joints and uncinate processes typical of the human neck are also not included. While this appears to be a limitation, it should be emphasized that the intent of the device is for use in occupant safety applications, such as side-facing seat performance tests; and, by correlating PMHS biomechanics (injuries and injury metrics), the overall response of the human is indirectly captured for crashworthiness use. Appendix B shows test-specific data. Test numbers shown in each plot correspond to the identification numbers in respective tables in this report.

## 11. THE ES-2-BASED IARVs.

Because matched-pair tests were conducted with the ES-2, it was possible to derive IARV data. The peak lateral bending moment of 73.6 Nm (rounded off to 75 Nm) represents the IRV for PMHS, as reported earlier. Lateral bending moments, as measured by the upper-neck load cell from the ES-2 tests in the second phase of the study, were compared with the OC PMHS moments using the integrated applied moment as the common factor between the two surrogates.

The integrated bending moment had a linear relationship with the lateral bending moment at the OC in both surrogates (R-squared ($R^2$) from linear regression was 0.83 and 0.87 for PMHS and ES-2 respectively, as shown in figure 18). The greatest moment achieved in PMHS tests was associated with an integrated bending moment of 1.72 Nm-s. Based on the regression line, at this integrated bending moment level, the ES-2 moment at the OC was 114.66 Nm.

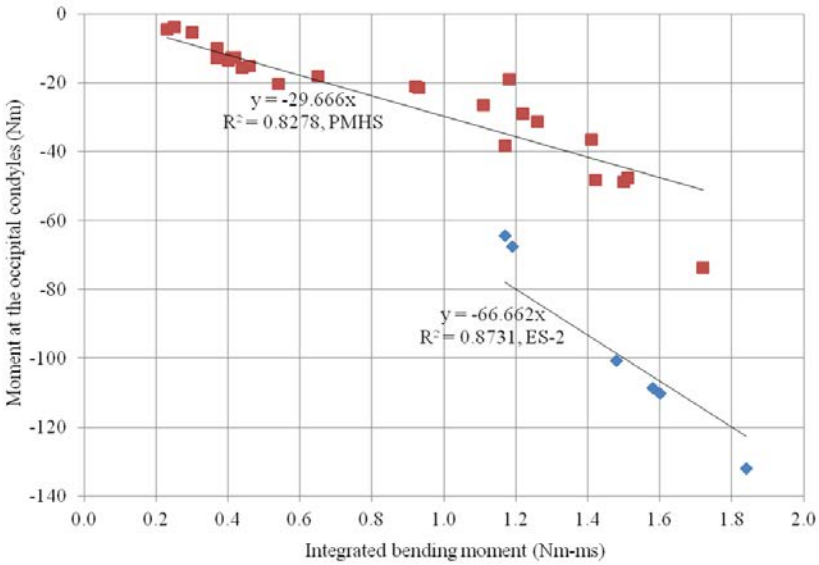


Figure 18. Variations of Integrated and OC Moments in PMHS and ES-2

The ES-2 data from tests FNMD 209-212 corresponded to input piston velocities ranging from 1.0 to 2.0 m/s. These velocities were considered to correspond to lower-energy inputs and, at these levels, the ES-2 is not recommended for crashworthiness evaluations. Therefore, these data were excluded from the regression analyses described above. Furthermore, the head angular velocities were also lower (less than 30 rad/s) in these ES-2 tests (table 11). It should be noted that peak head angular velocities greater than 30 rad/sec were obtained in earlier tests conducted using the sled equipment (Philippens et al., 2011). Therefore, tests at lower-energy inputs were not included in the analysis. As shown, the regression coefficient for ES-2 tests had a strikingly close correlation with the PMHS data (0.87 versus 0.83 for the two surrogates, respectively).

The use of the integrated, applied lateral bending moment to characterize the intrinsic neck response was based on the rationale that the purpose of this study was to determine the IARV stemming from high lateral bending moments associated with low levels of axial force; and the development of the high internal OC moment was due to the application of the pure lateral moment (with insignificant off-axis moments and forces) via a custom device capable of inducing high moments with low forces. In other words, other biomechanical input variables were deemed to play a secondary role. Use of a derived biomechanical metric has been adopted in the literature. For example, an applied chest compression to the surrogate, including animal models, has been used to characterize the viscous response of human tissues (Yoganandan et al., 2007a). From a modeling aspect, although acceleration time histories are frequently recorded in pendulum impactor tests (e.g., drop tests with human head-neck complexes), initial velocities are used to drive computational models (Yoganandan, et al., 1998). From another perspective, strain energy density functions, commonly obtained in stress analysis models of the human spine and soft tissues, use the integration of the primary output—strain in the mentioned case (Hallman et al., 2011 and Yoganandan et al., 1989a). The process of matching the two data sets (applied and resulting moments) from the matched-pair tests provided a methodology to obtain the IARV for the ES-2.

Although it is well known that the human head-neck response is not linear, the ES-2 response did appear to be linear. However, a second-order polynomial nonlinear regression analysis had a better fit with the PMHS data, with an improved R-square value of 0.9. While this appears to be a characterization of the biological behavior, the above analyses of matching the OC moment at the integrated bending moment of 1.72 Nm-s would not alter the ES-2 lateral bending moment of 114.66 Nm. From this perspective, either interpretations of the PMHS response may be used to obtain the IARV of 114.66 Nm for the ES-2. The likely reasons for the increased lateral bending moment in the ES-2, compared to the PMHS, are: the solid-beam structure of the ES-2 neck enhances moments more than the biological surrogate, in which column curvature, joints, and other segmental anatomical differences induce laxity and account for the decoupling behavior. A similar theory was presented for the Hybrid III neck in other modes of loading (Yoganandan et al., 1989b). Based on these analyses and discussions, this report suggests a peak lateral bending moment of 115 Nm as the IARV for the ES-2.

## 12. CONCLUSIONS.

This research supports the Federal Aviation Administration (FAA) efforts to develop aircraft side-facing seat neck injury criteria and tolerances for Title 14 Code of Federal Regulations. Because specific Injury Reference Values for the head-neck region in lateral impacts do not exist

in aviation environments, the FAA had to develop the necessary neck injury data. As summarized in FAA report DOT/FAA/AR-09/41, "Neck Injury Criteria for Side-Facing Aircraft Seats," sled tests and computational models were developed in the first phase of this study. Using different seat cushion, restraint, and impact energy combinations with limited sample sizes, the axial tensile force was found to be the discriminating parameter for predicting Abbreviated Injury Scale (AIS) 3+ neck injuries. The (ES-2) upper-neck forces of 2300 and 1800 Newtons corresponding to 50% and 25% risks were suggested Injury Assessment Reference Values (IARV), when combined with a minimum shear force, bending, or torque. The report stated "explicit tolerance values for pure bending or shear loads would be helpful to complete the dataset." The earlier phase of the FAA-sponsored study emphasized the need to develop a methodology to induce loading so that a high level of lateral bending moment accompanied by a low level of axial tensile force is applied to the head-neck complex of two postmortem human subjects (PMHS). The test results could then be used to determine the axial tensile and lateral bending moment data from the developed experimental and computational methodologies, and determine the potential head-neck injury criteria applicable to lateral impact loads with a focus on aviation environments.

To achieve these objectives, a component test methodology was developed to induce high lateral bending moment with low axial tensile force at the occipital condyles of the human head-neck complex. A custom fixture and sophisticated instrumentation and measurement techniques were used to obtain test data and PMHS-specific physical properties. Using this information, the IRV for the PMHS was developed. Using a matched-pair test procedure, the ES-2 anthropomorphic test dummy was subjected to lateral bending moment loads using the same loading fixtures and experimental setups as the PMHS. An IARV specific to the ES-2 was developed using the current PMHS and ES-2 research data. Acknowledging limitations in PMHS sample size, a peak lateral bending moment of 115 Nm is recommended as the IARV for the ES-2. The developed IARVs from the current (peak lateral moment) and previous FAA PMHS and ES-2 research data (axial tensile force) support the FAA in the development of a side-facing aircraft seat requirement and ES-2 test certification criteria to demonstrate compliance.

## 13. BIBLIOGRAPHY.

Association for the Advancement of Automotive Medicine, Committee on Injury Scaling, 1990, *The Abbreviated Injury Scale (AIS)—Update 98*, Des Plains, Illinois.

Cahane, C.J., , 1999, "Evaluation of FMVSS 214 Side Impact Protection Dynamic Performance Requirement," Washington, DC, National Highway Traffic Safety Administration.

Clark, C.R., 1998, *The Cervical Spine*, 3rd ed., Philadelphia, Pennsylvania, Lippincott-Raven.

DeWeese, R., D. Moorcroft, and M. Philippens, 2007, "Assessment of Injury Potential in Aircraft Side-Facing Seats Using the ES-2 ATD," FAA report DOT/FAA/AM-07/13.

Douglas, C.A., B.N. Fildes, T.J. Gibson, O. Bostrom, and F.A. Pintar, 2007, "Factors Influencing Occupant-to-Seat Belt Interaction in Far-Side Crashes," *Annual Proceedings of the Association for the Advancement of Automotive Medicine*, Vol. 51, pp. 319-339.

Eppinger, R., J. Marcus, and R. Morgan, 1984, "Development of Dummy and Injury Index for NHTSA's Thoracic Side Impact Protection Research Program," Government/Industry Meeting and Exposition, Washington, DC.

Fayon, A., C. Tarriere, G. Walfisch, C. Got, and A. Patel, 1977, "Contributions to Defining the Human Tolerance to Perpendicular Side Impact," *International Council on the Biomechanics of Impact*, Berlin, Germany, pp. 297-309.

Hallman, J.J., N. Yoganandan, and F.A. Pintar, 2011, "Prediction of Visceral Response to Multi-Directional Loading as Measured by the Chestband," *Medical Engineering and Physics*, pp. 906-913.

Kallieris, D., R. Mattern, G. Schmidt, and R. Eppinger, 1981, "Quantification of Side Impact Responses and Injuries," *Stapp Car Crash Conference*, San Francisco, California, pp. 329-366.

Klaus, G. and D. Kalleris, 1982, "Side Impact—A Comparison Between HSRI, APROD and HYBRID II Dummies and Cadavers," *Ninth International Tech Conference on Experimental Safety Vehicles*, Kyoto, Japan.

Klaus, G. and D. Kalleris, 1983, "Side Impact—A Comparison Between HSRI, APROD and HYBRID II Dummies and Cadavers," *Stapp Car Crash Conference*, San Diego, California, pp. 365-381.

Klaus, G., R. Sinnhuber, G. Hoffman, D. Kalleris, and R. Mattern, 1984, "Side Impact—A Comparison Between Dummies and Cadavers, Correlations Between Cadaver Loads and Injury Severity," *Stapp Car Crash Conference*, Chicago, Illinois, pp. 237-259.

Kleinberger, M., E. Sun, R. Eppinger, S. Kuppa, and R. Saul, 1998, "Development of Improved Injury Criteria for the Assessment of Advanced Automotive Restraint Systems," Washington, DC, National Highway Traffic Safety Administration.

Kuppa, S., F. Eppinger, M. Maltese, R. Naik, N. Yoganandan, F. Pintar, R. Saul, and J. McFadden, 2000, "Assessment of Thoracic Injury Criteria for Side Impact," *International Council on the Biomechanics of Impact*, Montpellier, France, pp. 131-146.

McIntosh, A.S., D. Kallieris, and B. Frechede, 2007, "Neck Injury Tolerance Under Inertial Loads in Side Impacts," *Accident Analysis and Prevention*, Vol. 39, pp. 326-333.

National Highway Traffic Safety Administration, 1990, Federal Register, Washington, DC, Department of Transportation.

Nightingale, R.W., B.A. Winkelstein, K.E. Knaub, W.J. Richardson, J.F. Luck, and B.S. Myers, 2002, "Comparative Strengths and Structural Properties of the Upper and Lower Cervical Spine in Flexion and Extension," *Journal Biomechanics*, Vol. 35, pp. 725-732.

Nusholtz, G.S., N. Alem, and J.W. Melvin, 1982, "Impact Response and Injury to the Pelvis," *Stapp Car Crash Conference*, Ann Arbor, Michigan, pp. 103-142.

Philippens, M., P. Forbes, J. Wismans, R. DeWeese, and D. Moorcroft, "Neck Injury Criteria for Side-Facing Aircraft Seats," FAA report DOT/FAA/AR-09/41, July 2011.

Philippens, M., J. Wismans, P.A. Forbes, N. Yoganandan, F.A. Pintar, and S.J. Soltis, 2009, "ES2 Neck Injury Assessment Reference Values for Lateral Loading in Side Facing Seats," *Stapp Car Crash Journal*, Vol. 53, pp. 421-441.

Pintar, F.A., N. Yoganandan, and J. Baisden, 2005, "Characterizing Occipital Condyle Loads Under High-Speed Head Rotation," *Stapp Car Crash Journal*, Vol. 49, pp. 33-47.

Pintar, F.A., N. Yoganandan, M.H. Hines, M.R. Maltese, J. McFadden, R. Saul, R. Eppinger, N. Khaewpong, and M. Kleinberger, 1997, "Chestband Analysis of Human Tolerance to Side Impact," *Stapp Car Crash Conference*, Lake Buena Vista, Florida, pp. 63-74.

Pintar, F.A., N. Yoganandan, and D.J. Maiman, 2010, "Lower Cervical Spine Loading in Frontal Sled Tests Using Inverse Dynamics: Potential Applications for Lower Neck Injury Criteria," *Stapp Car Crash Journal*, Vol. 54, pp. 133-166.

Pintar, F.A., N. Yoganandan, and L. Voo, 1998, "Effect of Age and Loading Rate on Human Cervical Spine Injury Threshold," *Spine*, Philadelphia, Pennsylvania, Vol. 23, pp. 1957-1962.

SAE International, 1994, *Sign Convention for Vehicle Crash Testing*, Warrendale, Pennsylvania, SAE International, SAE Surface Vehicle Information Report No. J1733.

SAE International, 2007, Society of Automotive Engineers: Instrumentation for Impact Test-Part 1-Electronic Instrumentation-SAE J211/1. Warrendale, Pennsylvania.

Shams, T. and N. Rangarajan, 2005, "THOR Instrumentation Data Processing Program," Boonsboro, Maryland, General Engineering and Systems Analysis, Inc.

Soltis, S., 2001, "An Overview of Existing and Needed Neck Impact Injury Criteria for Sideward Facing Aircraft Seats," *Third Triennial International Aircraft Fire and Cabin Safety Research Conference: Federal Aviation Administration*, Washington, DC.

Soltis, S., G. Frings, R. Gowdy, R. DeWeese, J. Hoof, and R. Meijer, 2003, "Development of Side Impact Neck Injury Criteria and Tolerances for Occupants of Sideward Facing Aircraft Seats," NATO, Koblenz, Germany, pp. 1-15.

Stemper, B.D., N. Yoganandan, and F.A. Pintar, 2003, "Gender Dependent Cervical Spine Segmental Kinematics During Whiplash," *Journal Biomechanics*, Vol. 36, pp. 1281-1289.

Stemper, B.D., N. Yoganandan, R.D. Rao, and F.A. Pintar, 2005, “Influence of Thoracic Ramping on Whiplash Kinematics,” *Clinical Biomechanics*, Vol. 20, Bristol, England, pp. 1019-1028.

Tarriere, C., G. Walfisch, A. Fayon, C. Got, and F. Guillon, 1979, “Synthesis of Human Impact Tolerance Obtained From Lateral Impact Simulations,” *Seventh International Technical Conference on Experimental Safety Vehicles*, Washington, DC, pp. 359-373.

Viano, D., I. Lau, C. Asbury, A. King, and P. Begeman, 1989, “Biomechanics of the Human Chest, Abdomen, and Pelvis in Lateral Impacts,” *33rd Association for the Advancement of Automotive Medicine*, Baltimore, Maryland.

Walfisch, G., A. Fayon, C. Tarriere, J. Rosey, F. Guillon, C. Got, A. Patel, and R. Stalnaker, 1980, “Designing of a Dummy’s Abdomen for Detecting Injuries in Side Impact Collisons,” *International Research Council on the Biomechanics of Impact*, pp. 149-164.

Yoganandan, N., D.J. Maiman, Y. Guan, and F. Pintar, 2009a, “Importance of Physical Properties of the Human Head on Head-Neck Injury Metrics,” *Traffic Injury Prevention*, Vol. 10, pp. 488-496.

Yoganandan, N. and F.A. Pintar, 2008, "Deflections from Two Types of Human Surrogates in Oblique Side Impacts," *Annals on Advances in Automotive Medicine*, Vol. 52, pp. 301-313.

Yoganandan, N., F.A. Pintar, S. Kumaresan, M. Haffner, and S. Kuppa, 1997, “Impact Biomechanics of the Human Thorax-Abdomen Complex,” *International Journal of Crashworthiness*, Vol. 2, pp. 219-228.

Yoganandan, N., F.A. Pintar, S. Kumaresan, A. Sances, and M. Haffner, 1996, “Response of Human Lower Thorax to Impact,” Association for the Advancement of Automotive Medicine, Vancouver, British Columbia, Canada, pp. 33-43.

Yoganandan, N., F.A. Pintar, S.J. Larson, and A. Sances, eds., 1998, *Frontiers in Head and Neck Trauma: Clinical and Biomechanical*, The Netherlands, IOS Press.

Yoganandan, N., F.A. Pintar, D.J. Maiman, M. Philippens, and J. Wismans, 2009b, “Neck Forces and Moments and Head Accelerations in Side Impact,” *Traffic Injury Prevention*, Vol. 10, pp. 51-57.

Yoganandan, N., F.A. Pintar, B.D. Stemper, T.A Gennarelli, and J.A. Weigelt, 2007a, “Biomechanics of Side Impact: Injury Criteria, Aging Occupants, and Airbag Technology,” *Journal of Biomechanics*, Vol. 40, pp. 227-243.

Yoganandan, N., F.A. Pintar, B.D. Stemper, C.E. Wolfla, B.S. Shender, and G. Paskoff, 2007b, “Level-Dependent Coronal and Axial Moment-Rotation Corridors of Degeneration-Free Cervical Spines in Lateral Flexion,” *The Journal of Bone and Joint Surgery (American)*, Vol. 89, pp. 1066-1074.

Yoganandan, N., F.A. Pintar, J. Zhang, and J.L. Baisden, 2009c, “Physical Properties of the Human Head: Mass, Center of Gravity and Moment of Inertia,” *Journal of Biomechanics*, Vol. 42, pp. 1177-1192.

Yoganandan, N., F.A. Pintar, J. Zhang, B.D. Stemper, and M. Philippens, 2008a, “Upper Neck Forces and Moments and Cranial Angular Accelerations in Lateral Impact,” *Annals of Biomedical Engineering*, Vol. 36, pp. 406-414.

Yoganandan, N., G. Ray, F.A. Pintar, J.B. Myklebust, and A. Sances, 1989a, “Stiffness and Strain Energy Criteria to Evaluate the Threshold of Injury to an Intervertebral Joint,” *Journal of Biomechanics*, Vol. 22, pp. 135-142.

Yoganandan, N., A. Sances, D.J. Maiman, J.B. Myklebust, P. Pech, and S.J. Larson, 1986, “Experimental Spinal Injuries with Vertical Impact,” *Spine*, Philadelphia, Pennsylvania, Vol. 11, pp. 855-860.

Yoganandan, N., A. Sances, and F. Pintar, 1989b, “Biomechanical Evaluation of the Axial Compressive Responses of the Human Cadaveric and Manikin Necks,” *Journal of Biomechanical Engineering*, Vol. 111, pp. 250-255.

Yoganandan, N., B.D. Stemper, F.A. Pintar, J.L. Baisden, B.S. Shender, and G. Paskoff, 2008b, “Normative Segment-Specific Axial and Coronal Angulation Corridors of Subaxial Cervical Column in Axial Rotation,” *Spine*, Philadelphia, Pennsylvania,
Vol. 33, pp. 490-496.

Yoganandan, N., J. Zhang, F.A. Pintar, and Y. King Liu, 2006, “Lightweight Low-Profile Nine-Accelerometer Package to Obtain Head Angular Accelerations in Short-Duration Impacts,” *Journal of Biomechanics*, Vol. 39, pp. 1347-1354.

# APPENDIX A—POSTMORTEM HUMAN SUBJECT TIME HISTORIES OF LOADS AT THE OCCIPITAL CONDYLES

Figures A-1 through A-24 show generalized time histories of loads at the occipital condyles (i.e., axial and shear forces and lateral bending moments) on a test-by-test basis. The test numbers correspond to the identification numbers in the respective tables in the main report.

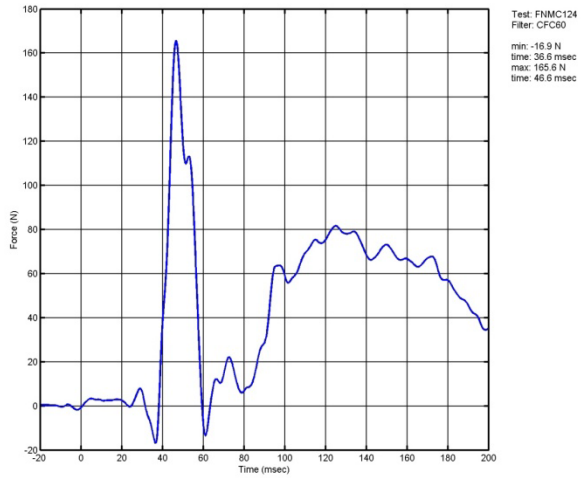


(a)

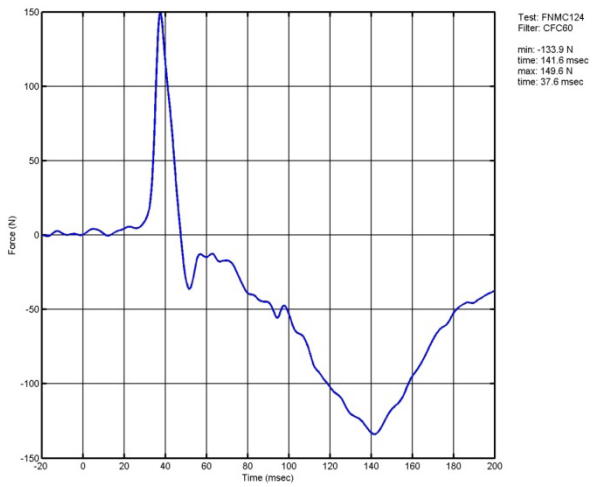


(b)

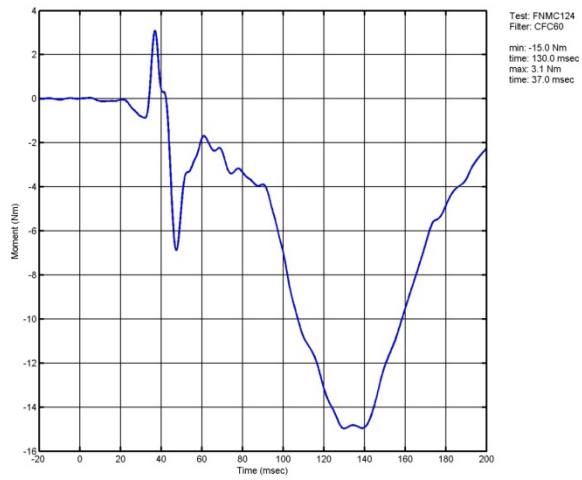


(c)

Figure A-1. Test FNMC124OC ((a) Force Y, (b) Force Z, and (c) Moment X)

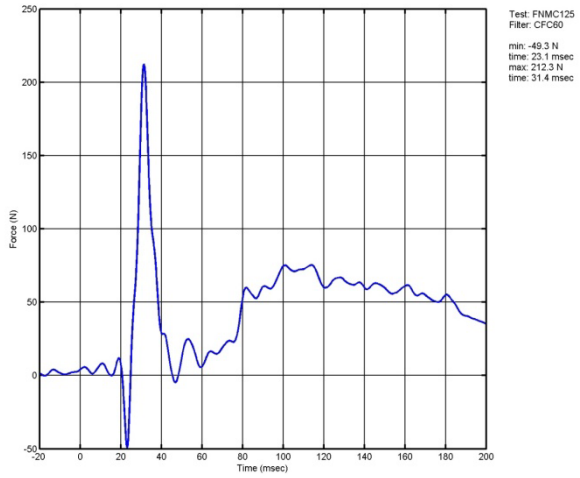


(a)

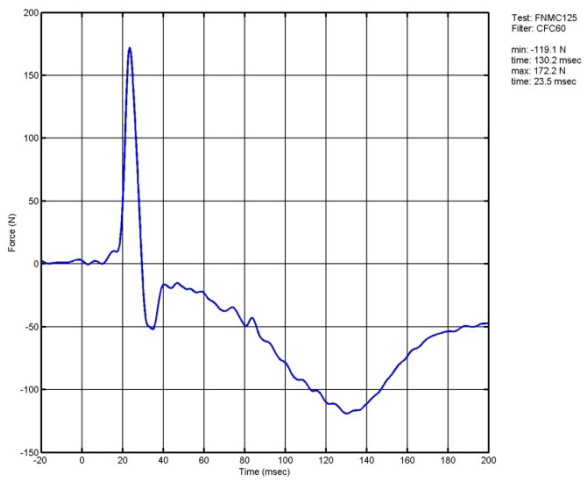


(b)

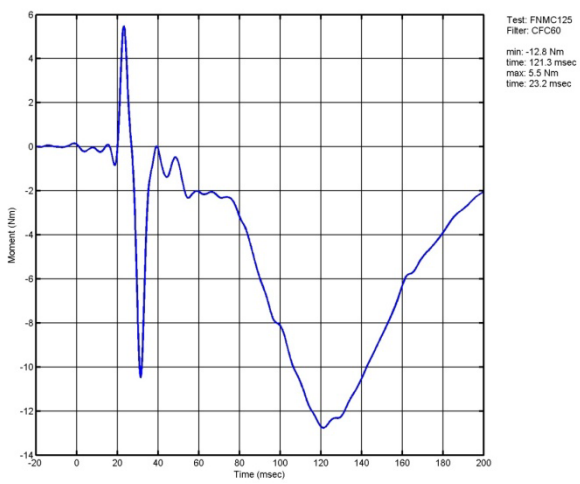


(c)

Figure A-2. Test FNMC125OC ((a) Force Y, (b) Force Z, and (c) Moment X)

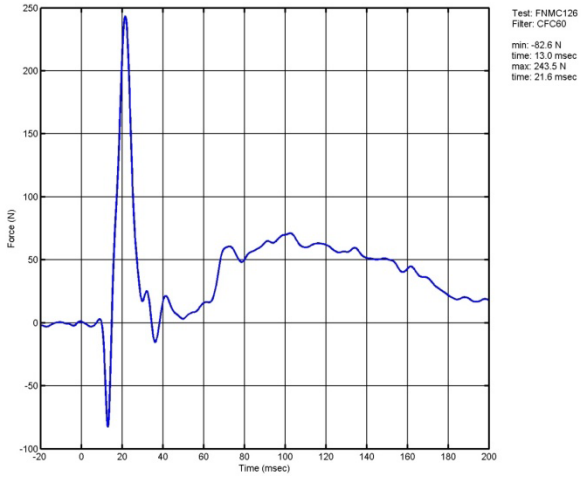


(a)

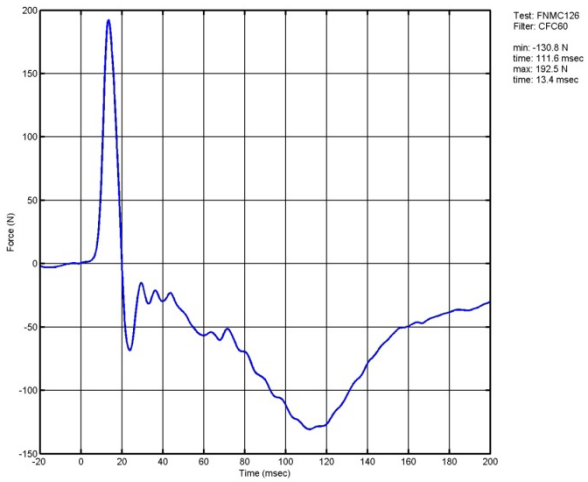


(b)

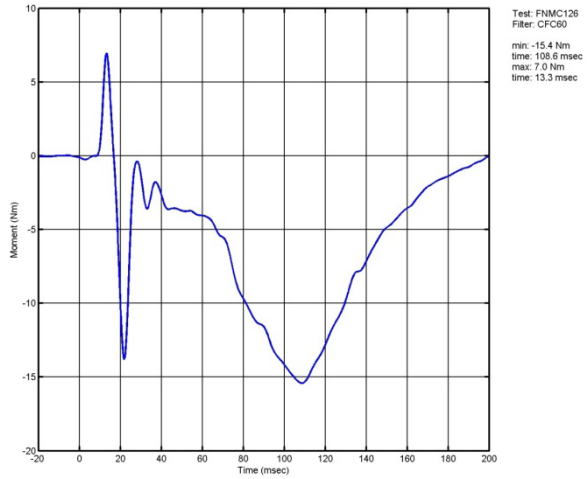


(c)

Figure A-3. Test FNMC126OC ((a) Force Y, (b) Force Z, and (c) Moment X)

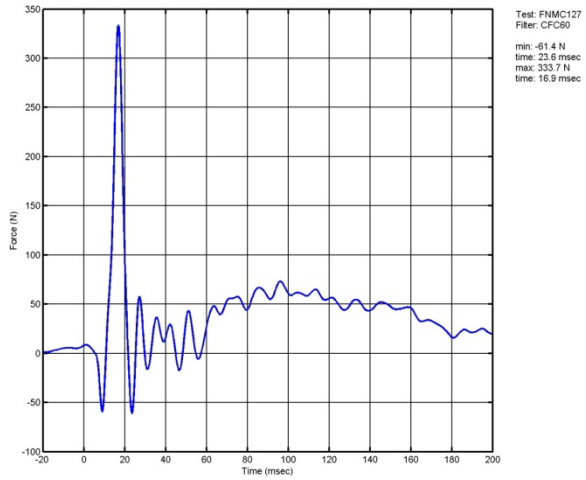


(a)

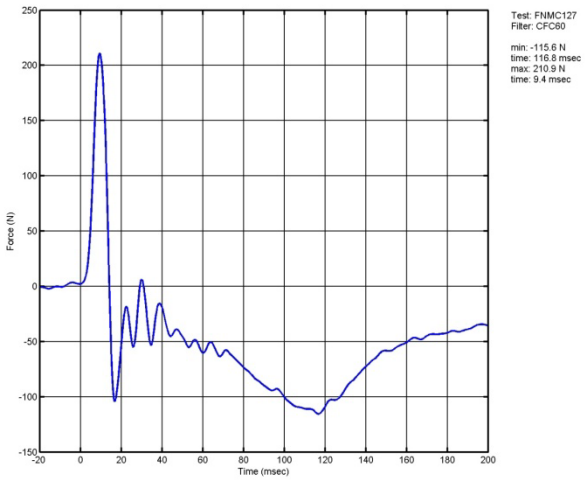


(b)

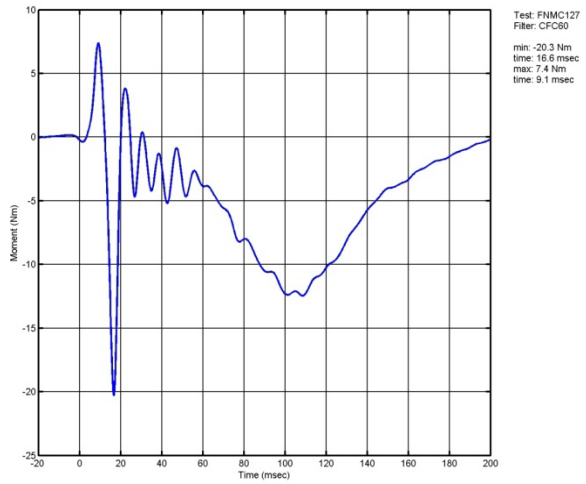


(c)

Figure A-4. Test FNMC127OC ((a) Force Y, (b) Force Z, and (c) Moment X)

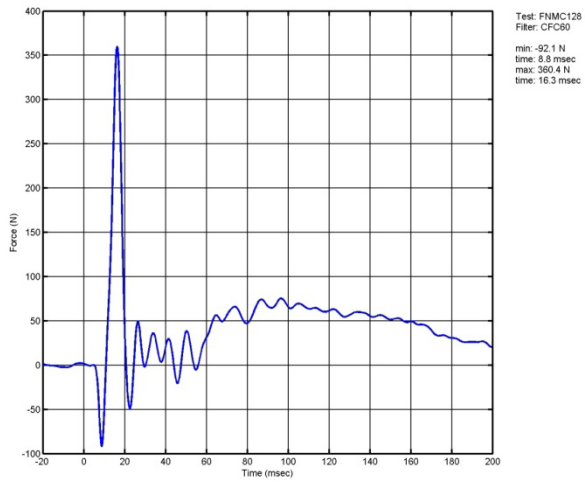


(a)

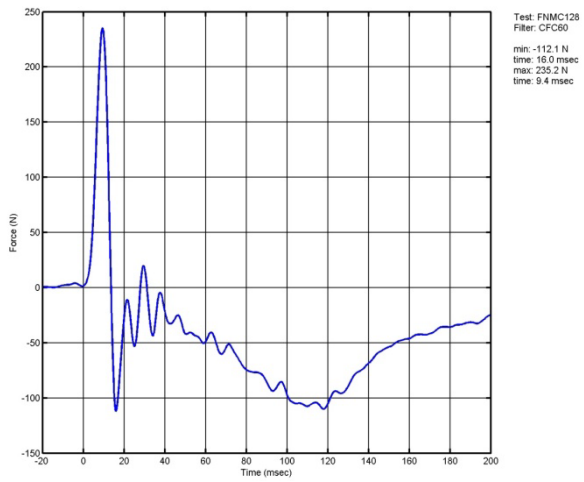


(b)

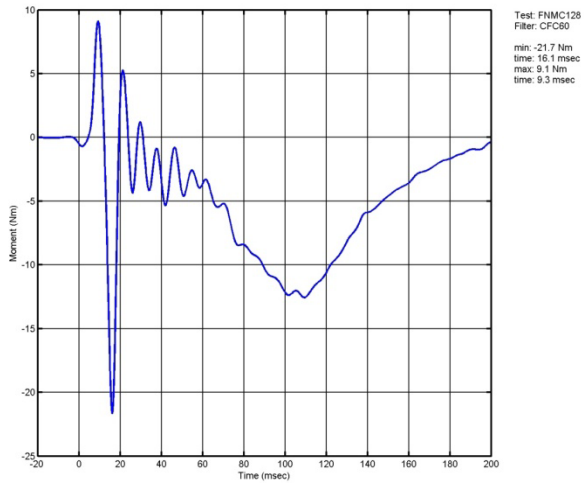


(c)

Figure A-5. Test FNMC128OC ((a) Force Y, (b) Force Z, and (c) Moment X)

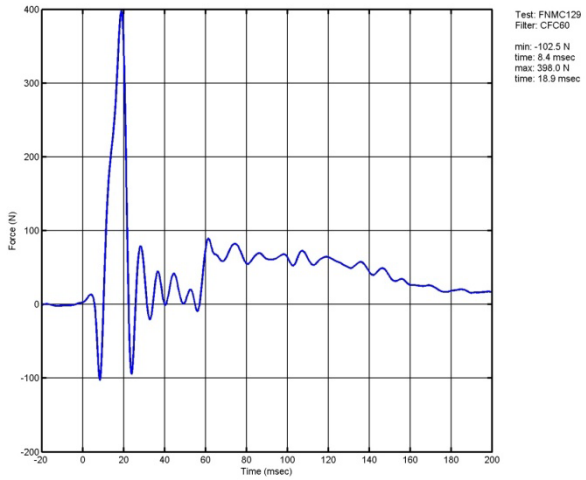


(a)

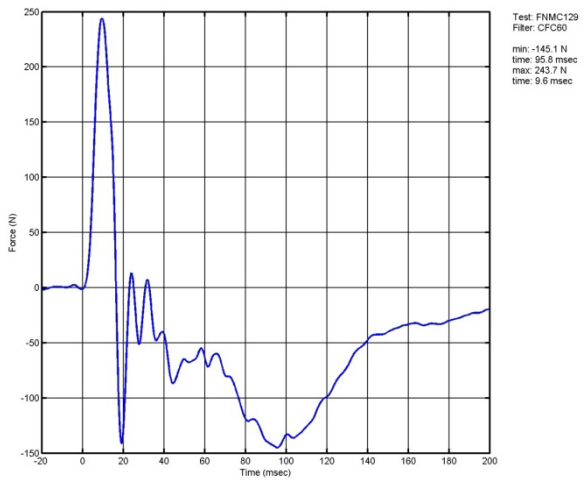


(b)

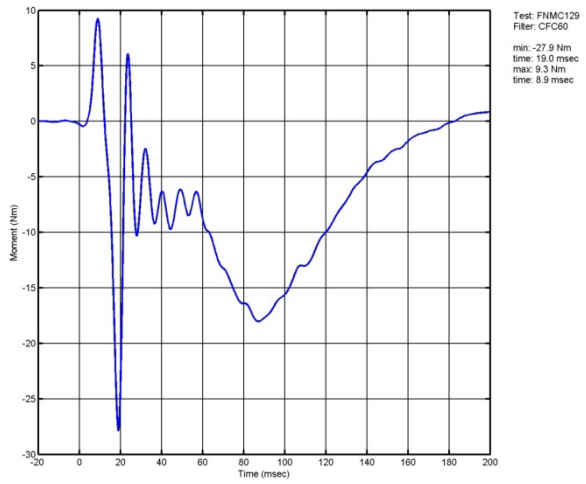


(c)

Figure A-6. Test FNMC129OC ((a) Force Y, (b) Force Z, and (c) Moment X)

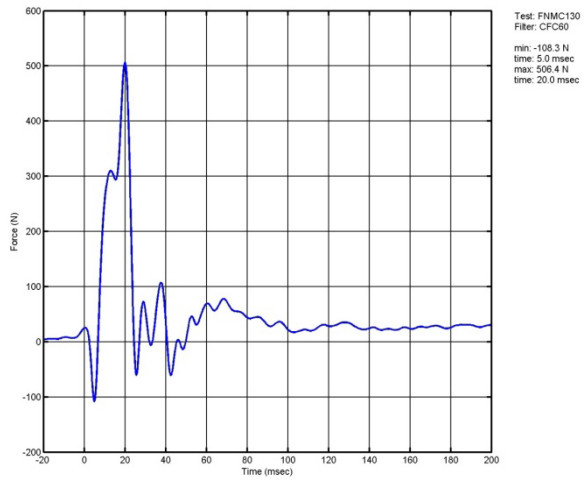


(a)

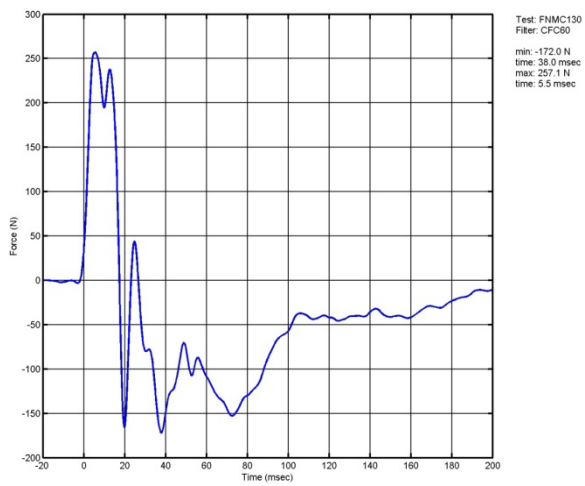


(b)

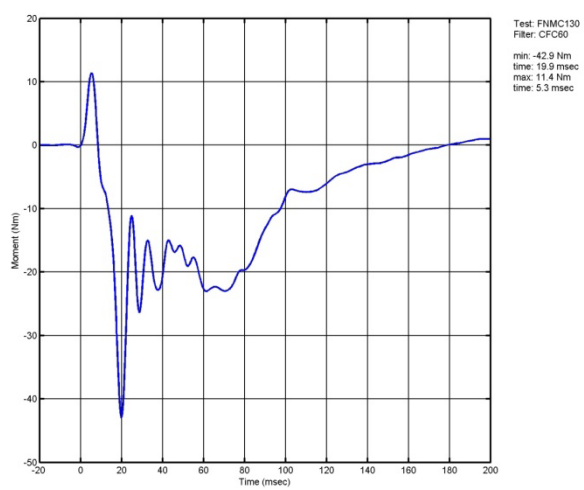


Figure A-7. Test FNMC130OC ((a) Force Y, (b) Force Z, and (c) Moment X)

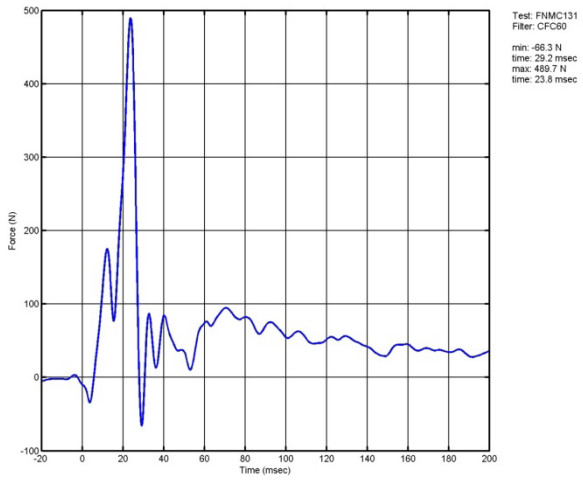


(a)

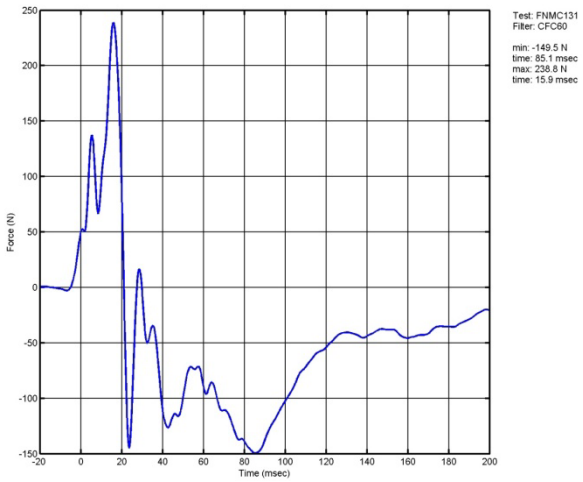


(b)

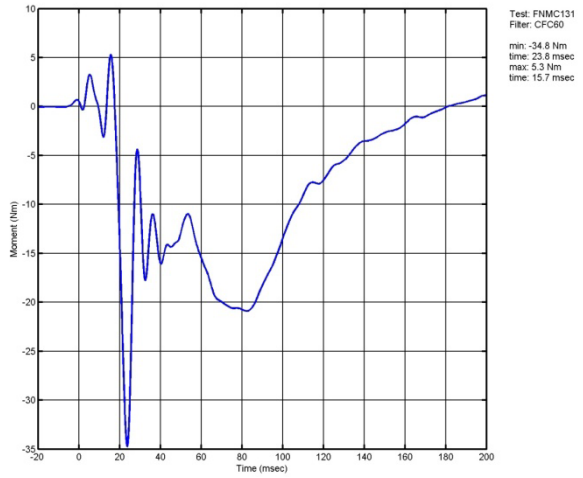


(c)

Figure A-8. Test FNMC131OC ((a) Force Y, (b) Force Z, and (c) Moment X)

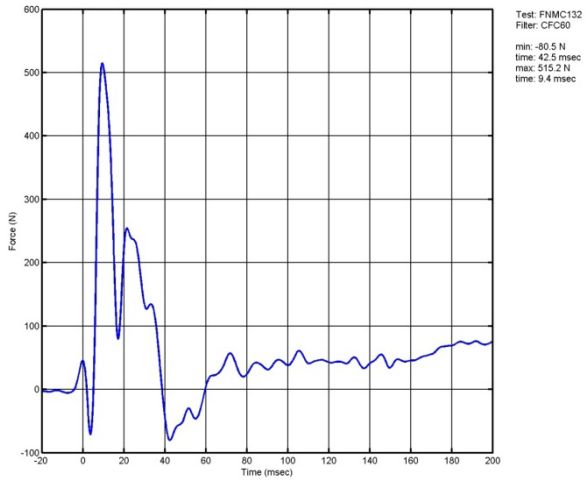


(a)

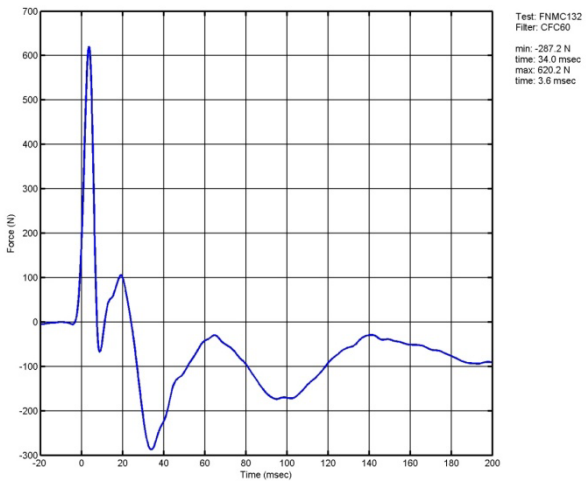


(b)

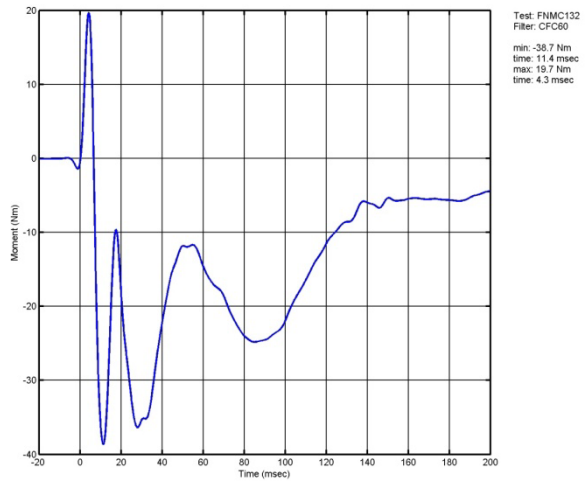


(c)

Figure A-9. Test FNMC132OC ((a) Force Y, (b) Force Z, and (c) Moment X)

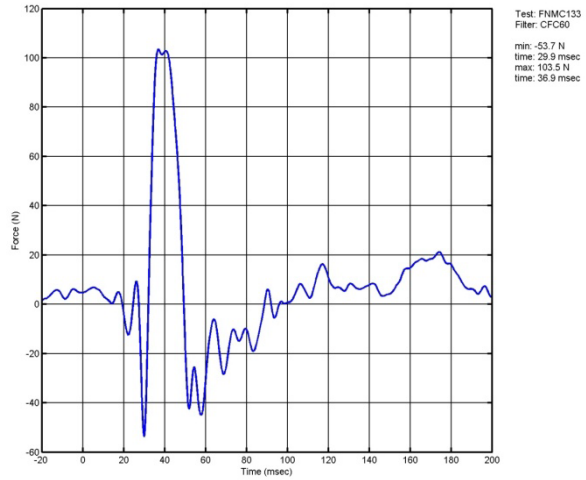


(a)

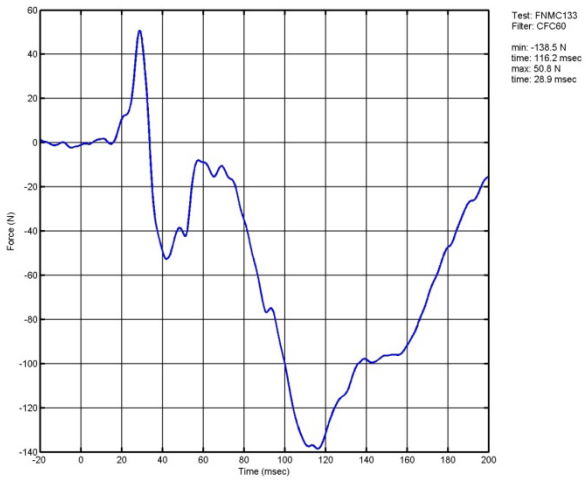


(b)

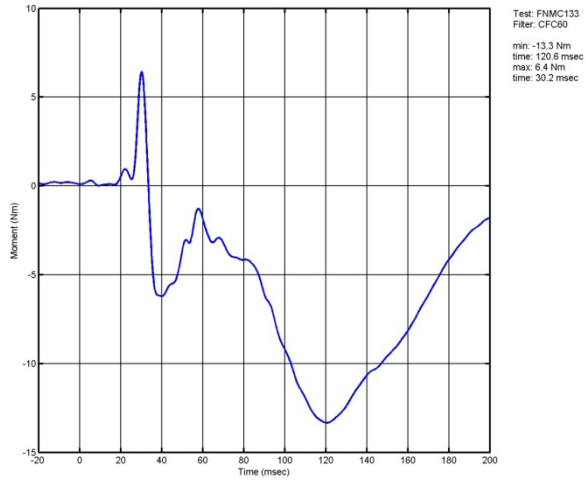


(c)

Figure A-10. Test FNMC133OC ((a) Force Y, (b) Force Z, and (c) Moment X)

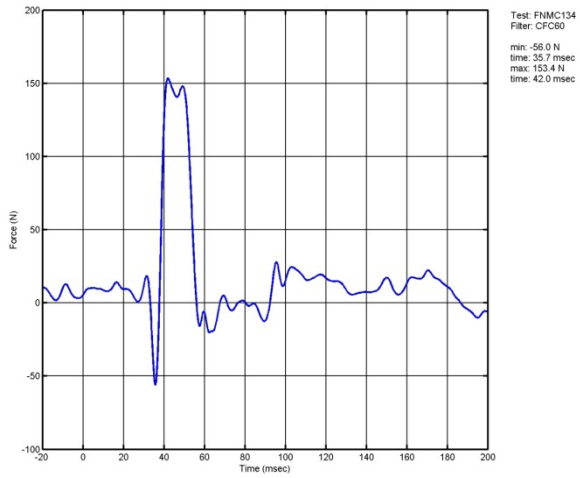


(a)

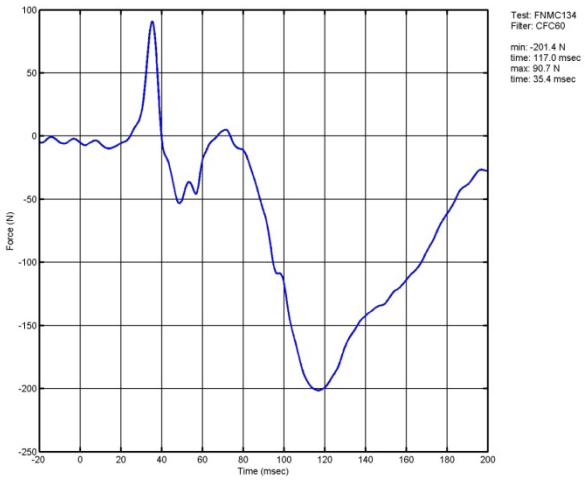


(b)

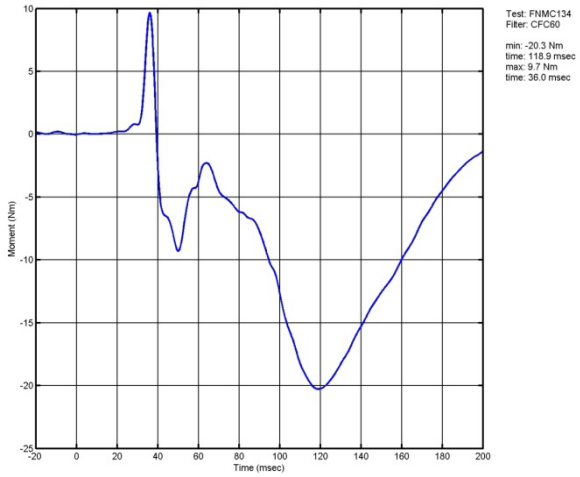


(c)

Figure A-11. Test FNMC134OC ((a) Force Y, (b) Force Z, and (c) Moment X)

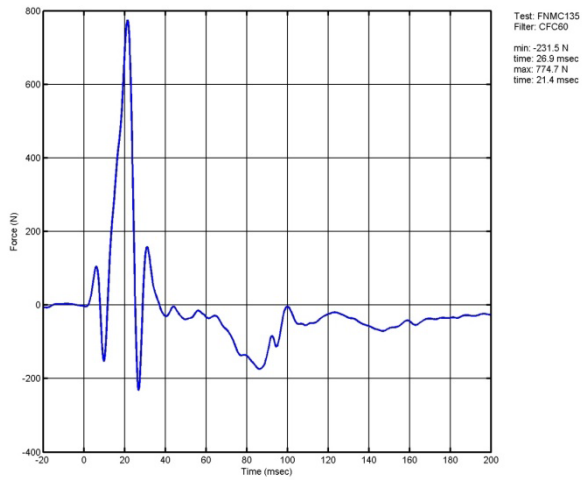


(a)

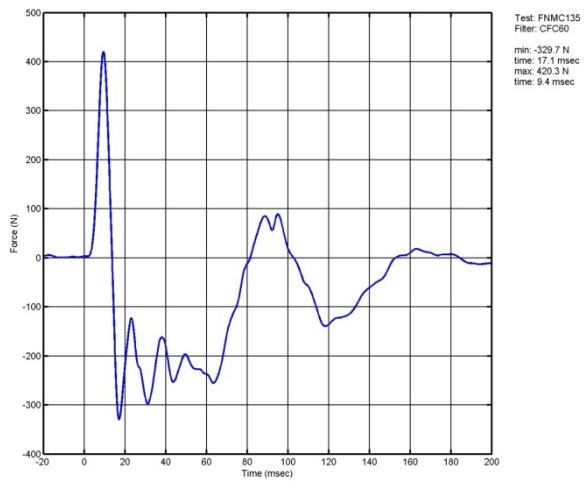


(b)

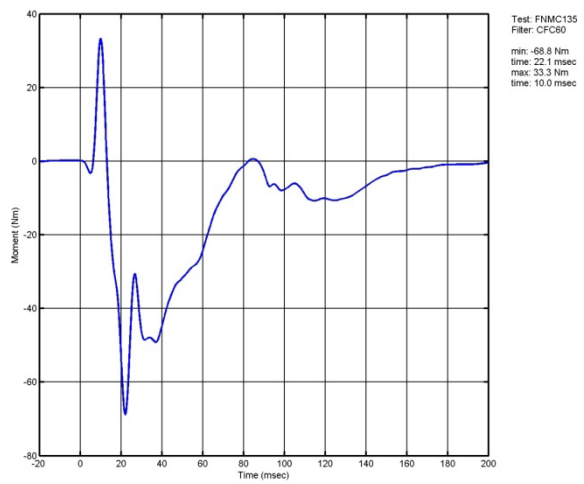


(c)

Figure A-12. Test FNMC135OC ((a) Force Y, (b) Force Z, and (c) Moment X)

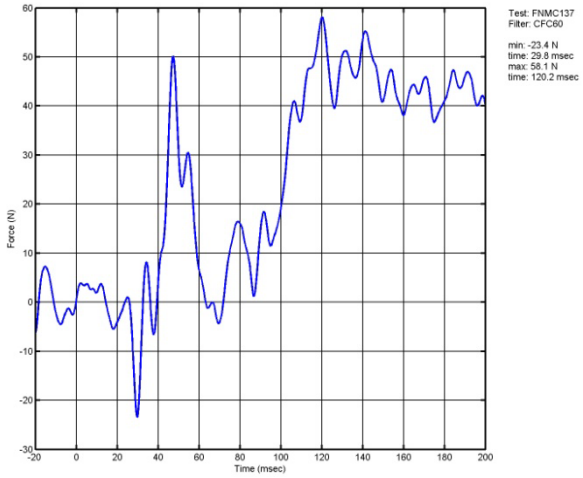


(a)

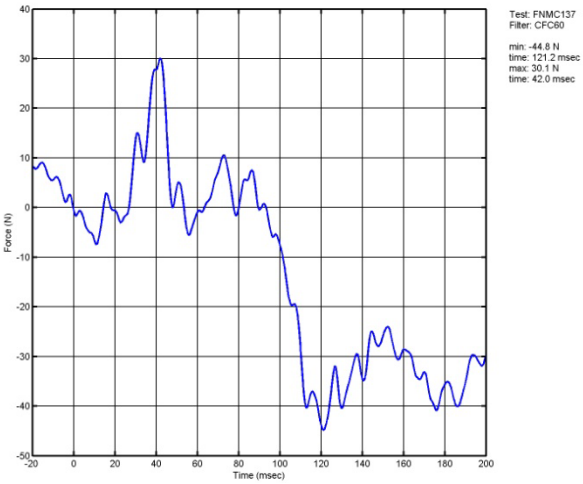


(b)

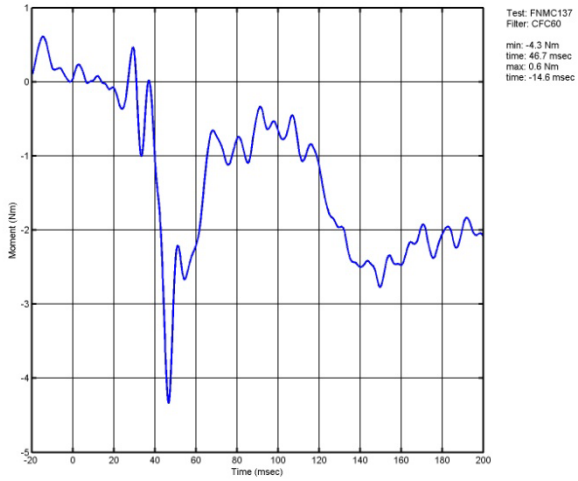


(c)

Figure A-13. Test FNMC137OC ((a) Force Y, (b) Force Z, and (c) Moment X)

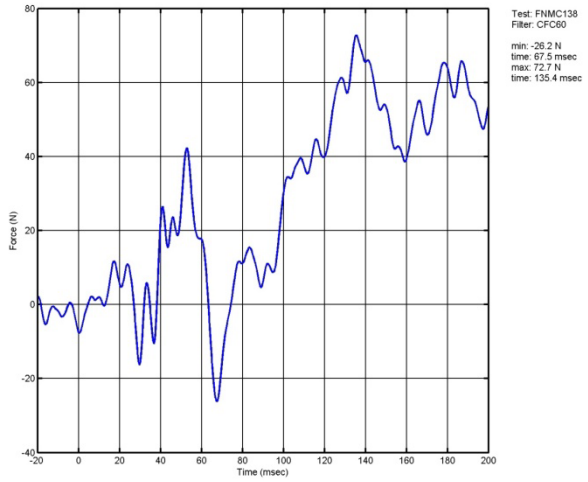


(a)

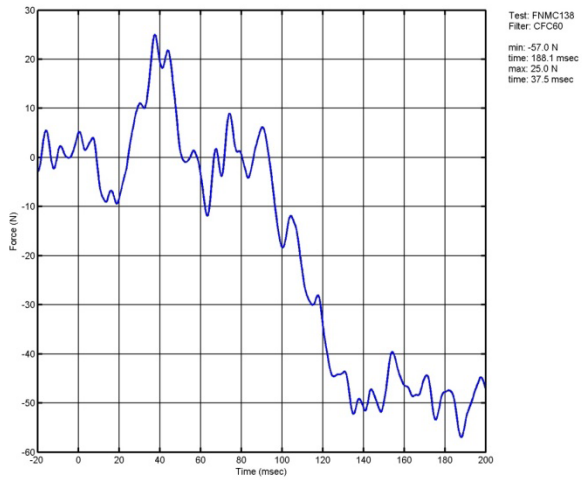


(b)

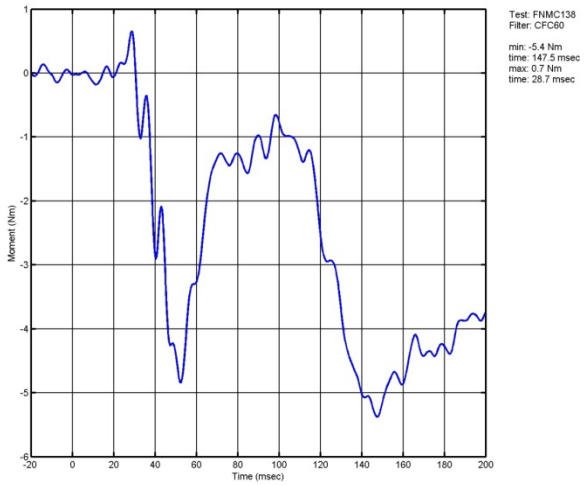


(c)

Figure A-14. Test FNMC138OC ((a) Force Y, (b) Force Z, and (c) Moment X)

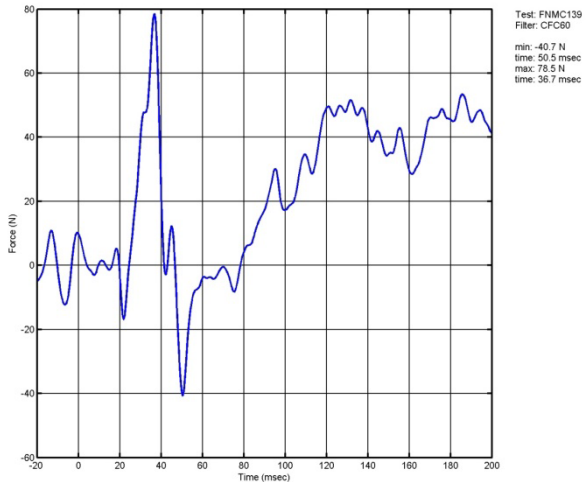


(a)

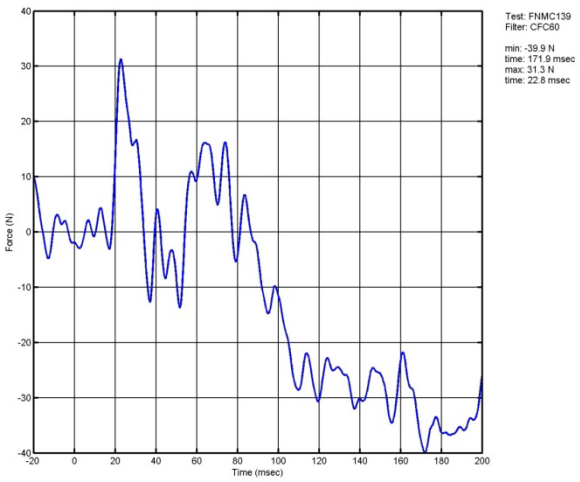


(b)

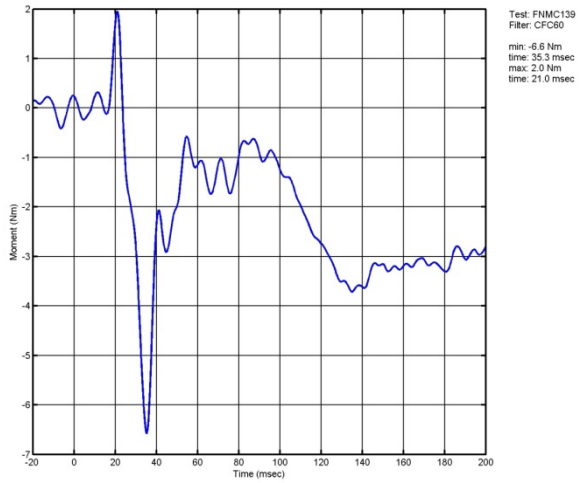


(c)

Figure A-15. Test FNMC139OC ((a) Force Y, (b) Force Z, and (c) Moment X)

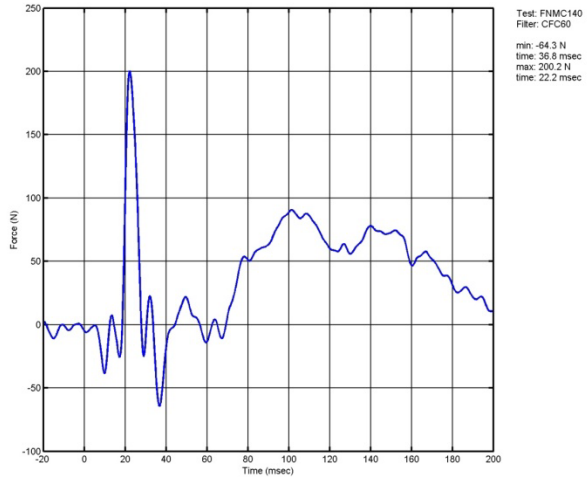


(a)

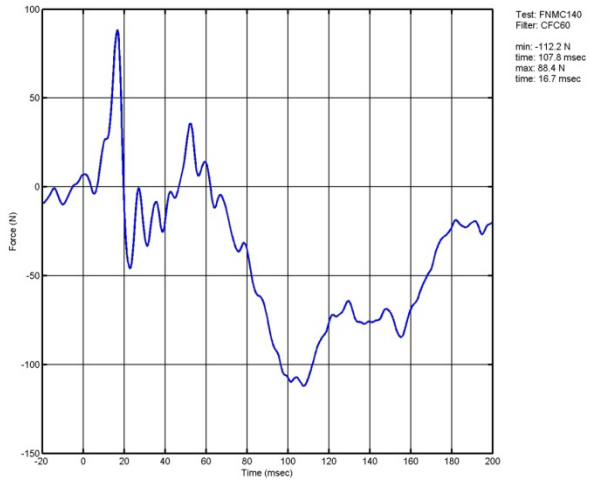


(b)

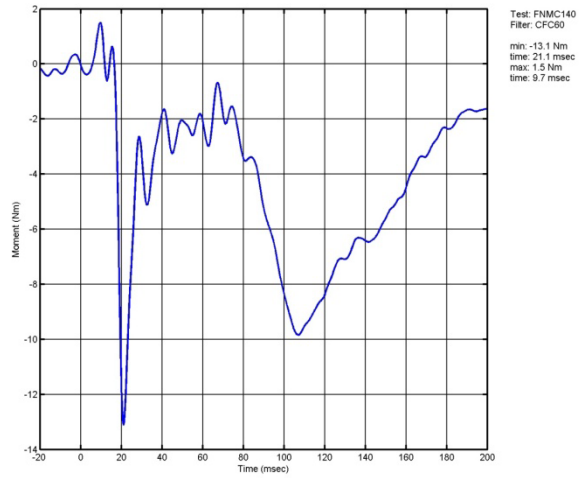


(c)

Figure A-16. Test FNMC140OC ((a) Force Y, (b) Force Z, and (c) Moment X)

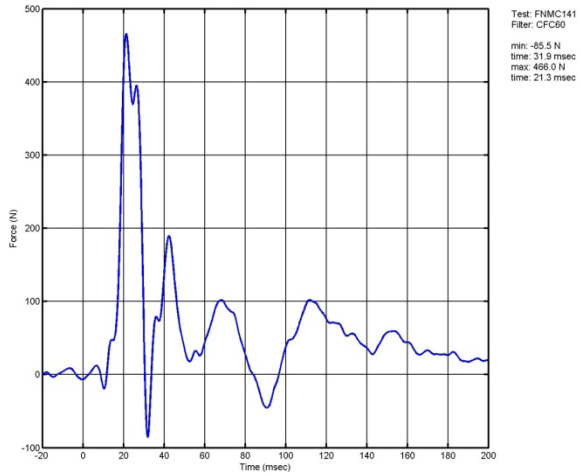


(a)

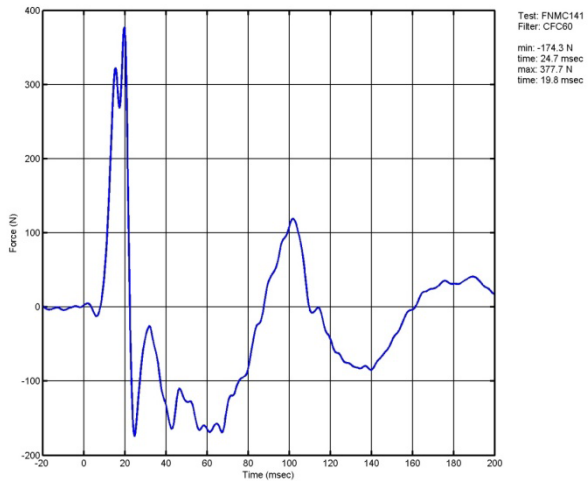


(b)

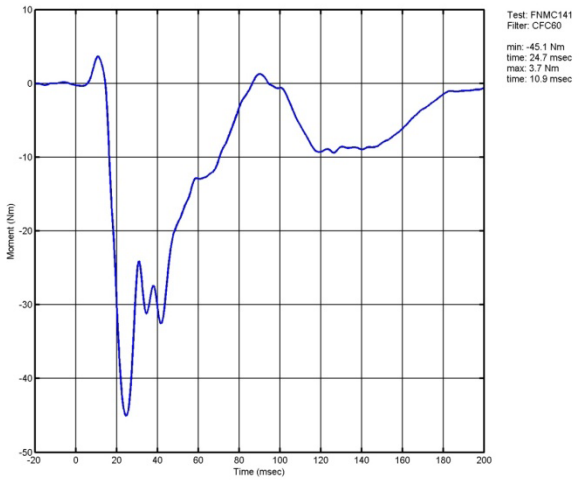


(c)

Figure A-17. Test FNMC141OC ((a) Force Y, (b) Force Z, and (c) Moment X)

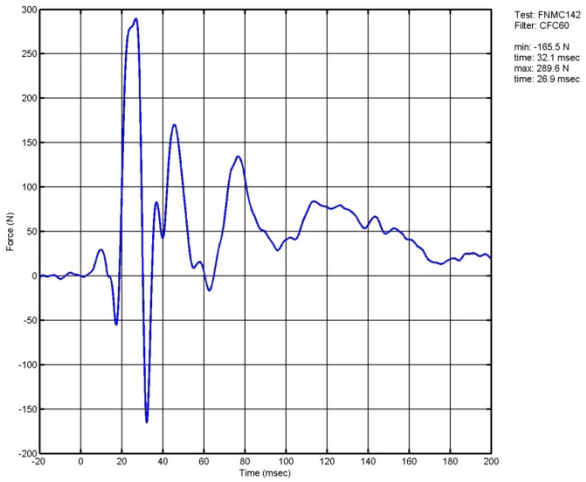


(a)

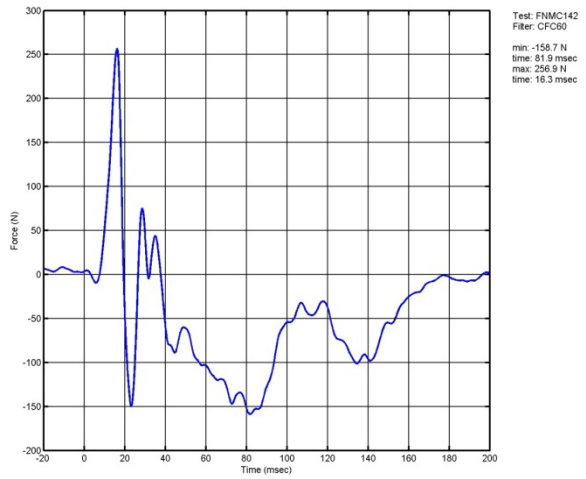


(b)

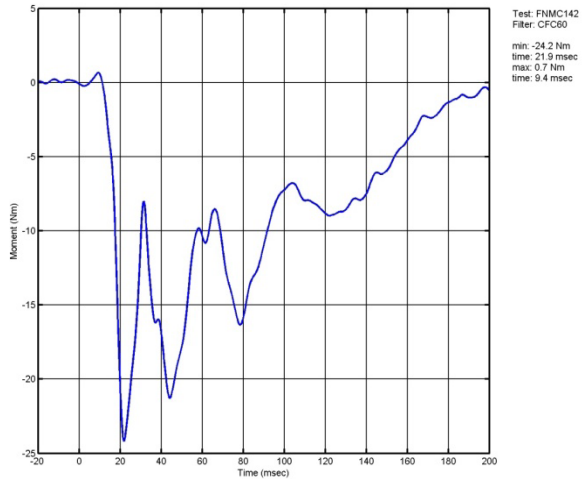


(c)

Figure A-18. Test FNMC142OC ((a) Force Y, (b) Force Z, and (c) Moment X)

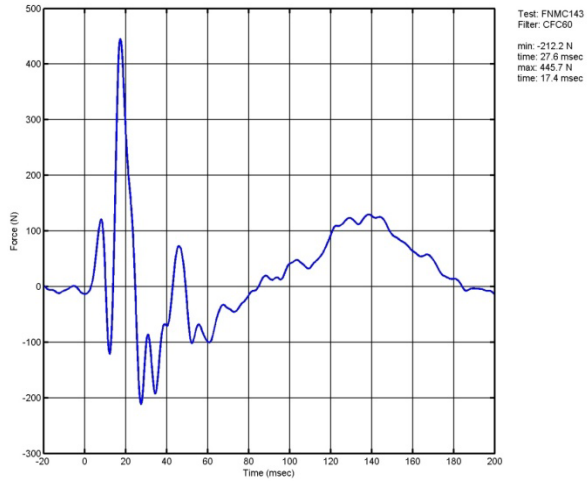


(a)

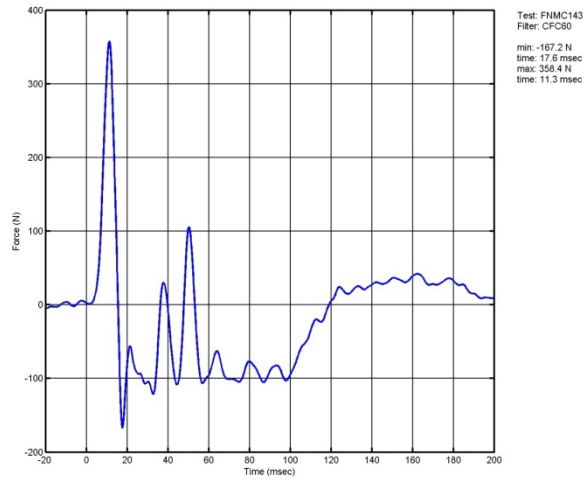


(b)

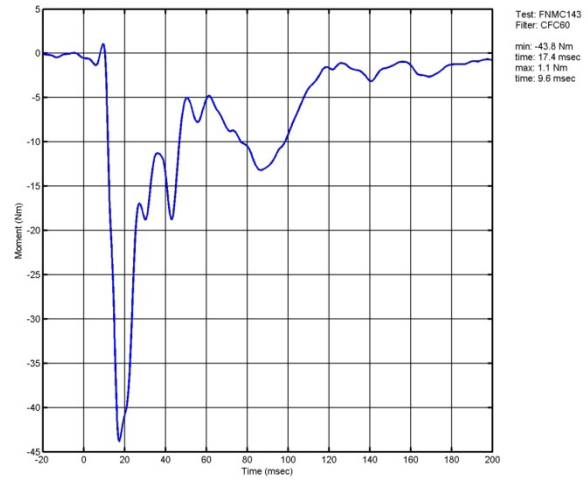


(c)

Figure A-19. Test FNMC143OC ((a) Force Y, (b) Force Z, and (c) Moment X)

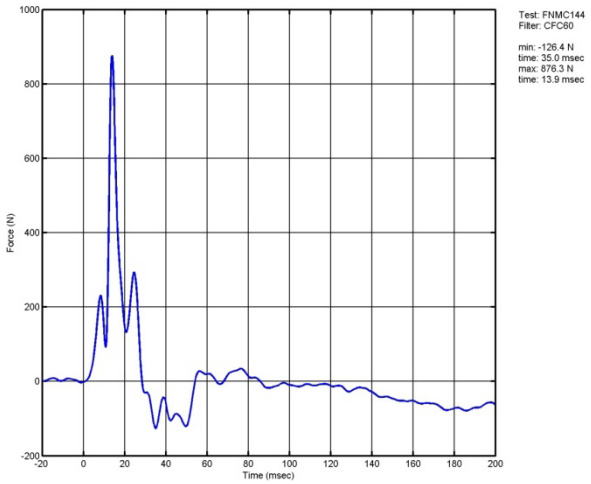


(a)

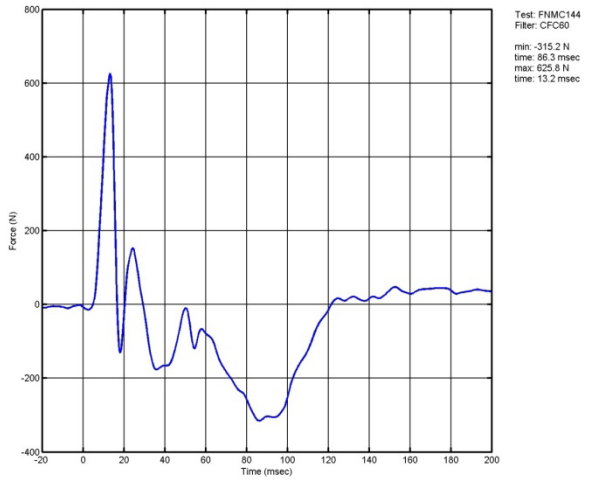


(b)

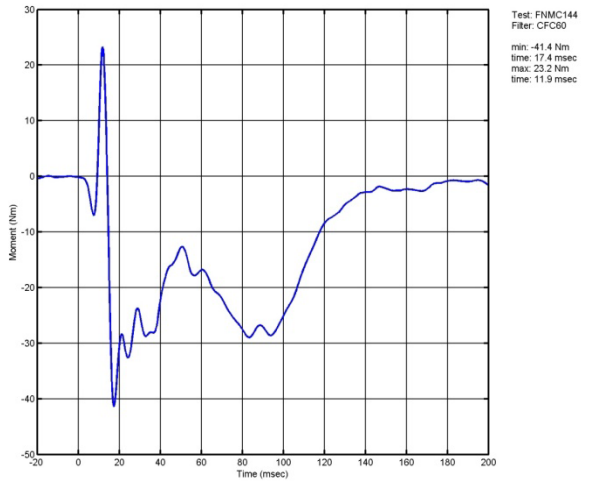


(c)

Figure A-20. Test FNMC144OC ((a) Force Y, (b) Force Z, and (c) Moment X)

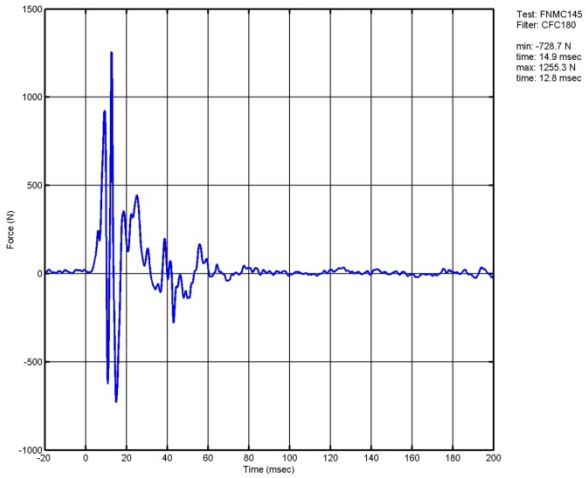


(a)

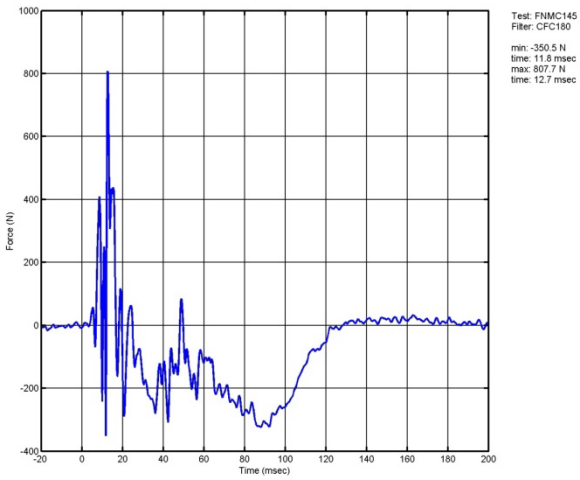


(b)

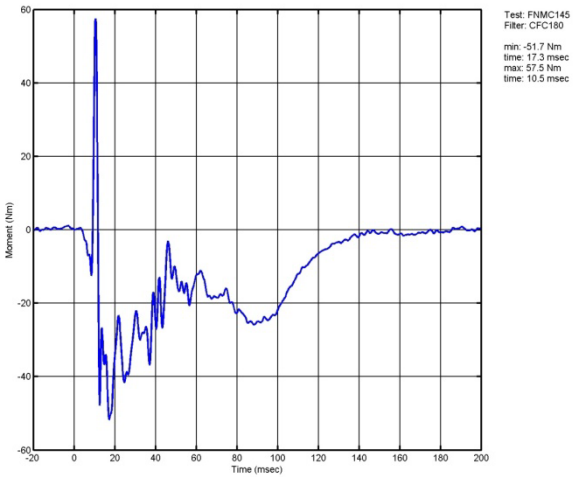


(c)

Figure A-21. Test FNMC145OC ((a) Force Y, (b) Force Z, and (c) Moment X)

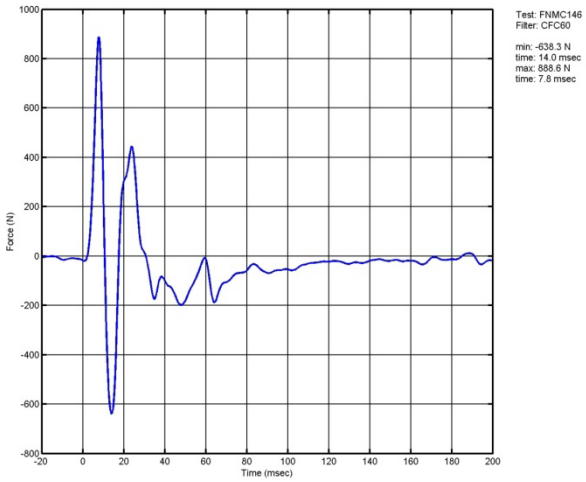


(a)

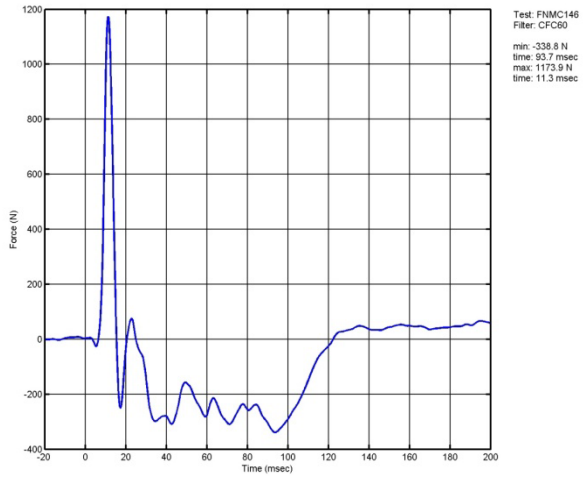


(b)

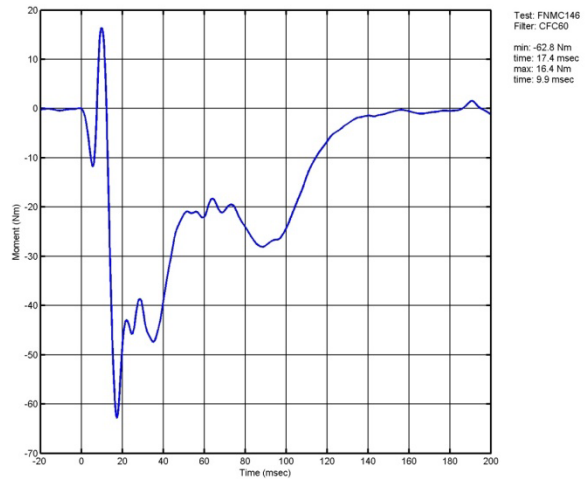


(c)

Figure A-22. Test FNMC146OC ((a) Force Y, (b) Force Z, and (c) Moment X)

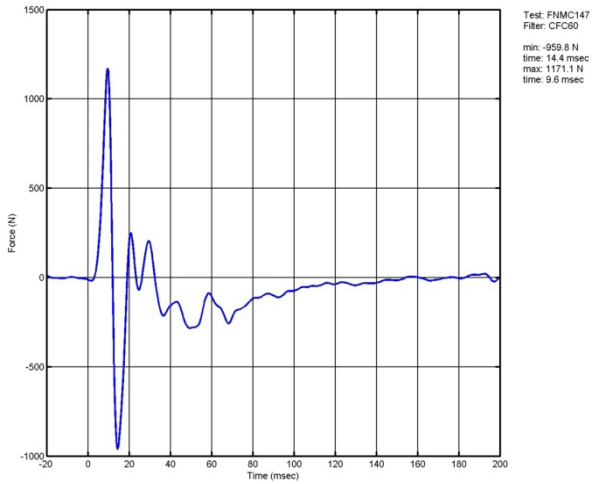


(a)

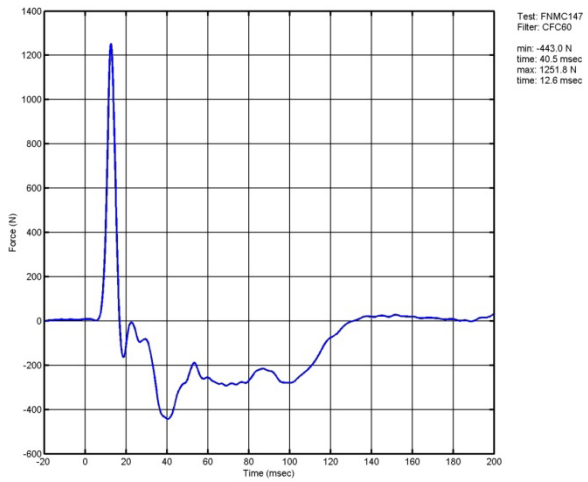


(b)

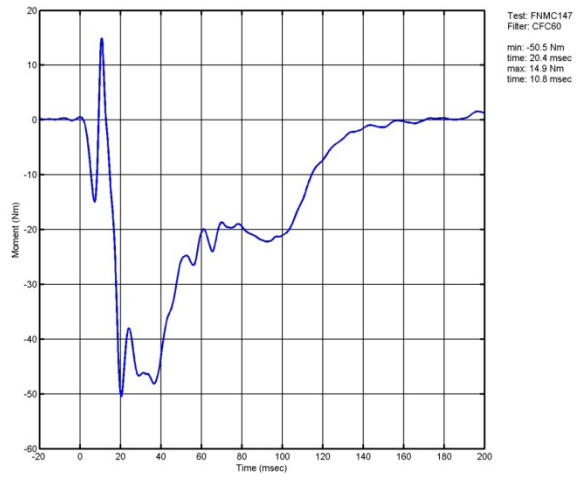


(c)

Figure A-23. Test FNMC147OC ((a) Force Y, (b) Force Z, and (c) Moment X)

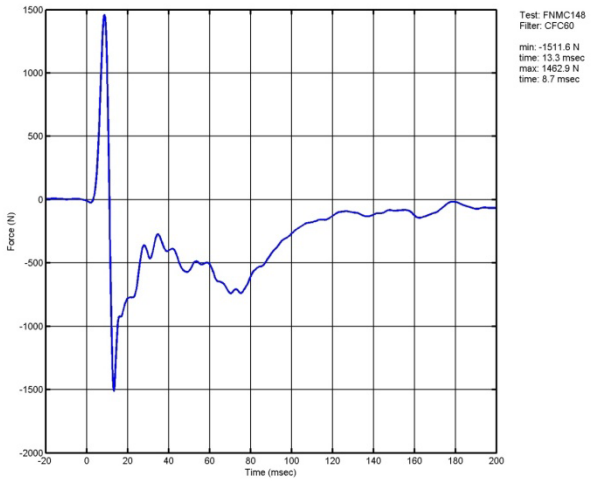


(a)

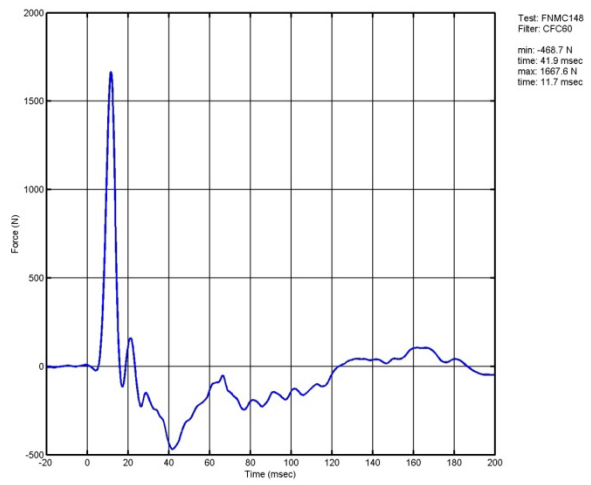


(b)

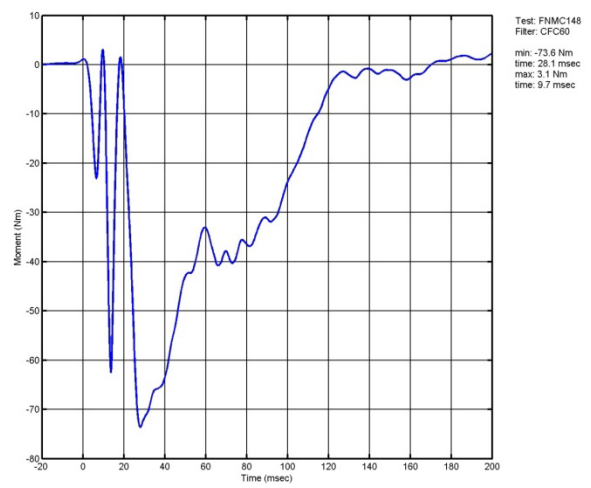


(c)

Figure A-24. Test FNMC148OC ((a) Force Y, (b) Force Z, and (c) Moment X)

# APPENDIX B—ANTHROPOMORPHIC TEST DEVICE TIME HISTORIES OF LOADS AT THE OCCIPITAL CONDYLES

Figures B-1 through B-10 show the anthropomorphic test dummy results.

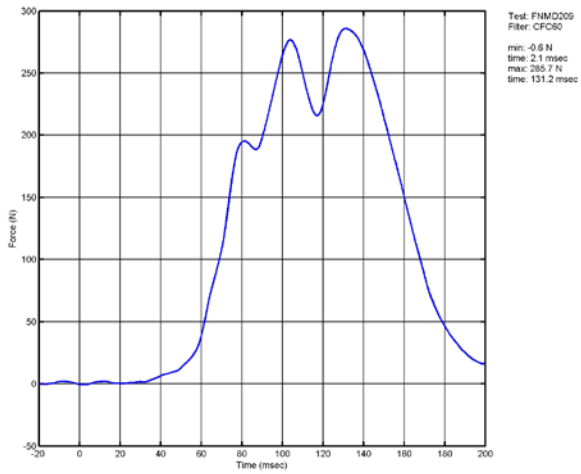


(a)

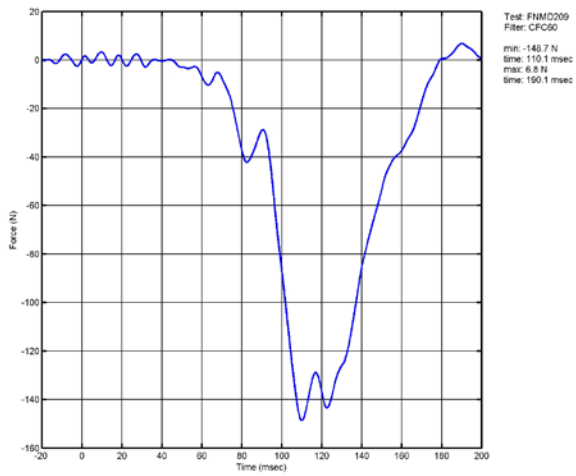


(b)

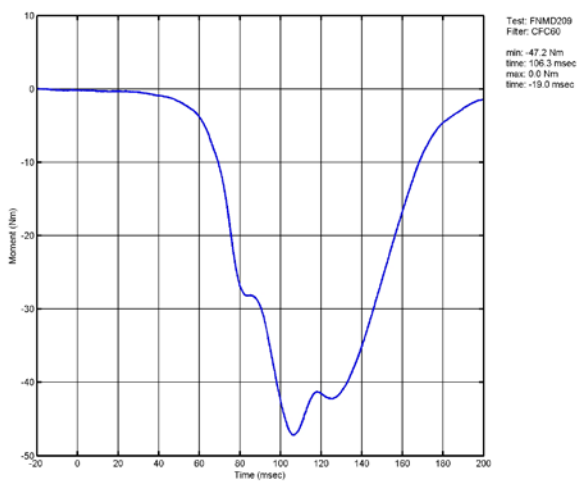


(c)

Figure B-1. Test FNMD209 ((a) Upper Neck Force Y, (b) Upper Neck Force Z, and (c) Corrected Measured Occipital Condyles (OC) Moment X)

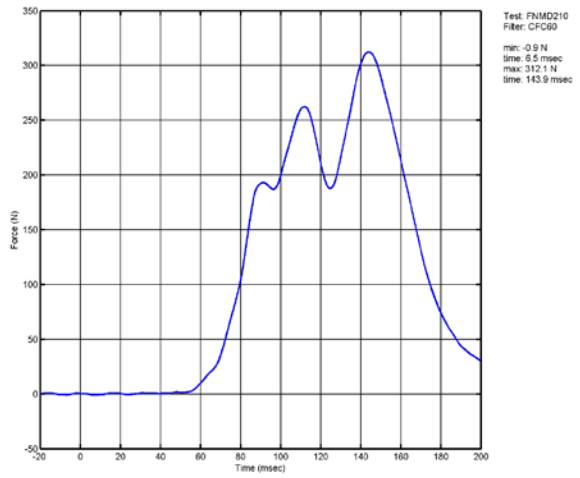


(a)

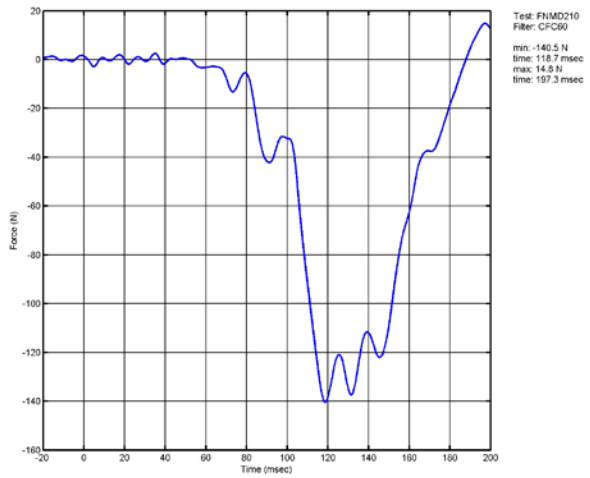


(b)

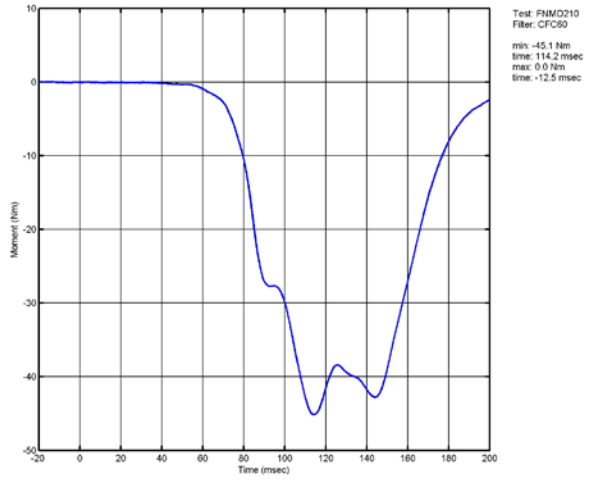


(c)

Figure B-2. Test FNMD210 ((a) Upper Neck Force Y, (b) Upper Neck Force Z, and (c) Corrected Measured OC Moment X)

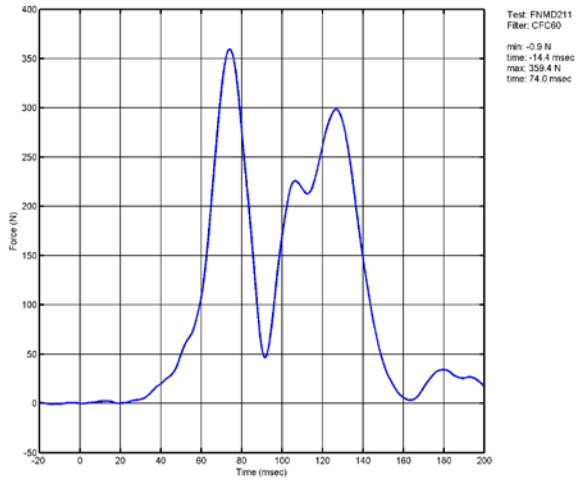


(a)

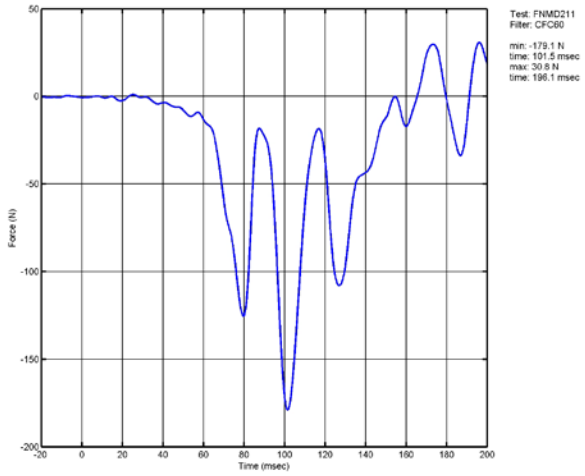


(b)

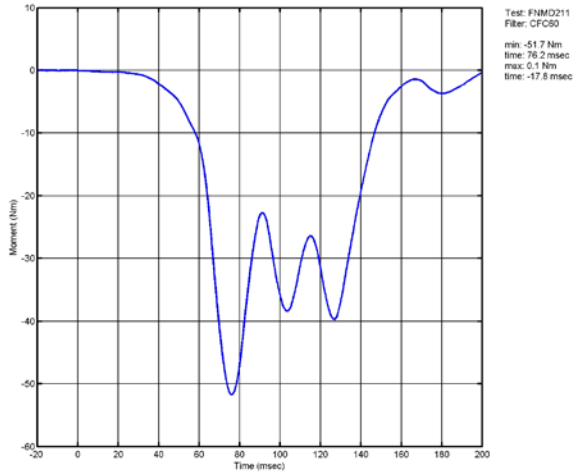


(c)

Figure B-3. Test FNMD211 ((a) Upper Neck Force Y, (b) Upper Neck Force Z, and (c) Corrected Measured OC Moment X)

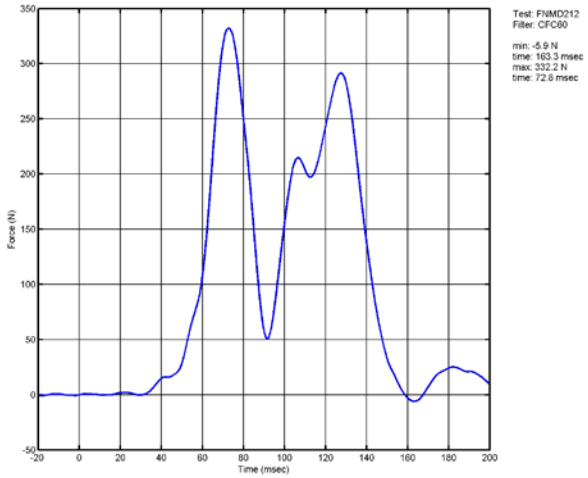


(a)

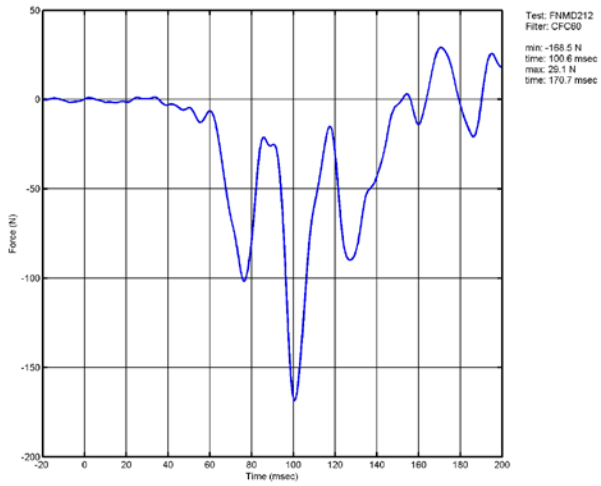


(b)

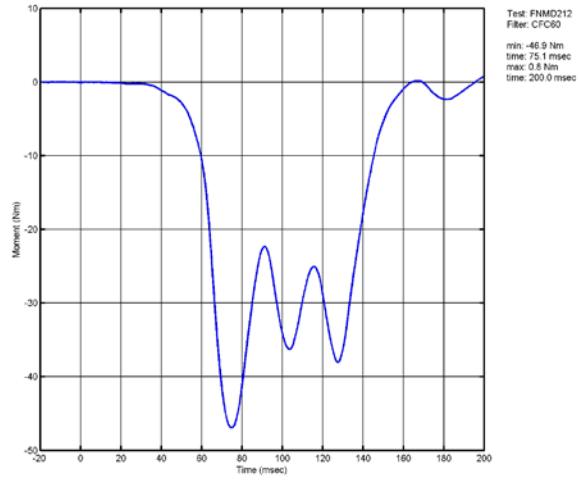


(c)

Figure B-4. Test FNMD212 ((a) Upper Neck Force Y, (b) Upper Neck Force Z, and (c) Corrected Measured OC Moment X)

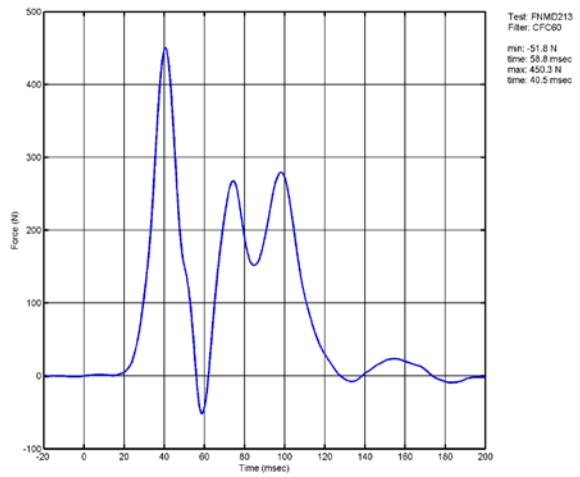


(a)

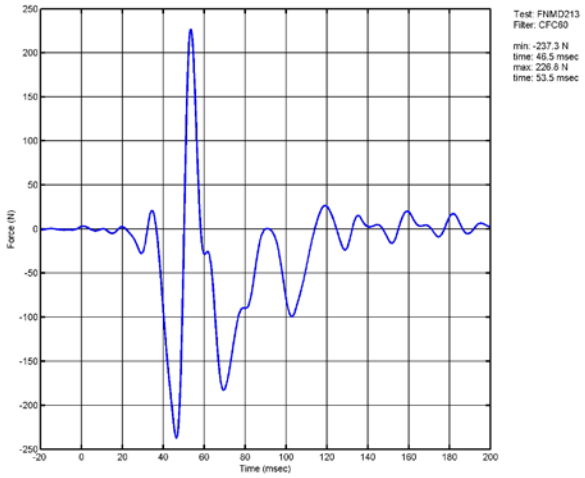


(b)

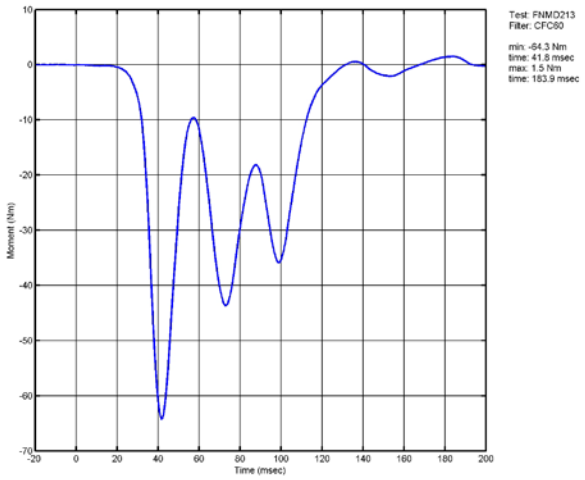


(c)

Figure B-5. Test FNMD213 ((a) Upper Neck Force Y, (b) Upper Neck Force Z, and (c) Corrected Measured OC Moment X)

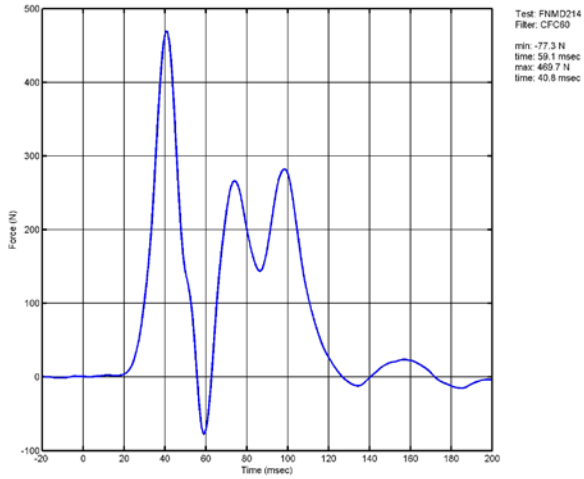


(a)

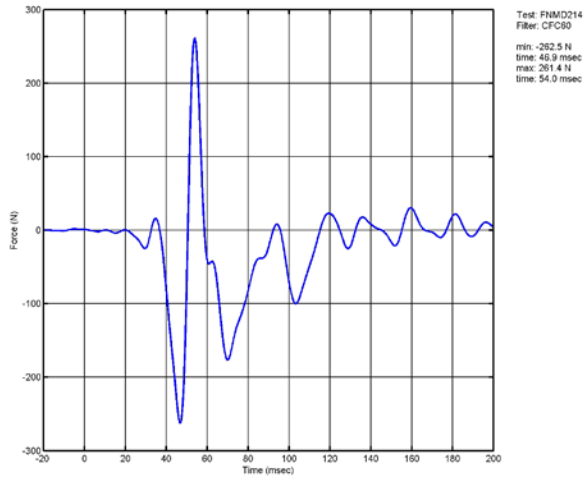


(b)

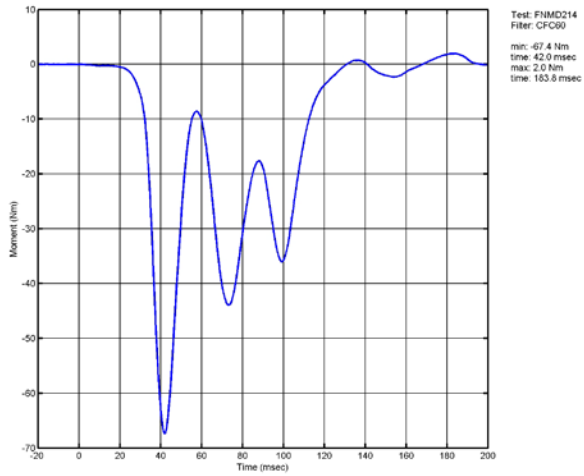


(c)

Figure B-6. Test FNMD214 ((a) Upper Neck Force Y, (b) Upper Neck Force Z, and (c) Corrected Measured OC Moment X)

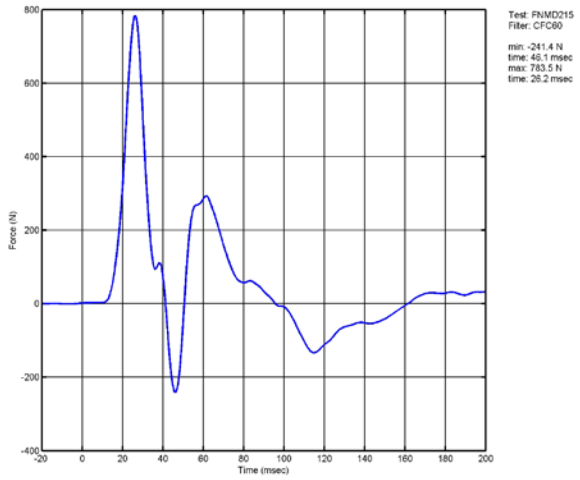


(a)

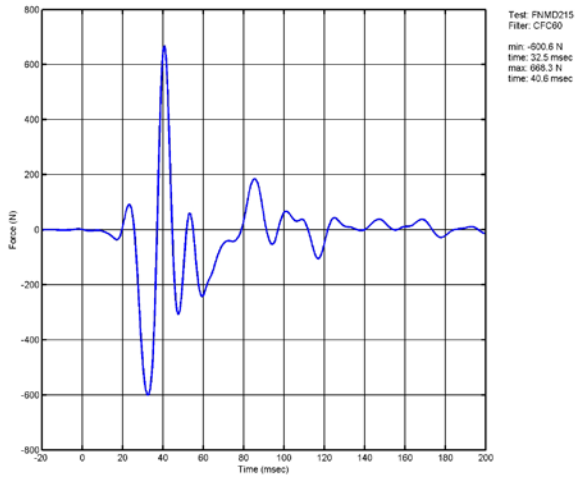


(b)

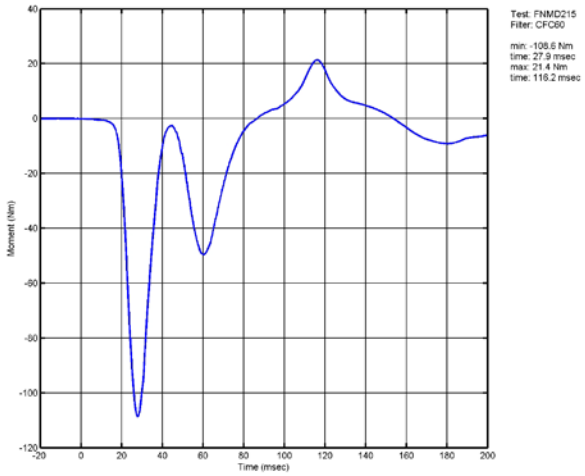


(c)

Figure B-7. Test FNMD215 ((a) Upper Neck Force Y, (b) Upper Neck Force Z, and (c) Corrected Measured OC Moment X)

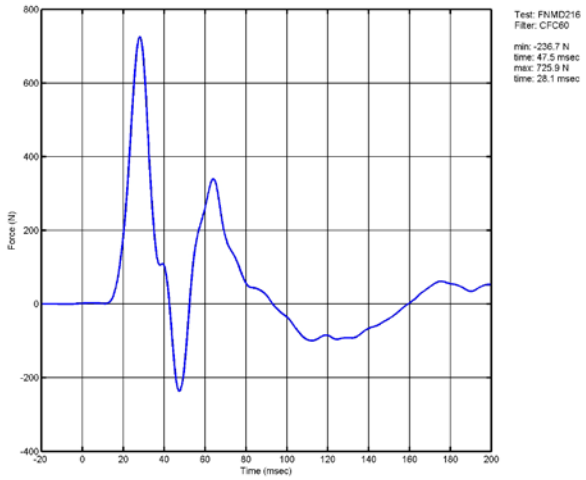


(a)

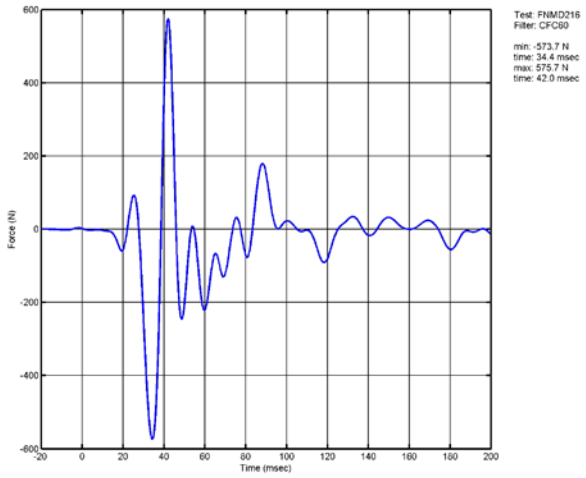


(b)

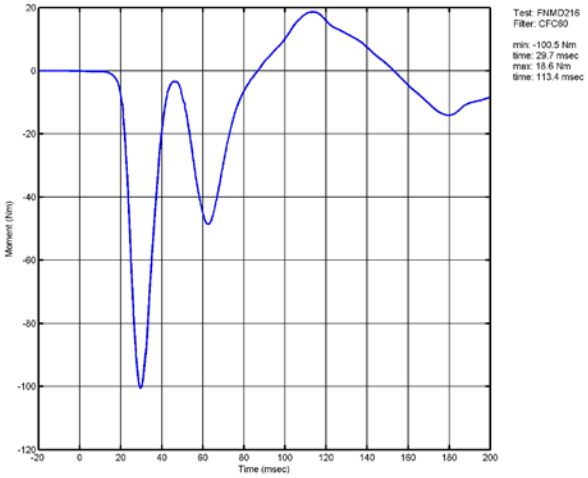


(c)

Figure B-8. Test FNMD216 ((a) Upper Neck Force Y, (b) Upper Neck Force Z, and (c) Corrected Measured OC Moment X)

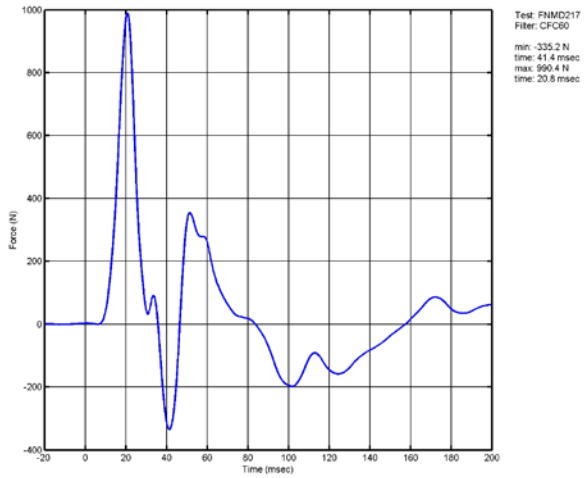


(a)

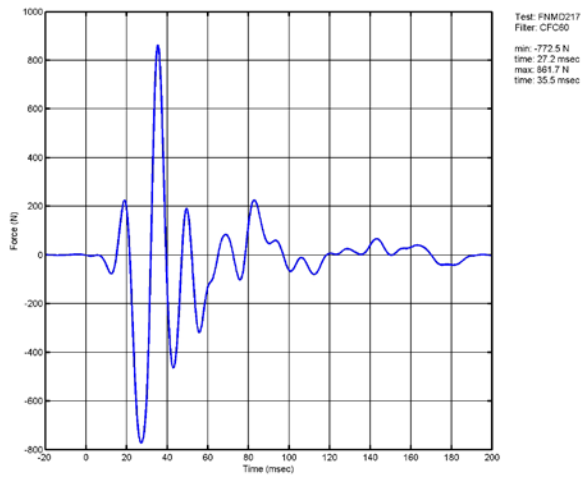


(b)

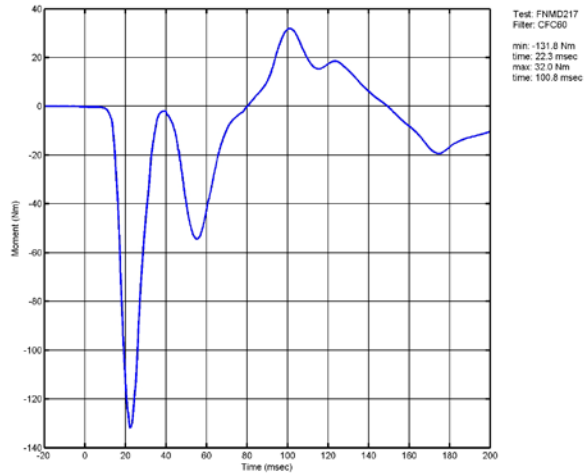


(c)

Figure B-9. Test FNMD217 ((a) Upper Neck Force Y, (b) Upper Neck Force Z, and (c) Corrected Measured OC Moment X)

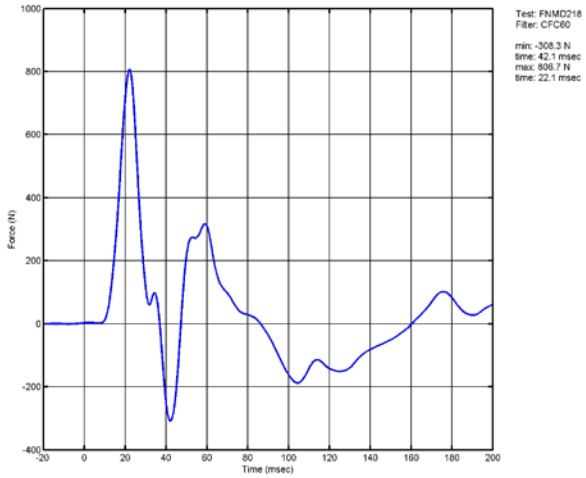


(a)

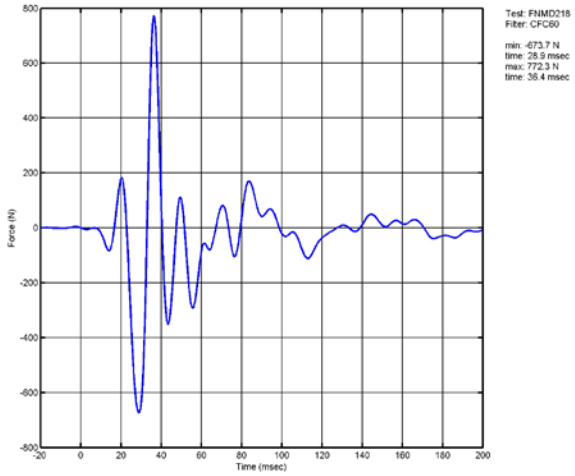


(b)

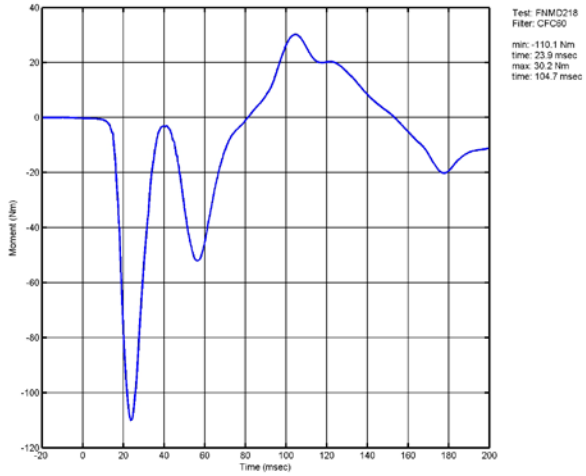


(c)

Figure B-10. Test FNMD218 ((a) Upper Neck Force Y, (b) Upper Neck Force Z, and (c) Corrected Measured OC Moment X)